



Durham E-Theses

Real-time digital signal processing system for normal probe diffraction technique

Zhang, Lei

How to cite:

Zhang, Lei (2006) *Real-time digital signal processing system for normal probe diffraction technique*, Durham theses, Durham University. Available at Durham E-Theses Online:
<http://etheses.dur.ac.uk/2843/>

Use policy

The full-text may be used and/or reproduced, and given to third parties in any format or medium, without prior permission or charge, for personal research or study, educational, or not-for-profit purposes provided that:

- a full bibliographic reference is made to the original source
- a [link](#) is made to the metadata record in Durham E-Theses
- the full-text is not changed in any way

The full-text must not be sold in any format or medium without the formal permission of the copyright holders.

Please consult the [full Durham E-Theses policy](#) for further details.

Real-Time Digital Signal Processing System for Normal Probe Diffraction Technique

Lei Zhang

2006

The copyright of this thesis rests with the author or the university to which it was submitted. No quotation from it, or information derived from it may be published without the prior written consent of the author or university, and any information derived from it should be acknowledged.

Thesis for the Degree of Master of Science

School of Engineering

University of Durham



0 1 JUN 2006

ABSTRACT

Ultrasonic systems are widely used in many fields of non-destructive testing. The increasing requirement for high quality steel product stirs the improvement of both ultrasonic instruments and testing methods. The thesis indicates the basics of ultrasonic testing and Digital Signal Processing (DSP) technology for the development of an ultrasonic system.

The aim of this project was to apply a new ultrasonic testing method - the Normal Probe Diffraction method to coarse grained steel in real-time and investigate whether the potential of probability of detection (POD) has been improved. The theories and corresponding experiment set-up of pulse-echo method, TOFD and NPD method are explained and demonstrated separately. A comparison of these methods shows different contributions made by these methods using different types of algorithms and signals. Non-real-time experiments were carried out on a V1 calibration block using an USPC 3100 ultrasonic testing card to implement pulse-echo and NPD method respectively. The experiments and algorithm were simulated and demonstrated in Matlab.

A low frequency Single-transmitter-multi-receiver ultrasonic system was designed and built with a digital development board and an analogue daughter card to transmit or receive signals asynchronously. A high frequency high voltage amplifier was designed to drive the ultrasonic probes. A Matlab simulation system built with Simulink indicates that the Signal to Noise Ratio (SNR) can be improved with an increment of up to 3dB theoretically based on the simulation results using DSP techniques. The DSP system hardware and software was investigated and a real-time DSP hardware system was supposed to be built to implement the high frequency system using a rapid code generated system based on Matlab Simulink model and the method was presented. However, extra effort needs to be taken to program the hardware using a low-level computer language to make the system work stably and efficiently.

Contents

Abstract.....	I
Content.....	II
List of Figures.....	VI
List of Tables.....	VII
Declarations.....	VIII
Statement of Copyright.....	IX
Acknowledgements.....	X
CHAPTER 1 Introduction.....	1
1.1 Ultrasonic Testing Fundamentals	2
1.1.1 Ultrasonic Waves	3
1.1.2 Longitudinal and Transverse Waves	4
1.1.3 Mode Conversion.....	4
1.1.5 Sound Field.....	6
1.1.6 Acoustic Impedance	7
1.1.7 Probability of Detection	8
1.2 Ultrasonic Testing in Industry fields.....	8
1.2.1 Ultrasonic Testing Application in Steel Industry.....	8
1.2.2 Steel products, Continuous Casting and Rolling	9
1.2.3 Inclusions of Steel Billet.....	10
1.2.4 Current Ultrasonic Testing System	11
1.2.5 Single Transmitter Multi Receivers System.....	13
1.3 Previous Research.....	13
1.4 Project Aims	15
CHAPTER 2 Ultrasonic Testing	17
2.1 Ultrasonic Transducers.....	18
2.1.1 Transducer Parameters	18
2.1.1.1 Resolution and Sensitivity	18
2.1.1.2 Impedance	18
2.1.1.3 Frequency.....	19
2.1.2 Transducer catalogue.....	19
2.1.2.1 Straight-Beam Probe.....	20
2.1.2.2 Angle-Beam Probe	21
2.1.2.3 Twin-crystal Probe	21
2.1.2.4 Delay-line Probe.....	21
2.1.3 Transducer for Steel Inspection	21
2.2 Scan Types	22

2.2.1 A-scan.....	22
2.2.2 B-scan.....	22
2.2.3 C-scan.....	23
2.3 Test Methods	23
2.3.1 Pulse–echo Method.....	23
2.3.2 TOFD Method.....	24
2.3.2.1 Reflection and Diffraction	24
2.3.2.2 TOFD Technique.....	25
2.3.2.3 Defect Location and Sizing.....	26
2.4 Normal Probe Diffraction Technique	27
2.4.1 Experiment Equipments	27
2.4.1.1 Socomate USPC 3100 PC based ultrasonic flaw detector.....	27
2.4.1.2 Hewlett Packard Infinium oscilloscope	28
2.4.1.3 V1 Calibration Block.....	28
2.4.1.4 Ultrasonic couplant Gel (Ultrigel II from Diagnostic Sonar Ltd)	28
2.4.2 Experimental Setup	29
2.4.3 Experiments with V1 calibration	29
2.4.4 Experiment Conclusion	32
2.5 PC-Based Ultrasonic Test System	32
2.5.1 Assembling an Ultrasonic Test System.....	32
2.5.1.1 Pulser/Receiver.....	33
2.5.1.2 Ultrasonic Transducer.....	33
2.5.1.3 Digitizer	33
2.5.1.4 Application software.....	33
2.5.1.5 Communication	33
2.5.2 Pulser/Receiver (P/R).....	33
2.5.3 Digitiser	34
2.5.4 Switching.....	35
2.5.5 Application Software.....	36
2.6 Summary	37
CHAPTER 3 NPD Algorithm	38
3.1 NPD Mathematical Model	38
3.2 NPD Simulink Model.....	40
3.3 Matlab GUI for NPD	42
3.4 Summary	42
CHAPTER 4 System Simulation Model.....	44
4.1 Simulink Model	45
4.2 Signal Generation	46
4.3 Attenuation	47
4.4 Time Delay and Environment Noise.....	48
4.5 Digital Filters	49
4.5.1 IIR Filter	49
4.5.2 FIR Filter	50
4.5.3 Correlation	51
4.6 Simulation Result.....	52
4.7 Summary	54

CHAPTER 5	DSP System Architecture	55
5.1	System Hardware.....	55
5.1.1	Texas Instruments TMS320C6713 DSK.....	55
5.1.1.1	C6713 DSP Core	58
5.1.1.2	EDMA (Enhanced Direct Memory Access)	58
5.1.1.3	Timer.....	59
5.1.1.4	EMIF (External Memory Interface)	59
5.1.1.5	CPLD (Complex Programmable Logic Device).....	60
5.1.1.6	SDRAM (Synchronous Dynamic Random Access Memory)	60
5.1.1.7	Daughter Card Interfaces	61
5.1.1.8	McBSP (Multi-channel Buffered Serial Ports)	61
5.1.1.9	AIC23 Codec.....	62
5.1.1.10	JTAG (Joint Team Action Group).....	62
5.1.2	Analogue Daughter card.....	63
5.1.2.1	FPGA	63
5.1.2.2	THS5661 DAC.....	64
5.1.2.3	THS1230 ADC.....	64
5.1.2.4	Digital I/O Connector	65
5.2	Development Tools.....	65
5.2.1	Code Composer Studio.....	65
5.2.2	DSP/BIOS.....	66
5.2.3	Software Libraries.....	67
5.2.4	Support for Daughterboard Interfaces.....	68
5.2.5	Matlab Tools	68
5.2.6	FPGA Configuration	69
5.2.6.1	Digital I/O Register	70
5.2.6.2	Digital I/O Control Register.....	70
5.2.6.3	Status register	70
5.2.6.4	Start register and Period register	71
5.2.6.5	A/D Clock Rate Register	71
5.2.6.6	D/A Clock Rate Register	71
5.3	Real-Time DSP Prototype	71
5.4	DSK Application Example	73
5.4.1	Description.....	74
5.4.2	Ping-Pong Buffering	75
5.4.3	EDMA Linked Transfers.....	76
5.4.4	DSP/BIOS Real-time Analysis and Schedule.....	76
5.5	Real-time Rapid Prototype Example	78
5.5.1	Simulink Model and RTDX Result.....	78
5.5.2	Board Support Blocks	79
5.5.3	From/To RTDX Block	80
5.6	Summary	80
CHAPTER 6	AED330 Daughter Card Experiments.....	81
6.1	Test Program Description.....	81
6.2	Test Program Source Files	83
6.2.1	AED_Main.....	83

6.2.2 AED_DMS_EDMA	83
6.2.3 AED_330	83
6.2.4 6x1x_BRD	84
6.3 Daughter Card Clock Frequency Test.....	84
6.4 40 kHz Ultrasonic Transceiver Circuit	86
6.5 High Voltage High Frequency (HVHF) Amplifier	88
6.6 Summary	90
 CHAPTER 7 Conclusion and Further Research.....	 91
7.1 Conclusion.....	91
7.2 Further Research.....	92
 References.....	 94

Appendix Published Papers

1. The Institute of Materials, Minerals and Mining Conference: Advances in on-line instrumentation for materials characterisation in metals industry Conference, 2005, London, UK
 “Normal Probe Diffraction – Improving the Capability of Industrial Ultrasonic Probe Arrays” - L.Zhang, S.Johnstone, P.Snowdon(University of Durham), S.Dewey(STC, Corus plc, UK)
2. To be published on The British Institute of Non-Destructive Testing (BINDT) 2005 Conference, September 2005, Harrogate, UK
 “Real-Time DSP System for Normal Probe Diffraction Technique” – L.Zhang, S.Johnstone, P.Snowdon, S.Dewey

Lists of Figures

Figure 1. 1 Reflection and Refraction.....	5
Figure 1. 2 Sound Field.....	7
Figure 1. 3 Relationship and size of probes	12
Figure 1. 4 The two banks of probes	12
Figure 1. 5 Divergence of Pulse/Echo Signal	13
Figure 1. 6 Normal Probe Diffraction Experiment Setup	14
Figure 1. 7 Comparison of Probability of Detection for NPD and Pulse-Echo	15
Figure 2. 1 5MHz Transducer Parameter Measurement.....	19
Figure 2. 2 Four Fundamental Transducer Types	20
Figure 2. 3 Block diagram: Pulse Echo Method	23
Figure 2. 4 Reflection and Diffraction.....	24
Figure 2. 5 TOFD wave paths	25
Figure 2. 6 TOFD A-scan Schematic.....	26
Figure 2. 7 (a) Pulse-echo A-scan form probe 1	29
Figure 2. 7 (b) Pulse-echo A-scan form probe 1	30
Figure 2. 7 (c) Pulse-echo A-scan form probe 1	30
Figure 2. 8 Transmitter-Receiver Mode Test Result	32
Figure 3. 1 Ellipse.....	39
Figure 3. 2 Double Probes NPD Scheme.....	40
Figure 3. 3 Triple Probes NPD Scheme.....	40
Figure 3. 4 NPD Algorithm Simulation Model.....	41
Figure 3. 5 Matlab NPD GUI	42
Figure 3. 6 NPD GUI Example	43
Figure 4. 1 Ultrasonic Detection System Simulink Model	46
Figure 4. 2 Transmission Subsystem	48
Figure 4. 3 IIR Butterworth Lowpass Filter.....	50
Figure 4. 4 FIR Kaiser Lowpass Filter	51
Figure 4. 5 Correlation Subsystem	52
Figure 4. 6 Simulation Result.....	54
Figure 5. 1 Taxes Instrument TMS320C6713 DSK.....	56
Figure 5. 2 TMS320C6713 DSK Block Diagram	56
Figure 5. 3 DSK Memory Map	58
Figure 5. 4 AED_330 Daughter Card Block Diagram.....	63
Figure 5. 5 A Rapid Real-Time DSP Prototype	72
Figure 5. 6 DSK Application Example Hardware Diagram	74
Figure 5. 7 Real-time analysis using DSP/BIOS.....	76
Figure 5. 8 CPU Load Graph.....	77
Figure 5. 9 Execution Graph.....	77
Figure 5. 10 Simulink Real-time Model: Time-Domain Acoustic Noise Canceller	79
Figure 5. 11 Waterfall Plot of Filter Parameters	79
Figure 6. 1 Test Program DAC_table	85
Figure 6. 2 Receive Circuit.....	87
Figure 6. 3 Tx-Rx using 3 Periods Square Wave	88
Figure 6. 4 Tx-Rx using Half Period Sine Wave.....	88
Figure 6. 5 Custom Amplifier Circuit.....	89
Figure 6. 6 PSPICE Simulation Result	89

List of Tables

Table 3. 1 Transmit Distance and Time.....	39
Table 3. 2 Propagation Angles	40
Table 4. 1 Signal-to-noise Ratio Comparison	53
Table 5. 1 TMS320C6713 DSK Features	57
Table 5. 2 CPLD Registers.....	60
Table 5. 3 FPGA Control Registers.....	70
Table 6. 1 Daughter Board Test Program Functions	84
Table 6. 2 PLL Multiplier Control Daughter Card Sampling Frequency	86
Table 6. 3 PLL Divider Control EMIF Frequency	86

Declarations

The author confirms that this thesis conforms to the word length prescribed for the degree to which it is submitted.

No part of the material offered in this thesis has been previously submitted by the author for a degree in this or any other University.

Statement of Copyright

The copyright of this thesis rests with the author. No quotation from it should be published without prior written consent and information derived from it should be acknowledged.

Acknowledgement

This project has been sponsored by Corus. I would like to thank Steve Dewey for all helpful comments and stimulating discussions.

I especially want to thank my supervisor Dr Sherri Johnstone, for her continuous support guides me to learn not only harder but smarter; her encouragement leads me to be self-confident in chasing my goal; her positive attitude and happy manner teach me how to treat research as a hobby and an art, rather than a tedious work; her consideration covers both my academic progress and my daily life, helps me to overcome any homesick and loneliness in a foreign country and focus on my study.

I also want to thank Paul Snowden for his previous research and testing; Adam Cluett for his detailed explanation with patience and a good humour; Tom Grocutt for sharing his knowledge and experience introducing me to hardware programming; Ian Hutchinson for providing all necessary equipments and everyone in the School of Engineering who has contributed to such a good scientific and technology environment and shared their knowledge impartially.

Acknowledgement

This project has been sponsored by Corus. I would like to thank Steve Dewey for all helpful comments and stimulating discussions.

I especially want to thank my supervisor Dr Sherri Johnstone, for her continuous support guides me to learn not only harder but smarter; her encouragement leads me to be self-confident in chasing my goal; her positive attitude and happy manner teach me how to treat research as a hobby and an art, rather than a tedious work; her consideration covers both my academic progress and my daily life, helps me to overcome any homesick and loneliness in a foreign country and focus on my study.

I also want to thank Paul Snowden for his previous research and testing; Adam Cluett for his detailed explanation with patience and a good humour; Tom Grocutt for sharing his knowledge and experience introducing me to hardware programming; Ian Hutchinson for providing all necessary equipments and everyone in the School of Engineering who has contributed to such a good scientific and technology environment and shared their knowledge impartially.

CHAPTER 1

Introduction

In the course of the casting process, a variety of internal discontinuities can occur in the metal. The main defects that lie in the final steel product include inclusions, bubbles and cracks, all of which can affect the quality of the steel product. Main body defects excluding near-field defects can be detected using appropriate NDT (Non-destructive Testing) methods.

In bloom and billet mills, traditional on-line pulse-echo defect detection systems exist, in which each probe is sequentially used to produce a radio frequency pulse, which is then reflected from the defect and detected by the same probe. The results of experiments carried out in previous research successfully show that the conventional method of ultrasonic billet inspection discards much information which could be used to improve the test integrity and sensitivity. Extra information can be obtained about the defect to increase the probability of detection (POD) if the diffracted signal is also collected by neighbouring probes. A standard Single-Transmitter-Multi-Receiver system was built to implement this. As this technique is similar to time-of-flight diffraction (TOFD), but does not require angle beam probes, it is referred to as Normal Probe Diffraction (NPD). The aim of this project was to build the necessary real-time hardware for the implementation of the NPD technique, thus giving the possibility of improved on-line defect detection. Furthermore, modern advances in electronic and signal processing are applied to improve the signal to noise ratio.

In chapter 1, basic ultrasonic theory which is relevant to NPD is described. Although metallurgy is not within the scope of this project, the desired ultrasonic testing system is to be used in steel mill to test the quality of products. Therefore, a brief outline of the steel manufacture process is also included to assist in the understanding of some of the potential problems within the manufacture of steel and the formation of internal defects that require the development of complex inspection techniques.



Chapter 2 describes the equipment, such as probes, test methods and standard representations of signals used in ultrasonic testing and then applies these to non-real-time tests using the NPD algorithm on both a V1 calibration block and an as-cast billet. It was found that the signal to noise ratio in the billet was low due to the large grain size, so a model of the system was created in Matlab Simulink. To implement this, an NPD simulation model was first created. This is described in Chapter 3. Chapter 4 then describes how it is incorporated into a model of the complete ultrasonic test system, using simulated input data. The model is then used to investigate and design different filtering techniques to improve the signal to noise ratio such that the probability of detection can be increased.

The next stage of the project was to implement the NPD algorithm in real-time. A TMS320C6713 DSK was chosen as the base hardware platform, together with a high-speed analogue daughter card. This hardware and the associated development tools are described in Chapter 5, together with some application examples for illustration. The Matlab Simulink real-time rapid prototyping method is described, but was not used in this project since it could not easily support the third party daughter card.

Finally, chapter 6 includes work carried out in applying the DSK and daughter card to transmit and receive signals from ultrasonic transducers with the ultimate aim of applying NPD in real-time. To test the basic principles, a 40 kHz system was investigated in which analogue interfacing hardware was designed and implemented. A high speed (MHz) high voltage amplifier was designed but not implemented during this project.

1.1 Ultrasonic Testing Fundamentals

Ultrasonics refers to any study or application of ultrasonic waves covering a range of frequencies between 18 kHz and 25 MHz, much higher than the human audible sound waves. Ultrasonic waves are used in many applications including plastic welding, medicine and NDT. Within NDT, ultrasonic waves give us the ability to “see through” solid/opaque material and internal flaws without affecting the material in an adverse manner.

Ultrasonic Testing is more than 40 years old. From the very first examinations, using ultrasonic oscillations for detection of flaws in different materials, it has become a classical test method based on measurements with due regard to all the important influencing factors. Today it is expected that ultrasonic testing, supported by great advances in instrument technology, give reproducible test results within narrow tolerances. This assumes exact knowledge of the influencing factors and the ability to apply these in the testing technology. Not all influences have to be seriously regarded by the operator. In many cases some of the influences can be neglected without exceeding the permitted measurement tolerances. Due to this, the test sequence is simplified and the testing time reduced. Despite this, the future belongs to the UT engineer who continuously endeavours to keep his knowledge at the latest state of the art and the well designed automatic testing system which can carry out the task efficiently.

1.1.1 Ultrasonic Waves

Ultrasonic waves are transmitted by high frequency particle vibrations. The ultrasonic principle is based on the fact that solid materials are good conductors of sound waves, whereby the waves are not only reflected at the interfaces but also by internal defects such as inclusions. When an ultrasonic wave is transmitted in homogenous solid material, the directed energy in it is reflected by boundaries between materials as well as by any cracks or voids in the object. The reflected waves caused by internal defects can be compared to the reflected waves from the external surfaces, enabling the size and severity of internal defects to be identified.

The following relationship between frequency $f(MHz)$, wave length λ (mm), and sound velocity, $c(km/s)$ is valid for all types of wave.

$$c = f * \lambda \dots\dots\dots (1.1)$$

Acoustic velocity is dependant on the material of propagation, and in general, is constant for any frequency and wavelength. This function indicates that ultrasonic waves, which are mainly used in a frequency range between about 0.5 MHz and 25 MHz, have wave lengths in mm. With lower frequencies, the interaction effect of the waves with internal flaws would be so small that detection becomes questionable.

1.1.2 Longitudinal and Transverse Waves

Two predominant types of waves, or wave modes, are generated within a material with ultrasonic waves: longitudinal and transverse. Longitudinal waves compress and decompress the material in the direction of motion, much like sound waves in air. Transverse waves vibrate particles at right angles compared to the motion of the ultrasonic wave. The velocity of transverse waves through a material is approximately half that of the longitudinal waves. The angle in which the ultrasonic wave enters the material determines whether longitudinal, transverse, or both waves are produced.

The mode of the wave affects the velocity, in that longitudinal waves have greater velocity than transverse waves. The velocities of the sound waves are calculated from the elastic constants of the material concerned, that is:

Modulus of elasticity E (measured in N/m^2)

Density ρ in kg/m^3

Poisson's ratio u

for longitudinal waves:

$$c_l = \sqrt{\frac{E}{\rho} \frac{1-u}{(1+u)(1-2u)}} \dots\dots\dots (1.2)$$

for transverse waves:

$$c_t = \sqrt{\frac{E}{\rho} \frac{1}{2(1+u)}} \dots\dots\dots (1.3)$$

1.1.3 Mode Conversion

Ultrasonic beam refraction and mode conversion occur when an ultrasonic wave passes from one medium to another. Refraction and mode conversion occur because of the change in L-wave velocity as it passes the boundary from one medium to another. The higher the difference in the velocity of sounds between two materials, the larger the resulting angle of refraction. L-waves and T-waves have different angles of refraction because they have dissimilar velocities within the same material.

The oscillations of longitudinal waves can be described by compression and decompression of the atoms propagating through the material (gas, liquid and solid). Transverse waves only occur in solid materials never in liquids or gases because these do not have a transverse modulus and therefore do not affect any transverse forces. In addition to this, they propagate much slower than longitudinal waves in the same

material. It is therefore longitudinal waves which are the main area of interest in this project.

1.1.4 Snell's Law

L-wave and T-wave refraction angles are calculated using Snell's Law, the equation and illustration figure are shown as follow. Snell's Law also can be used to determine the first critical angle for any combination of materials. The refraction angle of longitudinal waves is for steel approximately twice as large as that of the transverse waves because of the difference of their velocities.

$$\frac{\sin \alpha}{\sin \beta} = \frac{c_1}{c_2} \dots\dots\dots (4.1)$$

Where α = angle of incidence, β = angle of refraction, c_1 = sound velocity in medium 1
 c_2 = sound velocity in medium 2.

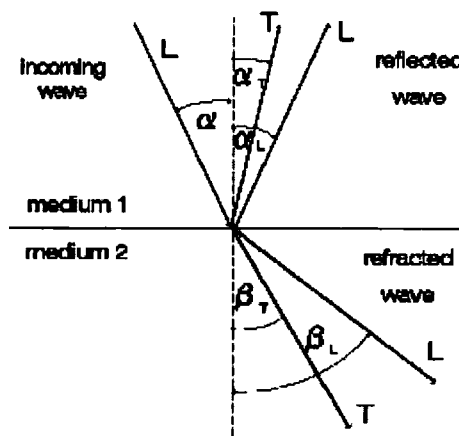


Figure 1. 1 Reflection and Refraction

By enlarging the angle of incidence, we will eventually get the longitudinal wave refracted through an angle of 90°. This means that it runs along the interface whilst the transverse wave is still transmitted into the test object. The angle of incident - α_{CL} is called the first critical angle. With further enlargement of the angle of incidence various refraction angles of the transverse wave (beam angle) can be set when the transverse wave reaches 90°, it is refracted and propagates along the surface of the test object, and it then becomes a surface wave. This angle of incident - α_{CT} is called the second critical angle.

1.1.5 Sound Field

The ultrasonic waves only cover a certain section of the test object depending on the certain directivity of the probe. The area effective for the ultrasonic test is called the sound beam which is characteristic for the applied probe and material in which sound waves propagate. A sound beam can be roughly divided into a convergent (focusing) area, the near-field, and a divergent (spreading) part, the far field. The near field is the region in an ultrasonic beam that is subject to variations of intensity due to diffraction effects. It extends from the source of radiation to a point just short of the far field. The length N of the near-field and the divergence angle is dependent on the diameter of the element and the wave length of the ultrasound in the tested material.

$$N = \frac{D^2 - \lambda^2}{4\lambda} \dots\dots\dots (1.5)$$

The ultrasonic field is cylindrical from the face of the transducer to the end of the near field[1]. In the far field the beam diverges conically with the apex at the centre of the transducer face. The sound pressure disperses according to the inverse square law, which is when the intensity is inversely proportional to the square of the distance. In the far field the angle of divergence for the extreme width of the beam is given by[2]

$$\sin \frac{\gamma}{2} = k_{dB} \frac{\lambda}{D} \dots\dots\dots (1.6)$$

Where k_{dB} = constant based on stated dB drop from centre maximum. Values of k_{dB} vary for the dB drop that is to be determined: $k_{dB}=0.37$ when dB=3, $k_{dB}=0.70$ when dB=6, $k_{dB} = 0.87$ when dB=20. Both the near field and beam angle are shown in Figure 1.2.

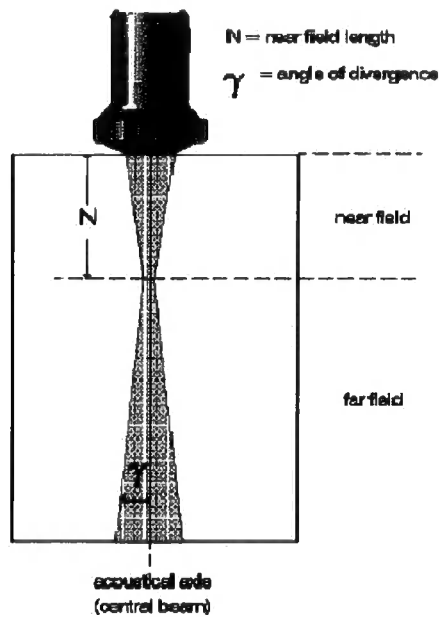


Figure 1. 2 Sound Field

1.1.6 Acoustic Impedance

When performing ultrasonic testing, it is important to understand how effectively ultrasonic waves pass from one medium to another. Generally, when an ultrasonic wave propagates from one medium into another, energy is partially reflected and partially transmitted. The relationship in this phenomenon is described by acoustical impedance and the acoustical impedance ratio.

$$Z = \rho V \dots \dots \dots (1.7)$$

where Z is the acoustical impedance, ρ is the density of the sound medium and V is the velocity of sound through medium.

For reference, air has low acoustical impedance, water has higher impedance than air, and steel has higher impedance than water. The acoustical impedance ratio is the impedance of the second material divided by the first. The higher the ratio, the more energy is reflected. For example, when ultrasonic waves are passed from water to steel, the acoustical impedance is approximately 20 to 1; whereas, when ultrasonic waves are passed from air to steel, the acoustical impedance is approximately 100,000 to 1. Almost 100% of the ultrasonic energy will be reflected when passing ultrasonic waves

from air to a solid such as steel, making air a very poor ultrasonic couplant. That is reason that the couplant gel is used in this project.

1.1.7 Probability of Detection

Probability of Detection (POD) is a term that describes the reliability of inspection techniques. Two main elements affect POD; the technique and the human factor. Broadly speaking the inspection reliability is defined as the probability of not overlooking an existing defect (probability of detection, POD) and correct sizing the defect. However simple this definition may appear, it encompasses many complex issues ranging from the specification of the nature of defects to influencing factors related with the inspection instrumentation, product nature, the involved human factor and the available expertise for inspection data processing and assessing.

1.2 Ultrasonic Testing in Industry fields

Among many UT methods developed for the detection of the steel defects, ultrasonic testing has commonly and long been used in the industry fields. Tasks of ultrasonic testing system include detection, location, evaluation and diagnosis of discontinuities. The term "discontinuity" is defined as being an "irregularity in the test object which is suspected as being a flaw". In reality, only after location, evaluation and diagnosis has been made, can it be determined whether or not there is a flaw which effects the purpose of the test object. The term "discontinuity" is therefore always used as long as it is not certain whether it concerns a flaw which means a non-permissible irregularity[3].

1.2.1 Ultrasonic Testing Application in Steel Industry

Ultrasonic testing has been used for many applications, among which, steel production and the manufacture of rods, tubes, and plates are ranked high for their importance and advance. In some cases, in order to detect the internal and surface-breaking defects without affecting the strength and integrity of the tested product and to guarantee that the test results can meet specific standards, UT turns out to be one of the best choices since it can fulfil these requirements easily Nowadays, the automated modern mills and their high production speed demand for fast testing system capable for high pulse repetition and real-time data processing. UT in this field operates ultrasonic probes close to the surface of the testing products and uses complex mechanical system to

handle the geometry, size and movement of the products under inspection. Ultrasound lamb waves provide a reliable test for tube inspection without the need of rotation and use relatively lower frequency. The lamb wave or guided wave is an interesting topic in modern UT and worth of further study in the steel industrial. It is considered that the real-time system discussed in this paper can also be amended and implemented with the guided waves. This requires further research of the present test method using guided waves. The structure of castings can highly attenuate the power of ultrasound, makes UT methods less effective. However, this deficiency can be compensated by increase the testing frequency and the output voltage of the pulse. 5MHz is chosen for this project to get a relatively high resolution within reasonable amplitude attenuation.

1.2.2 Steel products, Continuous Casting and Rolling

In the past, molten steel used to be poured (teemed) into a large mould where it would be allowed to cool and solidify to form an ingot. The ingot was then put into an oven called a soaking pit, where it would be gently heated to the correct and uniform temperature. This red hot ingot would then be rolled in primary mills, in the first stage of its transformation into a usable steel product, into one of three forms of semi-finished product: a slab (a long, thick, flat piece of steel, with a rectangular cross-section), a bloom (a long piece of steel with a square cross-section) or a billet (like a bloom, but with smaller cross-section).

In the UK, the continuous casting process has substituted the ingot route and become dominant, while the ingot route may still be the most suitable way of producing the required steel under certain circumstances.. For the continuous casting process, firstly, molten steel is poured into a reservoir at the top of the continuous casting machine. The outer shell of the molten steel is then solidified by a water cooled mould. After this, the steel is shaped by a series of rolls and fully solidified by water sprays at the same time. The last step of this continuous process is to cut the steel to the required length to form the final products like slabs, blooms and billets.

Rolling is to reduce the thickness of a material by passing it between two rolls. It is a very popular forming process. It is divided into hot-rolling and cold-rolling according to operating methods. Hot-rolling is mainly used for larger amounts of deformation and cold-rolling is applied to optimise the mechanical properties and surface finish.

Corus, formerly the British Steel Company, is one of the typical steel manufacturers in the UK processing and distributing metal products such as steel bar and steel billet. Scunthorpe Bloom and Billet Mill is part of the main Corus site in North East UK. The mill produces various types of steel in billets that are widely used in industry; the section of material of interest, for this project, a square section steel of sections ranging from 76mm x 76mm down to 36mm x 36mm. Corus employs several different methods of defect detection, which is dependant upon the positioning of the defect, i.e. surface, sub-surface and core defects. The remit of the project is to investigate the core section of the hot-rolled billet with a coarse grain structure using ultrasonic techniques.

A coarse grain structure metal contains fewer grains than a fine grain metal. A fine grained metal is therefore harder than a coarse grained metal. The coarse grain structure of steel product can scatter the pulse wave sent into the steel sample and form the randomly distributed background noise disturbing the recognition of the defect echoes[4]. Sometimes, grain refining agents are added to the molten metal before it is cast to provide nuclei around which grains can grow. This will tend to produce a finer grained material which is harder than it would have been with fewer grains.

An initial Eddy current inspection of the material (for surface breaching cracks) is done prior to the steel leaving the mill. The steel is then transferred in billet form to the finishing mill. At the finishing mill it is reheated to 1200°C and rolled down to the final size required of between 30-75mm. The ultrasonic inspection process takes place after the material has been hot rolled down to the final size and cooled. The evaluation of the ultrasonic signals is carried out with multi-channel electronics[5]. The coarse grain structure of the as-cast bloom causes high attenuation of ultrasound[6]; it is more practical therefore to inspect the steel post hot rolling. This process of working the steel also improves the quality of the steel by refining its crystalline structure and making the metal harder and tougher.

1.2.3 Inclusions of Steel Billet

At the Primary Mill the molten steel is continuously cast as a 400mm square bloom. A bloom is a bar of steel prepared for rolling. The casting process during which the refractory shrouds cover the vessel and pore to prevent atmospheric exposure is the main cause of inclusions being formed in the molten steel [7][8]. Inclusions are small

patches of impurities such as non metallic elements (e.g. carbon); or their oxides, sulphides which are mixed into steel. These can be either something quite simple in nature containing just one component or very often a much more complex multi-component construction. In addition to chemistry, inclusions are characterised by their size and shape[9] ; inclusions can be angular, globular or highly elongated. They usually have to be removed from the steel in order for it to have good structural and mechanical properties. Inclusions can have a major impact on the processing characteristics of steel, and also the final in-service physical properties of the steel. The hot rolling process elongates and concentrates these inclusions to the core of the billet, making the defect in a billet rolled down from a bloom different from that of a direct cast billet.

There are two classes of inclusions which are dependent on elongation during hot rolling:

- Non-deformable inclusions - such inclusions are hard at rolling temperatures and maintain their original shape as the steel is deformed.
- Deformable inclusions - such species are soft at steel rolling temperatures and deform and elongate as the steel is rolled.

1.2.4 Current Ultrasonic Testing System

Scunthorpe Billet Mill uses an immersion ultrasonic inspection system to detect defects, cracks, and inclusions etc. within the core area of the material. The immersion system has a stationary multi-probe array of eight 3/8 inch diameter piezoelectric transducers, arranged at normal incidence to the material. Figure 1.3 shows the layout of the probes in relation to each other. The piezoelectric transducers create a receive ultrasound to convert energy between mechanical and electrical forms. The probes are set overlapping so that no part of the material is left un-inspected. The ultrasonic system currently in use is shown in Figure 1.4.

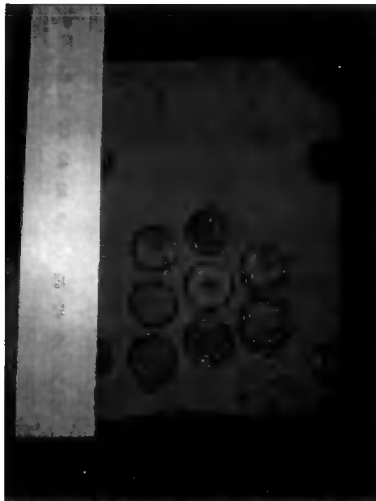


Figure 1. 3 Relationship and size of probes **Figure 1. 4** The two banks of probes

Each probe works independently in a pulse echo mode. That is, the transducer that transmits the signal also receives that signal. The probes are held at a distance of 70mm from the material. This is to alleviate the possibility that they will be struck by the front end of the moving bar, remove the complications involved with the near field of the probe, and will be in the correct alignment to optimise the quality of the signals achieved from the product. A high pulse repetition rate leads to full coverage of the area to be inspected and the system is capable of detecting a 2mm defect because a smaller wavelength can increase the testing precision.

When the front end of the bar has passed beyond the inspection probes, the inspection system is 'enabled'. This results in a short length of bar at the extreme front end which has not been inspected (50mm - 100mm typically); this is known as "front end loss". There is, therefore, an untested region at the ends of the bar, which is necessary to suppress the alarm output from the inspection system, caused by distorted signals which occur when probes pick up the abrupt edge of the bar end. If any defects are encountered by the inspection system, fixed paint jets at a position beyond the actual Inspection Zone will subsequently mark the defective regions. The inspection is terminated prior to the tail end of the bar passing over the inspection probes and again suppressing the alarm output similar the front end. This again results in an undetected region at the tail end of the bar length known as back end loss. Bars, for which the line control logic has been alerted to the defective nature of the product, are tracked through the line and subsequently sorted into good or defective groups. The defective bars are then manually re-inspected to qualify and define the nature of the defect.

1.2.5 Single Transmitter Multi Receivers System

The above system can be amended to process the received transmission using several of the probes. That is a single transmitter with multiple receivers. This idea is viable because of the divergence of the ultrasonic wave as it is transmitted. When an ultrasonic probe is fired, the pulse of ultrasound is transmitted through the water coupling into the steel billet, and is reflected off the back wall of the steel (pulse/echo). Figure 1.5 shows the beam diverges when transmitting. The signal is received back at the probe is only a small proportion of the total reflected signals.

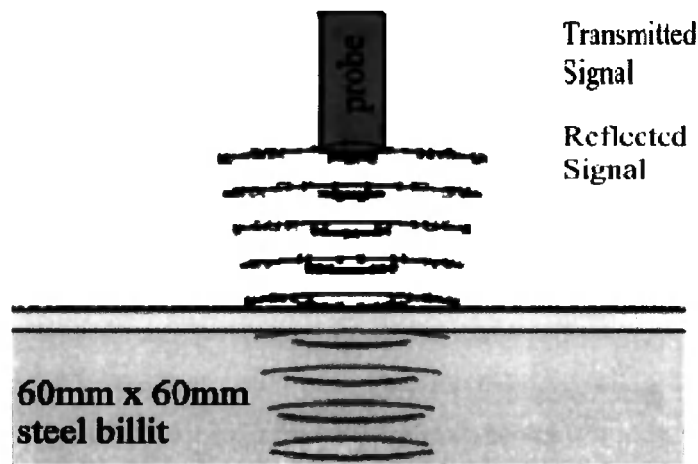


Figure 1. 5 Divergence of Pulse/Echo Signal

The remit of the project is to investigate and develop the latent potential within the present system. The belief is that the system is not being used to its full potential in that only one probe is in use at any time. If more than one or all probes could be used simultaneously, the system would have greater efficiency. This could lead theoretically to a faster throughput of material or a greater sensitivity of defect detection, and higher reliability of defect detection.

1.3 Previous Research

The previous research has investigated the potential within a current multi-probe ultrasonic detection system installed at a steel mill. Extensive laboratory experiments were carried out using the transducer array geometry, to extract additional information from passive probes. The apparatus was set up as shown in Figure 1.6.

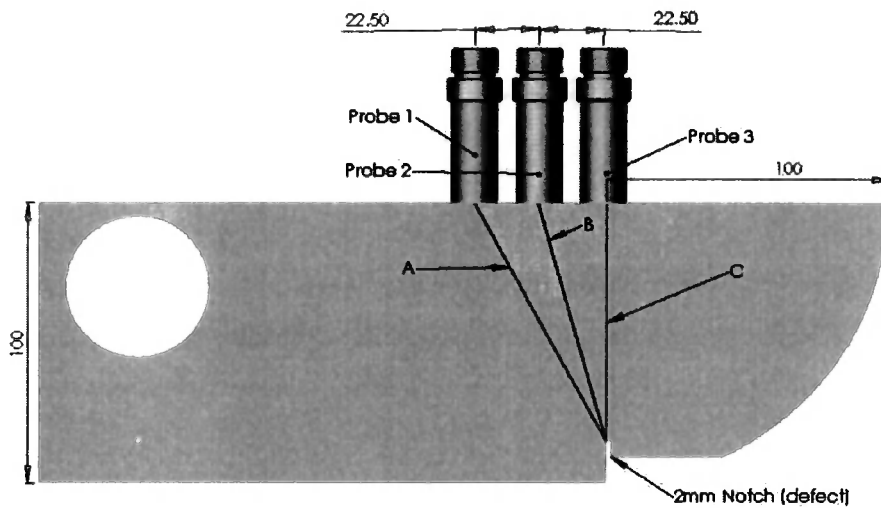


Figure 1. 6 Normal Probe Diffraction Experiment Setup

Figure 1.7 shows the increase of detection ability using the standard single-probe-multi-receiver (SPMR) system over the conventional single-probe-single-receiver (SPSR) system. It shows that the NPD system starts detecting the defect at a lateral distance of 41mm from the defect whereas the pulse-echo probe needs to be within a range of 15mm. The physical principle behind this system uses diffracted waves from the edge of the defects and thus it is particularly effective for the increased detection and sizing of centre-line defects. This technique is defined as Normal Probe Diffraction (NPD), which has been successfully applied offline on a V1 calibration block and a single billet, but has not yet been applied for real-time control.

Experiments show that the defect detection range can be increased by collecting the diffracted pulse on all the neighbouring probes. This is due to the defect being detected several times per pulse. The research project involves developing a real-time laboratory based prototype which can detect defects using two methods: the standard single probe pulse echo technique and NPD, and testing the system on a V1 calibration block and a steel billet. In this project, the transmitting and receiving electronics are developed to enable the NPD technique to be applied in real-time[10].

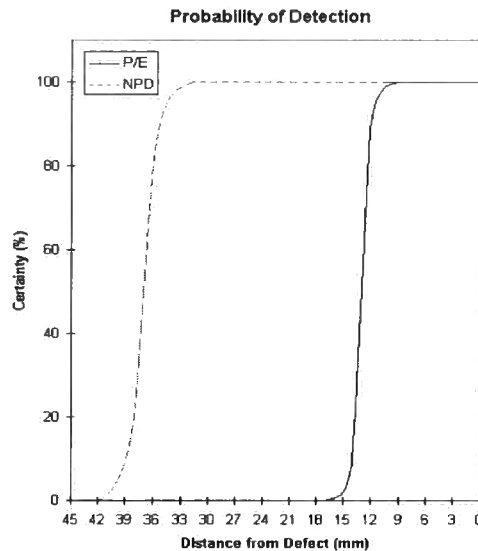


Figure 1. 7 Comparison of Probability of Detection for NPD and Pulse-Echo

A coarse grain steel billet was tested based on the previous research discussed above. A slice was cut as a pseudo back wall and a 2mm diameter hole was drilled as a pseudo defect, both were 30mm from the upper surface. The slice could be tested while the hole could not. Therefore, further research has been made in both the field of ultrasonic testing and the digital signal processing technique to improve the probability of detection.

1.4 Project Aims

- Study the principles of ultrasonic defect detection including NPD
- Investigate large grain steel billets using off-line NPD, found needed better S/N ratio
- Simulate the NPD system to investigate methods of improving S/N ratio and aid in finding the defect
- Use simulation as a base for the real-time DSP rapid prototyping system.

Real-time DSP System

In this project, a rapid Digital Signal Processing (DSP) prototype for the necessary real-time system is modelled and simulated to implement the NPD technique. TMSC320C6713 DSK and AED_330 analog expansion daughter card were used to process digital signals in real-time to gain a fast Digital to Analogue conversion speed

for the desired high frequency pulse signal. The desired real-time system was to help increase the probability of detection of defects in steel billets and produce a low-cost system solution for ultrasonic billet inspection in the steel industry.

A good real-time implementation should be reliable, low power consuming, compact and always runs in real-time[11]. Sufficient amount of instructions per second and quick enough transport speed must be considered and calculated during the design procedure to meet the requirement of short delays between inputs and outputs in real-time implementation.

This system uses general purpose digital signal processors for solving problems in real-time, and particularly focuses on using the Texas Instruments (TI) TMS320C6713 DSK (Digital Signal Processing Starter Kit) with the C6713 kernel floating point processor to implement programs written in assembly and C. The TI C6713 DSK is for general real-time signal processing applications. The main applications taking place in this project are digital filter design using different DSP algorithms. These filters are characterized and applied on the received data. TI Hardware/software development tools (Code Composer Studio and DSP/BIOS) provide I/O channels for data exchange with Matlab in real-time.

System testing uses MATLAB and Simulink including several toolboxes. The MATLAB Embedded Target for TI C6000 DSP enables the rapid prototyping of real-time software for C6713 floating-point processor and generates efficient code for the processor directly from a Simulink model using MATLAB Real-Time Workshop. The generated code is readable and editable, and the code profiler identifies regions of generated code that may benefit from manual optimization. The Embedded Target for TI C6000 DSP automates the creation of Link for the Code Composer Studio project, provides board support for the C6713 DSK board, invokes Link for Code Composer Studio to create a DSP executable and downloads the executable to the DSK board for real-time algorithm evaluation. It also employs the link to enable interactive debugging and systematic testing of the DSP programs.

CHAPTER 2

Ultrasonic Testing

This chapter gives an overview of the basics of ultrasonic testing techniques, classification of ultrasonic probes and their applications, the main defect that occurs in the steel industry and the existing ultrasonic testing system and method used to detect them.

Ultrasonic detection techniques have developed at a tremendous rate to fulfil the requirement for high quality defect free material in many industrial and research applications. The basic method is the Conventional Pulse-Echo Method. As dictated by its name, the Pulse-Echo method use an array of probes in which each probe pulses and receives sequentially. This method was replaced gradually by some new techniques based on Time-of-Flight Diffraction (TOFD), because these new methods collect extra information from diffracted signal which was previously discarded by the pulse-echo detection.

When Ultrasound is incident at a linear discontinuity such as a crack, diffraction takes place at its extremities in addition to the normal reflected wave. This diffracted energy is emitted over a wide angular range and is assumed to originate at the extremities of the crack. This is in marked contrast with conventional ultrasonic detection which relies on the amount of energy reflected by discontinuities.

The TOFD technique, which is an off-line method, uses angled beam probes to pick up the diffracted signal, while the NPD technique can get the same result with normal probes by using multi-receivers, thus enabling the method to be implemented in real-time on a production line.

Both the TOFD and NPD ultrasonic technique relies on the diffraction of ultrasonic energies from 'corners' and 'ends' of internal structures in a component under test. This is in contrast to the conventional pulse echo method which relies on directly reflected signals from internal structures and only can test the depth of the defect, while the

former two methods can detect the defect in 2D and could be improved to 3D detection by using an array of probes.

2.1 Ultrasonic Transducers

Ultrasonic transducers are built around piezoelectric ceramics that vibrate at ultrasonic frequencies when a voltage is applied, and generate voltages when vibrated. The transducer is one of the most critical components of any ultrasonic system. A literature search has been carried out to investigate the correlation between transducer properties, defect size and depths, and the signal to noise ratio during ultrasonic inspection of steel with coarse grain structure. However practical test have been made to select the appropriate transducer for the application.

2.1.1 Transducer Parameters

2.1.1.1 Resolution and Sensitivity

Ultrasonic transducers perform according to two main parameters: resolution and sensitivity. The resolution of a particular transducer is denoted by its ability to discern between two discontinuities that are on top of one another. A transducer with sufficient resolution will stop ringing, or vibrating, from the first discontinuity before receiving the echo from the second discontinuity. If the ceramic does not stop ringing before the second echo is received, the second echo is masked from the test system. Sensitivity of an ultrasonic transducer refers to the ability to detect small discontinuities. Reference blocks with standard sized defects are used to gauge the sensitivity of a particular transducer.

2.1.1.2 Impedance

Impedance (Z) is the resistance of a circuit to alternating current, such as an audio signal. Technically, impedance is the total opposition (including resistance and reactance) that a circuit has to passing alternating current. A high impedance circuit tends to have high voltage and low current. A low impedance circuit tends to have relatively low voltage and high current.

Figure 2.1 shows that the measured impedance of the transducer at the frequency of 5MHz is 7.5 ohm (phase 10.7°).

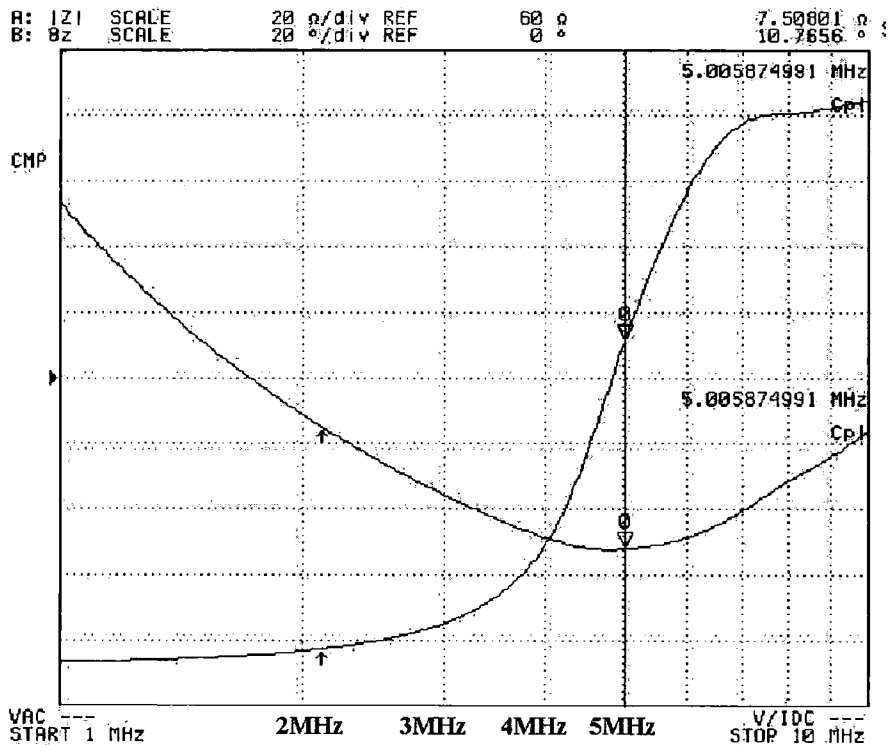


Figure 2.1 5MHz Transducer Parameter Measurement

2.1.1.3 Frequency

The frequency of the ultrasonic transducer is chosen based on several factors including detectable defect size, depth of penetration, and grain size of the material. Materials made up of fine grained material, such as metals, permit deep penetration by ultrasonic waves of all frequencies. However, coarse grained materials, including many plastics, scatter high frequency ultrasonic waves. The higher the frequency, the smaller defects the system will detect, but the depth of penetration decreases. So a trade-off has to be made between the required sensitivity and depth of penetration.

2.1.2 Transducer catalogue

Ultrasonic transducers generate and detect ultrasonic waves. Piezoelectric ceramics within ultrasonic transducers are excited by an extremely short electrical discharge, typically between 50 and 1000 Volts to produce the ultrasonic wave. The same element

on the other hand generates an electrical signal when it receives an ultrasonic signal thus causing it to oscillate. The probe is coupled to the surface of the test object with a liquid or coupling paste so that the sound waves from the probe are able to be transmitted into the test object.

Ultrasonic transducers work almost exclusively according to the piezoelectric effect and are classified into four fundamental types: Straight beam transducers, Angle beam transducers, Delay line transducers and Twin crystal transducers[12]. Transducers also differ with respect to the size of the active piezoelectric elements, their frequency, bandwidth and the basic design. The selection of bandwidth is essential for achieving certain test results; a narrow bandwidth for highly sensitive testing, or broad banded for high resolution testing.

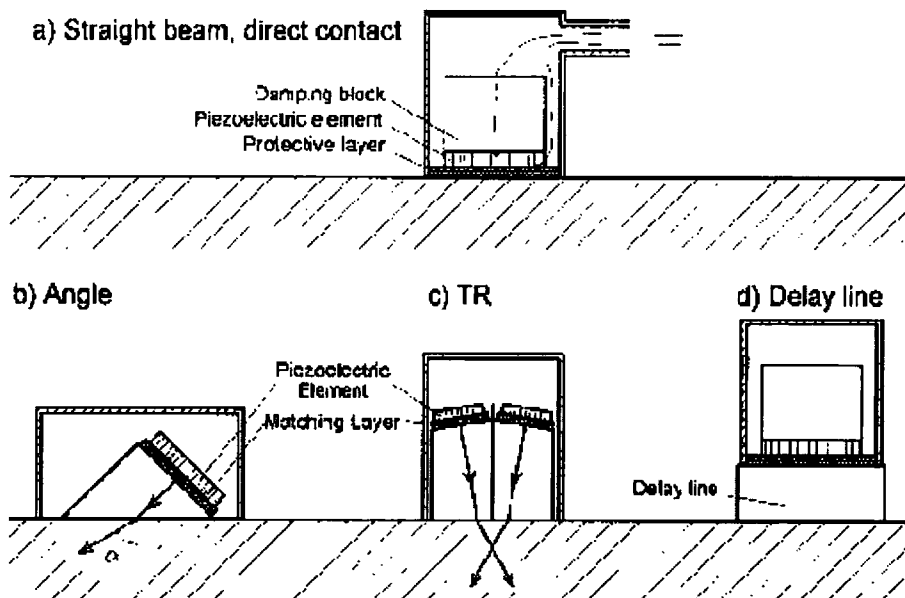


Figure 2. 2 Four Fundamental Transducer Types

2.1.2.1 Straight-Beam Probe

Probes whose beams are normal to the surface are called straight-beam probes as shown in Figure 2.2(a). Most standard straight-beam probes transmit and receive longitudinal waves. There is a large selection of straight-beam probes in various sizes and range from frequencies of approximately 0.5 MHz to 25 MHz. Distances of over 10 inch can be obtained thus enabling large test objects to be tested. The wide range enables individual matching of probe characteristics to every test task, even under difficult testing conditions.

2.1.2.2 Angle-Beam Probe

Angle beam transducers are single element transducers used with a wedge to introduce a refracted transverse wave or longitudinal wave into a test piece. An angle-beam probe is shown in Figure 2.2(b). Most standard angle-beam probes transmit and receive, due to technical reasons. Angle-beam probes do not transmit longitudinal waves. Due to the fact that steel is tested in most applications, the angle-beam probes are designed so that suitable angles of incidence are produced in steel. Angle-beam probes do not have such a wide selection as straight-beam probes. This is primarily due to the fact that high frequency transverse waves in non-alloyed fine grain steels are subjected to high attenuation. As the sound energy of the waves travels through the material it is so strongly absorbed and scattered that only relatively small test objects can be tested with sufficient sensitivity.

2.1.2.3 Twin-crystal Probe

A twin crystal probe is a single transducer containing two piezoelectric elements, one for transmitting and one for receiving. The crystal assemblies are separated by some form of an acoustic barrier (usually cork) in order to prevent cross noise. Figure 2.2 (c) shows a Twin-crystal Probe.

2.1.2.4 Delay-line Probe

The construction of the Delay-line probe is shown in Figure 2.2(d). Basically it is a straight beam probe with an additional delay-line made of plastics with low ultrasonic absorption. The time delay avoids echoes from defects close to the surface appear within the dead zones of the ultrasonic defect detector, which are caused by the high voltage excitation pulses[3]. Dead zone refers to the non-testable area immediately beneath the surface. Use of delay-line probes is a simple measure to have an excellent near field resolution.

2.1.3 Transducer for Steel Inspection

The type of transducer used is dictated to by the conditions in which they are to operate. In the inspection of steel, consideration must be given to the metallurgical structure; grain type, size and distribution all influence the propagation of the ultrasonic sound

beam. Large or directionally oriented grains tend to scatter and otherwise absorb the ultrasonic energy, to a greater extent than fine, randomly oriented grains. The combination of these two effects, that is scattering and absorption, is termed attenuation. To minimise this attenuation it is therefore necessary to use a probe with the optimum frequency for steel, generally between 2 and 5 MHz. The probe chosen for the project was also used in water and therefore required a special immersion type transducer and cables.

2.2 Scan Types

There are several ways to look at ultrasonic test data ranging from TOF to surface scan. The most common scans are referred to as A-, B- and C-scans.

2.2.1 A-scan

The most primitive method to analyze the reflected ultrasonic signals is time-of-flight (TOF) scan, or A-Scan, which displays voltage amplitude versus depth. The depth is calculated by multiplying the speed of sound through the medium by the time of flight.

Defects that are closer to the ultrasonic transducer are received sooner than those further away from the transducer. The x-axis on the A-scan is not typically units of time, but is converted to distance. This conversion is accomplished by measuring, or looking up, the speed of sound through the material that the ultrasonic wave is travelling and performing the conversion. Although there are a few exceptions, the speed of sound through a material is governed largely by the density and elasticity of the material. For most materials, the nominal speed of sound within homogenous material is easy to research and find.

2.2.2 B-scan

B-scan is a two dimensional graphical presentation, in rectangular coordinates, in which the travel time of an ultrasonic pulse is represented as a displacement along one axis, and transducer movement is represented as a displacement along the other axis.

In other words, B-scan images the voltage peaks in the A-scan moving back-and-forth over time. This movement is caused by the varying thickness of the test object as the

transducer is moved over the surface. Put all of those A-scan images together and the result is a B-scan.

2.2.3 C-scan

C-scan is also a two dimensional graphical presentation, in which the defect echoes are displayed in a top view on the test surface. C-scans display x- and y-position, while the colour represents depth.

2.3 Test Methods

There are two operating modes for ultrasonic probes, pulse-echo and through-transmission. In pulse-echo mode, each ultrasonic transducer transmits a signal out and receives the echo. The reflected ultrasonic waves vibrate the piezoelectric crystal within the ultrasonic transducer and generate voltages that are measurable by data acquisition hardware. In through-transmission mode, two ultrasonic transducers are used; one transducer generates the pulse signal and the other receives the echo.

2.3.1 Pulse-echo Method

Sound reflections in the audio range are called echoes. The name of the method came into being which is applied in most areas of application for material testing with ultrasonics is the Pulse Echo Method as shown in Figure 2.3[13].

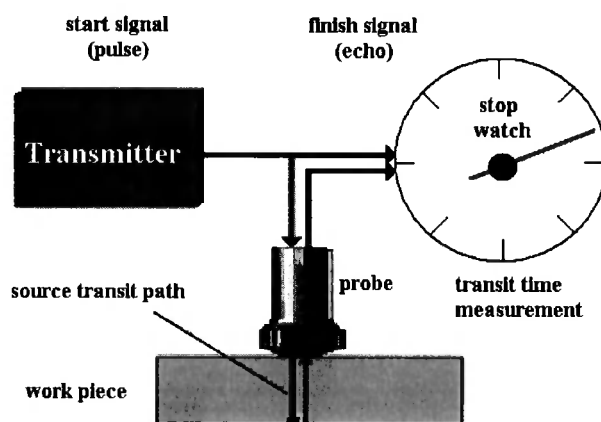


Figure 2. 3 Block diagram: Pulse Echo Method

The time measurement starts with the electrical transmission pulse, the initial pulse. This is an extremely short electrical discharge which triggers a sound pulse at the probe crystal. This pulse travels through the material and is reflected by a discontinuity or the opposing wall and returns back to the probe. The received oscillations are converted into an electrical pulse which stops the time measurement. The distance to the reflector can now be instantly determined by the following formula:

$$s = \frac{c * t}{2} \dots\dots\dots (2.1)$$

Where s is the length of the sound path in mm, c is sound velocity in km/s and t is the time of flight in ms.

The problem with the pulse-echo technique is that it is based on the assumption that echoes come from planar features within normal angle of incidence to give a specular reflection back to the transducer. Clearly it is quite rare for defects to be exactly normal to the beam as would be required for a perfectly smooth large specular reflector.

2.3.2 TOFD Method

2.3.2.1 Reflection and Diffraction

When ultrasound is incident at linear discontinuity such as a crack, diffraction takes place at its extremities in addition to the normal reflected wave. This diffracted energy is emitted over a wide angular range and is assumed to originate at the extremities of the defect. Figure 2.4 shows both reflection and diffraction of a crack. This is in marked contrast with conventional pulse echo method, which relies on the amount of energy reflected by defects.

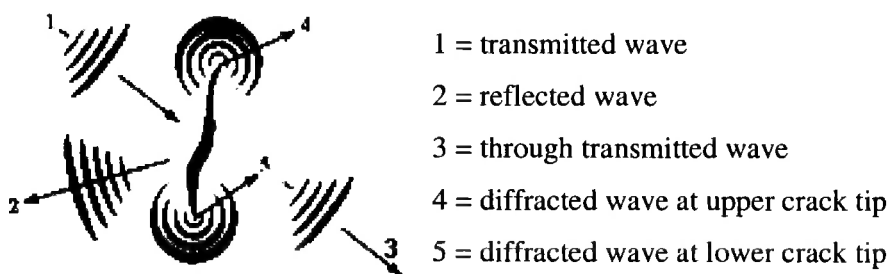


Figure 2. 4 Reflection and Diffraction

2.3.2.2 TOFD Technique

The TOFD technique uses a single probe pair in a transmitter-receiver arrangement. Usually longitudinal probes are applied with an angle of incidence range of 45° to 70° . The received data consist of signals transmitted between transmitter and receiver and diffracted signals from defects. In addition to energies diffracted by defects, the TOFD method will also detect a surface wave travelling directly between the probes and also a back wall echo from energies that reach the back of the tested object without interference from defects. Because the technique relies on detection of the forward scattered diffracted signals originating at the defect edges, precise measurement of defect size, location, and orientation is possible, and inspection reliability improves. Point reflectors are precisely determined by using geometric considerations, beam angles, and the appropriate sound propagation velocity.

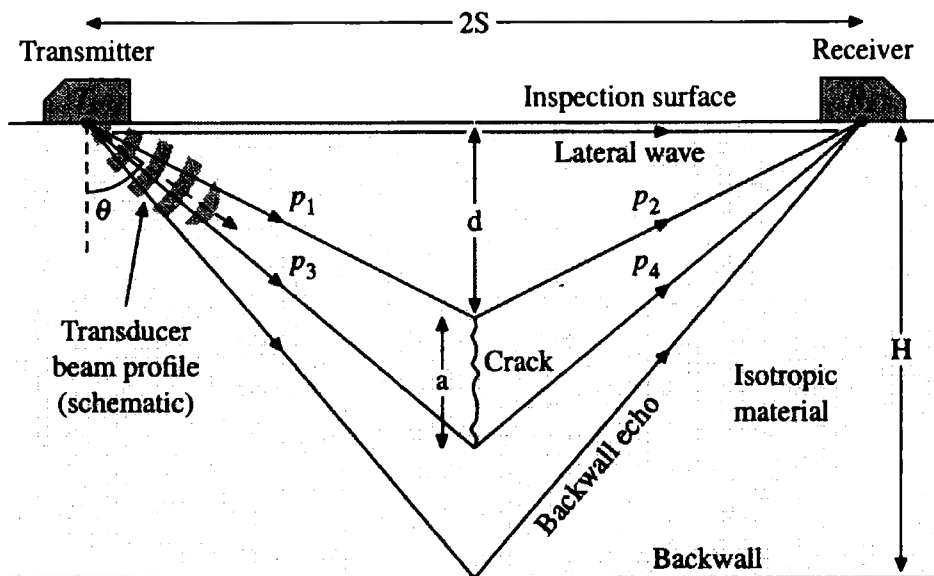


Figure 2. 5 TOFD wave paths

- $2S$ = Distance between probes
- a = Length of defect
- θ = Refracted beam angle in material
- H = Material thickness
- d = Depth of defect

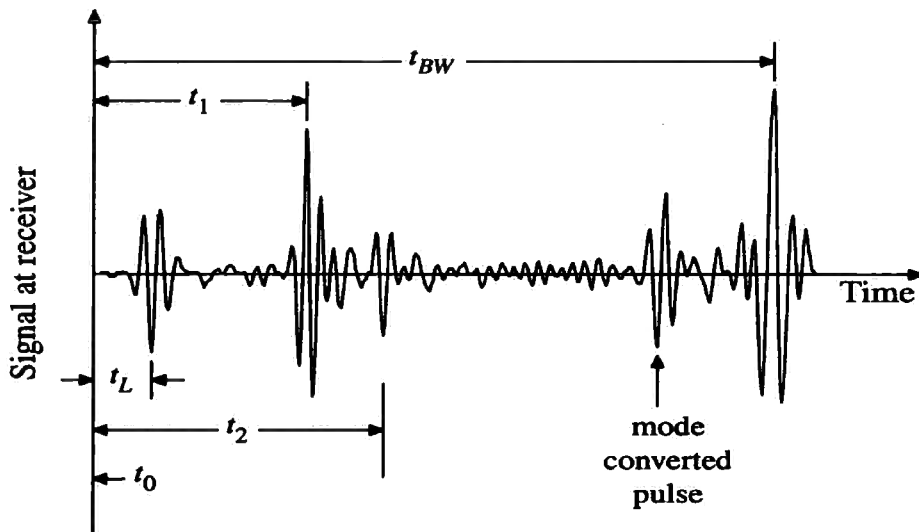


Figure 2. 6 TOFD A-scan Schematic

2.3.2.3 Defect Location and Sizing

Location of the crack tips is determined from the time differences between the lateral wave and the pulses that follow the paths;

$$P_1 + P_2 \text{ or } P_3 + P_4 \dots\dots\dots(2.2)$$

These paths correspond to t_1 (top of crack) and t_2 (crack bottom) respectively. Figure 2.5 shows the four wave paths and Figure 2.6 shows the detection of four main signals and a mode converted signal from the top of the crack.

t_L : the surface or lateral signal which travels along the surface of the component and has the shortest arrival time

$$t_L = \frac{2S}{C} \dots\dots\dots (2.3)$$

t_1 : the top tip of the defect

$$t_1 = \frac{2\sqrt{S^2 + d^2}}{C} \dots\dots\dots (2.4)$$

t_2 : the bottom tip of the defect

$$t_2 = \frac{2\sqrt{S^2 + (d+a)^2}}{C} \dots\dots\dots (2.5)$$

t_{BW} : the back-wall echo, which has the longest transit time

$$t_{BW} = \frac{2\sqrt{S^2 + H^2}}{C} \dots\dots\dots (2.6)$$

Rearranging the equations,

$$d = \frac{1}{2}\sqrt{C^2 t_1^2 - 4S^2} \dots\dots\dots (2.7)$$

Length of defect (a)

$$a = \frac{1}{2}\sqrt{C^2 t_2^2 - 4S^2} - d \dots\dots\dots (2.8)$$

C is taken to be the velocity of the bulk compression wave.

Equation 2.7 and 2.8 are used generally in the analysis of TOFD data and are thus of basic importance. The assumption that the defect is positioned symmetrically between the probes introduces an error but this can be arranged to have little effect on the accuracy of the estimated defect depth[14]. By use of today's advanced computer techniques it is possible to evaluate signals very rapidly. That makes it possible to perform scans with a speed of hundreds of millimetres per second. In practice speed is limited only by the mechanic.

2.4 Normal Probe Diffraction Technique

Normal Probe Diffraction (NPD) Technique firstly debuted in 2003 by Paul C. Snowdon, Sherri Johnstone and Stephen Dewey[15]. Experiments were conducted to investigate that the probability of detection can be increased by using passive normal incidence transducers to pick up diffraction signal. On one hand, NPD technique makes use of the diffraction signal previously discarded by the conventional pulse-echo ultrasonic detection system for the on-line steel inspection. On the other hand, compared to TOFD, NPD does not require special beam-angle probes thus decreases the cost of testing.

2.4.1 Experiment Equipments

2.4.1.1 Socomate USPC 3100 PC based ultrasonic flaw detector

The USPC is a Plug & Play windows based PC Card flaw detector with two transmit/receive channel. It is a real time DSP system for in-line ultrasonic inspection and is supplied with the application software written in Labview. Various options are available for A-Scan, B-Scan & C-Scan Acquisition.

2.4.1.2 Hewlett Packard Infinium oscilloscope

The 2-channel oscilloscope has a window-based graphical interface and an integrated 3.5" floppy disc drive for data transfer. The bandwidth of the oscilloscope is 500MHz. The acquisition filter was set to a 16 average filter to improve the signal to noise ratio and signal stability. This was the optimum setting for the oscilloscope because a greater numerical average would affect the refresh rate and sample length at the chosen sampling frequency of 50MHz. The 50MHz sampling frequency is above the Nyquist sampling frequency to avoid signal aliasing problems[16]. The 5kHz system slowest repeat rate was selected to be the pulse repetition frequency to facilitate signal decay and reduce spurious echoes.

2.4.1.3 V1 Calibration Block

The reference piece used for calibration is called the Calibration Block, or Standard Calibration Block, if the block used is standardized. The Standard Calibration Block 1, also simply referred to as V1 block (according to BS 2704 - A2), which is shown in Figure 1.6, has a thickness x width x length of 25x100x300mm and is made of low-alloyed fine grained steel so that it can be used for nearly all types of calibration when similar steels are to be tested. The 2 mm-wide notch, 85 mm from the inspection surface was chosen as a pseudo defect.

2.4.1.4 Ultrasonic couplant Gel (Ultrigel II from Diagnostic Sonar Ltd)

Ultrasonic Couplant Gel is necessary because sound energy at the ultrasonic frequencies typically used for non-destructive testing is not effectively transmitted through air. Even an extremely thin air gap between the transducer and the test piece will prevent efficient

sound energy transmission and make conventional testing impossible. The general purpose propylene glycol based couplant used in these experiment was chosen because it has good surface wetting properties, thus will not corrode or otherwise attack materials, and it is easily washed off by water and chemically non-reactive and does not evaporate quickly at room temperature. Propylene glycol has an acoustic impedance of $1.61 \times 10^5 \text{ gm} - \text{cm}^2 / \text{sec}$ which is close to that of $1.48 \times 10^5 \text{ gm} - \text{cm}^2 / \text{sec}$ for water.

2.4.2 Experimental Setup

The experiment equipments were set up as shown in Figure 1.6. Three straight-beam probes placed in a linear arrangement, normal and in contact with the upper surface of the V1 standard calibration block. The probes were used in a single transmitter with double receiver in alternate positions. Receiver probes were located at distances of 22.5 mm and 45 mm from the transmitter. This experimental setup was used to reveal the clearest interpretation of the received reflection and diffraction signals.

2.4.3 Experiments with V1 calibration

In experiments, each of the three probes was excited in turn using the USPC 3100 in A-scan pulse-echo mode. The received signals were displayed on the oscilloscope and transferred digitally to the PC for further processing and analysis using MATLAB. The signal velocity measured using probe 1 in pulse-echo mode[17] within the V1 block is $5900 \text{ms}^{-1} \pm 1\%$.

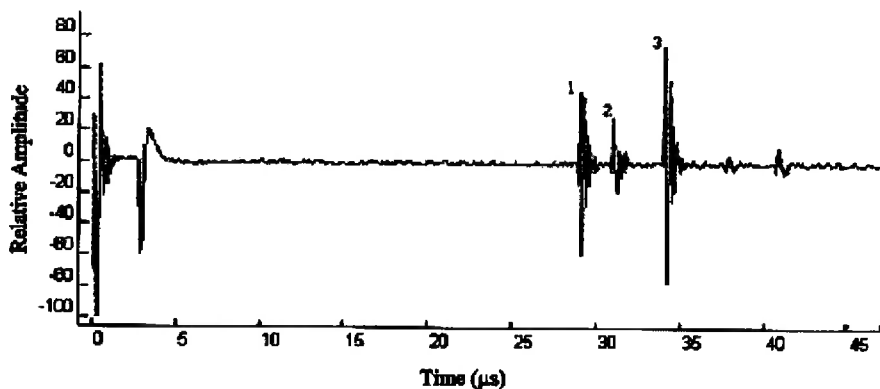
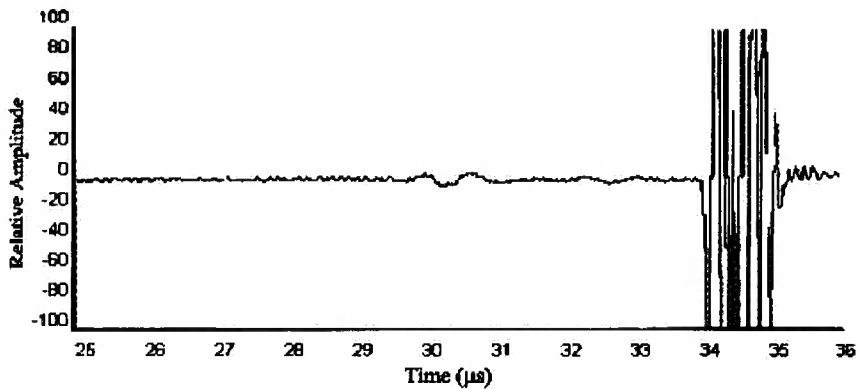
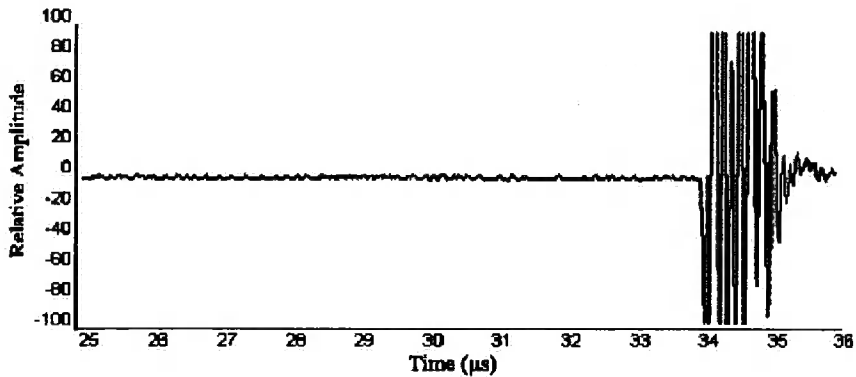


Figure 2. 7 (a) Pulse-echo A-scan form probe 1



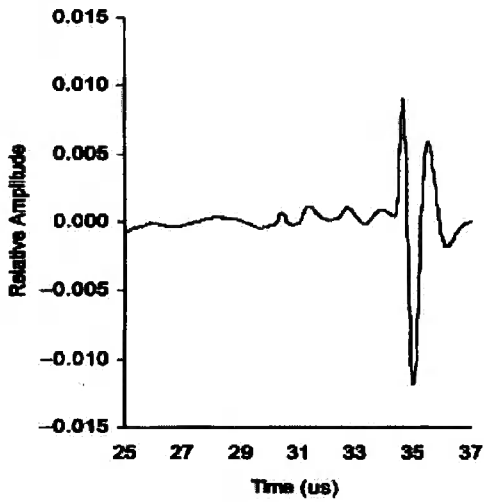
(b) Pulse-echo A-scan from probe 2



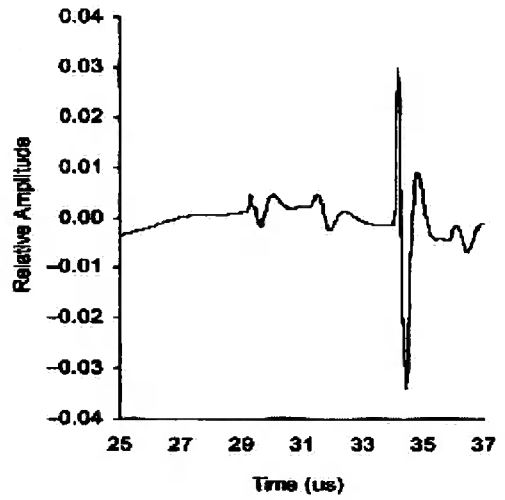
(c) Pulse-echo A-scan from probe 3

Figure 2.7 (a) (b) (c) shows the pulse-echo A-scans from probe 1, probe 2 and probe 3 respectively. The A-scans indicate that the 2mm notch is undetectable at probe 1 and distinguishable at probe 2 at a 50dB gain. In the A-scan from probe 3, point 1 is the notch, point 2 is the 91mm step back wall and point 3 is the 100 mm back wall. This verifies that in the following transmitter-receiver mode experiment, the signals received by two receivers are non-specular reflection or diffraction signals rather than directional reflection signals.

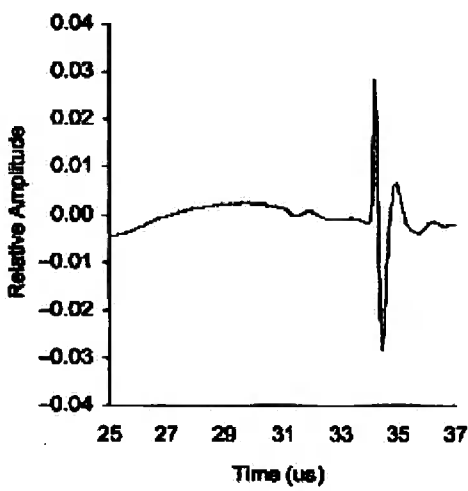
Figure 2.8 (a) to (e) display the signal from the defect and first back wall echo as after the back wall, it is impossible to distinguish between signals due to multiple internal reflections. Each probe was excited in turn and the left two probes acted as passive receivers and acquired diffracted signal.



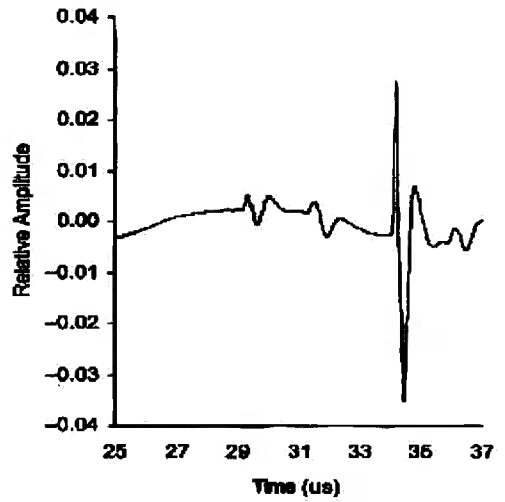
(a) Transmitter-Probe 3/Receiver-Probe 1



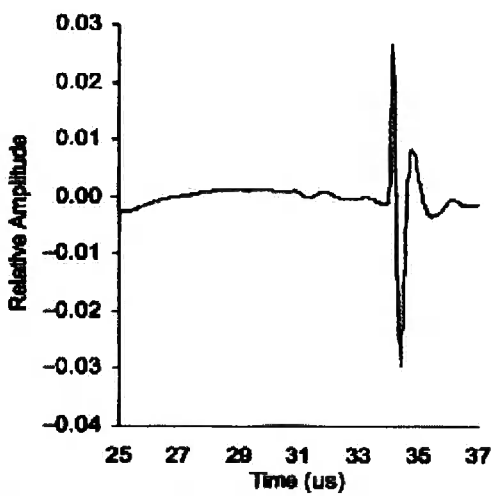
(b) Transmitter-Probe 3/Receiver-Probe 2



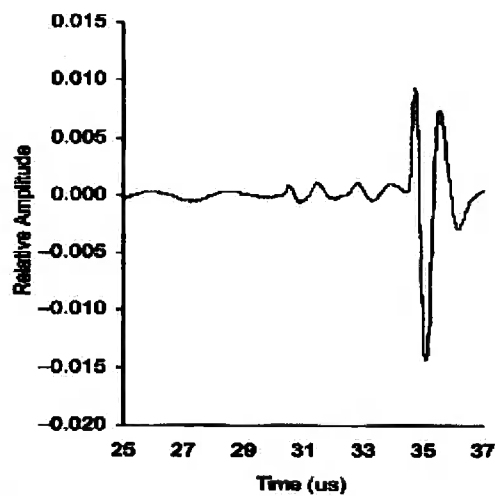
(c) Transmitter-Probe 2/Receiver-Probe 1



(d) Transmitter-Probe 2/Receiver-Probe 3



(e) Transmitter-Probe 1/Receiver-Probe 2



(f) Transmitter-Probe 1/Receiver-Probe 3

Figure 2. 8 Transmitter-Receiver Mode Test Result

2.4.4 Experiment Conclusion

The experiment results show that passive probes setup next to the transmitter can detect the signals correspond to the shortest signal paths via defects that are outside the normal detection range of the transmitting probe shown in Figure 1.6. The NPD technique was therefore proved to be able to improve the potential of the POD within a static array system. Three mechanisms were considered to explain the result of the experiments: directional reflection, electromagnetic coupling and diffraction[10]. A PC based DSP system and control software were to be designed and built based on this technique to carry out ultrasonic testing in real-time in this project. The architecture of this system is represented in chapter 3.

2.5 PC-Based Ultrasonic Test System

The performance of the system as a whole is of great importance. Variations in instrument characteristics and settings as well as material properties and coupling conditions play a major role in system performance. The hardware and software components must interact effectively for even the simplest ultrasonic test system to work properly. When assembling the custom ultrasonic test system, there are several factors to consider for each component of the system, including how well the components interact with one another. The Ultrasonic Transducer section describes each component of the test system in detail as well as the important features required for ultrasonic testing.

Several PC-based and external components make up each ultrasonic test system. Each of these components has a unique set of features and considerations. Some considerations are limited to the component itself while others depend on the various components in the system. The features/issues of these components are considered to build the ultrasonic test system to implement the NPD algorithm.

2.5.1 Assembling an Ultrasonic Test System

Ultrasonic test systems can take several forms, but the most common for automated test is immersion testing. The offline experiments carried out in previous research of this project use an immersion tank filled with water to have good acoustical impedance

matching between the couplant and the tested object and free range over the entire surface of the object.

The test system uses one or more ultrasonic transducers, which are moved over the surface of the tested object. As the transducer is moved over the surface, it is pulsed and receives echoes from various surfaces. This process is repeated many times a second. There are several pieces of the test system that must work together to get expected results. The following list includes the steps, and the accompanying hardware and software pieces, required to get one pulse and the subsequent echoes:

2.5.1.1 Pulsar/Receiver

This device generates the high voltage pulse that is required by the ultrasonic transducer. The analogue signal from the ultrasonic transducer is amplified and filtered before it is sent back to the digitizer within the PC.

2.5.1.2 Ultrasonic Transducer

The transducer is pulsed, sending out an ultrasonic wave. The subsequent echoes generate a voltage in the transducer, which is sent back to the pulser/receiver.

2.5.1.3 Digitizer

The waveform sent from the pulser/receiver is converted from voltage to bits using an analogue-to-digital converter.

2.5.1.4 Application software

The user interacts with the application software to set up the test and presentation parameters. Data from the digitizer is processed, analyzed, and presented according to the user-defined parameters

2.5.1.5 Communication

The pulser/receiver operation parameters, such as pulse energy, pulse damping, and bandpass filtering, are set. The communication path is typically RS-232 or USB.

2.5.2 Pulsar/Receiver (P/R)

These devices provide the high-voltage pulse required by the ultrasonic transducer as well as signal conditioning before the analogue signal is passed to the digitizer. For use within an automated test system, the P/R should be computer programmable via a standard PC bus such as RS-232 or USB. The USPC 3100 flaw detector uses a RS-232 while the TI C6713DSK uses a USB port. The devices are typically programmed once at the beginning of the test to set the pulse voltage level, pulse repetition frequency, damping, band pass filtering settings, and several other parameters. After these parameters are set, these devices are passive and do not send any information back to the PC during operation. Digitizer and P/R must operate as one tightly-timed unit during the test to ensure accuracy of results and brevity of test time.

2.5.3 Digitiser

This part of the test system converts the echo waveforms returned by the ultrasonic transducer into digital information using an analogue-to-digital converter (ADC). Some factors such as sample rate, bandwidth, vertical resolution, triggering features, memory, and bus type need to be considered for digitiser selection.

For applications that require well-shaped waveforms in the time-domain, such as research, a sample rate 10 times higher than the resonant frequency of the transducers is desirable. In these applications, a transducer that has a resonant frequency of 5 MHz requires 50 MHz to accurately represent the shape of the signal. In this project accurate time-domain waveform is required, so 50MHz sample rate is used. However, for applications that require less amplitude and echo-timing accuracy, 4~5 times the resonant frequency is acceptable.

Vertical resolution establishes the minimum voltage step size within a voltage range. 16-bits is equivalent to 65,536 (2^{16}) steps. When a 16-bit ADC is applied to a voltage range of 0-1 Volts (AIC23 codec ADC of TI C6713 DSK board), the minimum voltage step size is 15.3 μ V ($1V / 65,536$). However, when a 12-bit ADC is applied to a voltage range of 2V (THS1230 ADC on the AED daughter card), the minimum voltage step size is 0.49 mV ($2V / 4096$). In ultrasonics, the voltage amplitude is proportional to the amount of energy echoed by the discontinuity or defect. The front face and back wall of the tested object generally reflect the most energy, while defects reflect much less. To see the energy reflected from small flaws, the signal from the transducer must be

amplified or the digitiser must have high resolution. Amplifying the signal to detect a small defect can cause the front surface and back surface reflection voltages to swing outside the voltage range of the digitizer. On the other hand, additional resolution permits the user to zoom in on small defects and not distort main surface reflections at the same time. High resolution also relaxes the amplification levels required by the P/R component.

Flexibility of internal or external timing is essential for ultrasonic test applications. A programmable trigger delay is also a useful feature for ultrasonic testing. In immersion testing, the ultrasonic wave must travel through a significant distance of water before arriving at the tested object. If this distance is known, a trigger delay can be implemented to minimise the amount unnecessary data that is recorded and stored.

Because of the high frequencies associated with ultrasonic test, the amounts of collected data can be staggering. This data can be handled in many ways depending on the computer bus being used and the data collection rate. For instance, the PCI bus can realistically handle 80 MB/s (or 40 MSample/s at 16-bit) of continuous data throughput to PC memory. As this application requires more than 40 MSample/s sample rate, onboard device memory must be a consideration. In either case, the speed at which the data can be transferred back to permanent PC storage, such as a hard drive, after device onboard memory is full, must be a consideration. If data is transferred over a slow bus, such as USB 1.0 at 10 MB/s, the amount of time required to transfer data can easily double or triple the amount of time required for testing the object.

There is a trade-off between resolution, speed, channel count, data throughput, and cost. However, as ADC technology, PC memory, and data transfer rates evolve, many of these trade-offs have become or will become insignificant with respect to cost.

2.5.4 Switching

For ultrasound applications that have one digitiser and pulser/reciever for multiple ultrasonic sensors, switching is required to route the signals properly. This topology is common in applications that use arrays of sensors in order to create images. Arrays of ultrasonic sensors are common in non-destructive test applications since the sound energy can be steered in multiple directions without moving the sensor array. Multi-

transducer applications are also common when speed of test is an issue. Although switching was not yet employed in this project, its factors are introduced and discussed in the preparation for the further development of a multi channel system.

The three main factors to consider when choosing a switch for ultrasound applications are voltage rating, bandwidth, and switch topology. Common switch topologies include matrix and multiplexing. In large test systems, it is common to use a matrix topology which connects multiple instruments with multiple test points. In ultrasound applications it is more common to use the multiplexing topology, which connects one digitizer/pulser/receiver combination to multiple sensors.

Ultrasound pulser/receivers can create very high voltages. It was expected to be 250 volts in this project. The switching devices should have the clearances and creepages necessary to withstand these transient voltages, the appropriate amount of bandwidth compared to the ultrasonic transducer and also should be impedance matched to the rest of the system. Either the signal generated by the pulser or the echo returning from the transducer can be attenuated due to insufficient switch bandwidth. Proper impedance matching, typically 50 ohm, is required to minimize reflections and keep the signal clean.

2.5.5 Application Software

Ultrasonic test application software combines many types of I/O, analysis algorithms, and presentation techniques to form one software interface. The application software can be separated into three basic parts: acquisition/control, analysis, and presentation. Acquisition/control refers to the interface between the application software and the hardware that you have assembled for your ultrasonic application. For the most flexibility as test parameters change, make certain that a wide variety of hardware is supported by the application software.

Some of the required analysis algorithms for ultrasonic test are peak detection, computation of distances based on material properties, wave rectification, statistics, Fast-Fourier Transforms (FFT), level crossing, and filtering. Some of these algorithms are simple while others are complex and computationally intensive. Computationally

intensive algorithms included in the application software should be optimized, especially in ultrasonics applications where the presentation is graphically intensive.

Because of the wide variety of requirements in ultrasonic test, it is difficult to find turn-key software that utilizes the hardware components, specialized algorithms, and unique displays that one application requires. The alternative to turn-key software is application development software, or programming. Custom application development can integrate all of the hardware, analysis, and presentation components required by one application. The graphical application development environments of TI C6713 DSK allow a novice programmer to create advanced ultrasonic test programs easily and quickly.

2.6 Summary

In this chapter some of the theory and workings of ultrasonic testing have been investigated. Firstly, the parameters and main types of ultrasonic transducers were described. Then three commonly used scan types - A-scan, B-scan and C-scan were presented. The introductions of the conventional pulse-echo method and the popular TOFD method were also included to compare with the novel NPD testing method which was discussed in the succeeding section. It was concluded that NPD was a viable method of improving the probability of detection of defects in billets without the need for manual testing. Finally, the structure of a PC-based ultrasonic test system was introduced for the implementation of the NPD technique.

CHAPTER 3

NPD Algorithm

This chapter firstly reviews the mathematic fundamental for NPD algorithm and describes the NPD mathematical Model. NPD Simulink model was also built to be used for the rapid DSP prototype discussed in chapter 5. A static state Matlab GUI was designed to demonstrate the NPD testing procedure.

3.1 NPD Mathematical Model

In mathematics, an ellipse is a curve where the sum of the distances from any point on the curve to two fixed points is constant. An ellipse and the coefficients are shown in the left diagram in Figure 3.1. The two fixed points (F1 and F2) are called foci. The line which passes through the foci is called the major axis represented by $2a$. The line passing through the centre which is vertical to the major axis is called the minor axis represented by $2b$. An ellipse centred at the origin of an x - y coordinate system with its major axis along the x -axis is defined by equation 3.1:

$$\left(\frac{x}{a}\right)^2 + \left(\frac{y}{b}\right)^2 = 1 \quad \dots\dots\dots 3.1$$

The right diagram in Figure 4 shows an ellipse demonstrating the Pythagoras equation:

$$a^2 = b^2 + c^2 \quad \dots\dots\dots 3.2$$

as a special case of the non-parametric equation above ($x=0, y=\pm b$).

Another equation can be derived from the definition of ellipse:

$$r_1 + r_2 = 2 * a \quad \dots\dots\dots 3.3$$

Imagine that two probes are set separately on each focus of the ellipse, one transmitter and one receiver, the distance of $r_1 + r_2$ is the path of the transmitted ultrasound. The

NPD algorithm uses three probes – one transmitter and two receivers. The transmitter and each receiver can form an ellipse. By solving these two ellipse equations, both the vertical offset/defect depth (y_0) and the horizontal offset (x_0) can be calculated to locate the defect.

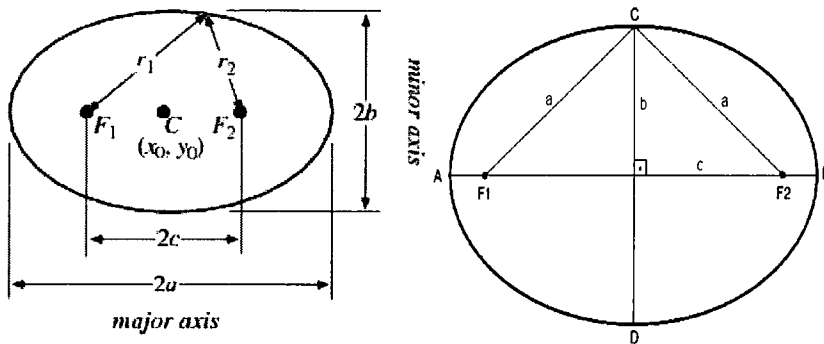


Figure3. 1 Ellipse

Table 3. 1 Transmit Distance and Time

Path	Distance (mm)	Time (us)
A	96.18	16.3
B	87.93	14.9
C	85	14.4
Backwall	100	16.95

Note: $d = v * t$; $v = 5900 \text{ m/s}$

Experiment setup was illustrated in previous chapters and shown in Figure 1.6. Table 3.1 gives out the tested distances of paths A, B and C in millimetres, with the theoretical time in microseconds calculated from the distances with the velocity of 5900m/s. The experiment setups and ellipse graphs for double probes and triple probes are shown separately in Figure 3.2 and Figure 3.3. The distance between each two probes is set to 22.5mm and the depth of the defect (notch) is 85mm (2).

For double probe NPD, probe 1 transmits signal and then receives the reflected signal, so the first path is 2 x B and forms a circle whose radius (R) is B. The second path is formed by transmitter probe 1 and receiver probe 2, making an ellipse whose major axis equals to B plus C. The signal received by probe 2 via this path is diffracted signal. In this case, both reflected signal and diffracted signal are acquired and analysed for defect location.

Similarly, for triple probes NPD, probe 1 only transmits signal and forms two ellipses with receiver probe 2 and receiver probe 3. The major axes for each are A plus B and A plus C separately.

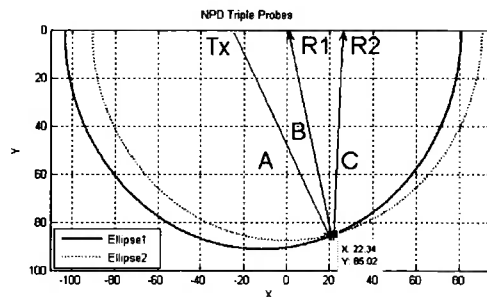
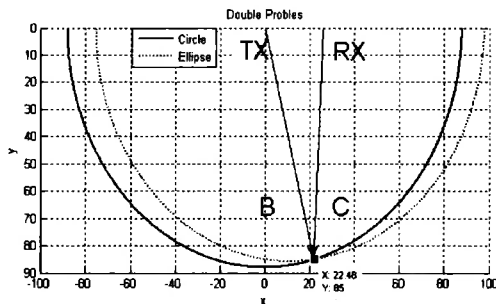
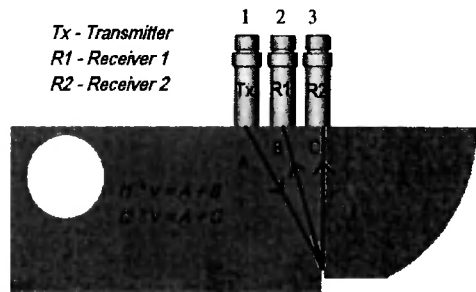
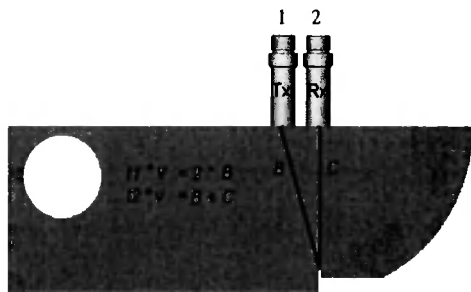


Figure3. 2 Double Probes NPD Scheme

Figure3. 3 Triple Probes NPD Scheme

Table 3. 2 Propagation Angles

Path	Propagation Angles
AC	27.90°
BC	14.83°

When probe 3 is set directly above the pseudo defect as shown in Figure 3.3, the angles formed by the path AC and BC in this static position are shown in Table 3.2. In this case, the defect is not centrally located. It is outside of the near-field (equation 1.5) and is located significantly outside the -20dB drop angle of 6° (equation 1.6) from the center of the transmitted beam, so that the detected signal is not reflected signal.

3.2 NPD Simulink Model

A SIMULINK Model was built to simulate the Pulse-echo, Double Probes NPD and Triple Probes NPD algorithms. The single probe pulse-echo method can only locate the depth of the defect by moving the probe along the upper surface of the calibration block, while the double probes and triple probes NPD algorithm can locate both the depth and the horizontal offset of the defect without changing the position of the probes. The

double probe and triple probe NPD algorithm share the same principle. Although the double probes NPD algorithm only need two probes, it requires more critical software programming including event timing and hardware interrupt (HWI) control. Figure 3.4 shows that by calculating the time delay of two transmit paths – t_1 and t_2 , the algorithm can locate the pseudo defect in 2 dimensions. In practice, the values of t_1 and t_2 can be tested by setting thresholds of received signal.

The algorithm was written in Matlab M file and included in Simulink embedded function block so that each block can be used in a rapid DSP prototype. This Rapid DSP prototype is introduced and evaluated in chapter 5 in detail. Theoretically, this procedure can save effort in building C program manually. Instead, by using the Simulink Embedded Target for TI C6713 DSK toolbox, Simulink block can be automatically convert into C code in a Code Composer Studio project, then compiled, downloaded and run on the target DSP board. In practice, software compatibility can be a big problem when using a high level language without knowing the fundamental architecture and programming processing of a system. Therefore, to build Code Composer Studio project manually using DSP/BIOS and the Chip Support Library is considered to be an optimum method in order to understand the performance of both hardware and software, although more time and effort is required.

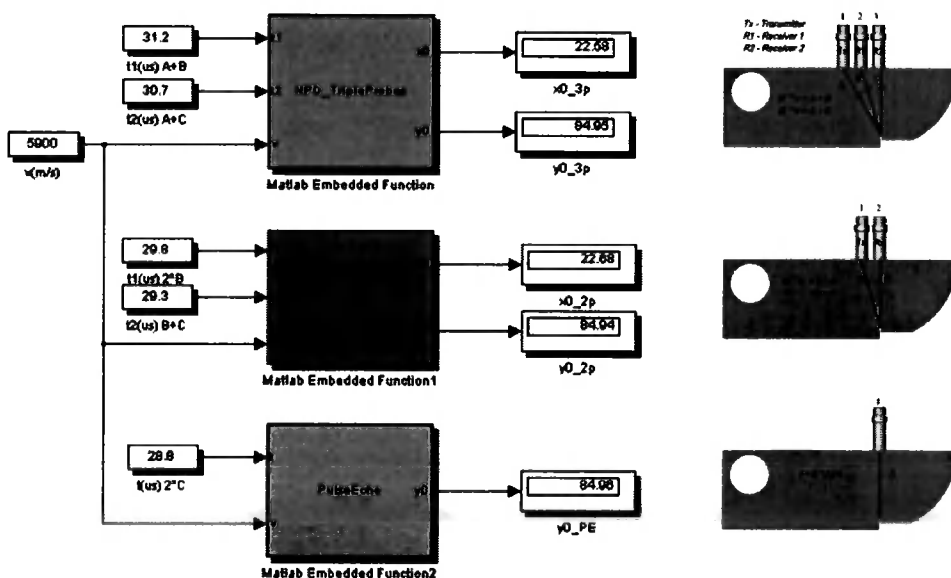


Figure3. 4 NPD Algorithm Simulation Model

3.3 Matlab GUI for NPD

A GUI (Graphical User Interface) programme has been designed and created to demonstrate the NPD algorithm using Matlab GUIDE (Graphical User Interface Development Environment). GUIDE automatically generates an M-file that controls how the GUI operates. The M-file initializes the GUI and contains a framework for all the GUI callbacks -- the commands that are executed when a user clicks a GUI component [18].

Figure 3.5 shows the NPD GUI initial window. When the value of offset and the transmitter probe are set, the GUI moves the transducer array to the right position, calculates the relative position of the defect, draw two ellipses and locate the pseudo defect. One execution example is also shown in Figure 3.6. In the example, the offset of these three transducers from their original position is set to be 40mm to the left and Probe 3 is chosen to be the transmitter, while Probe 1 and Probe 2 are two receivers, each of which constructs an ellipse with the transmitter. For the first ellipse formed by Probe 3 and Probe 1, the length between two foci is 45mm and the transmission path ($C + A$) equals to the major axis ($2*a$). Similarly, the length between Probe 3 and Probe 2 is 22.5mm and the value of the major axis is path C plus B.

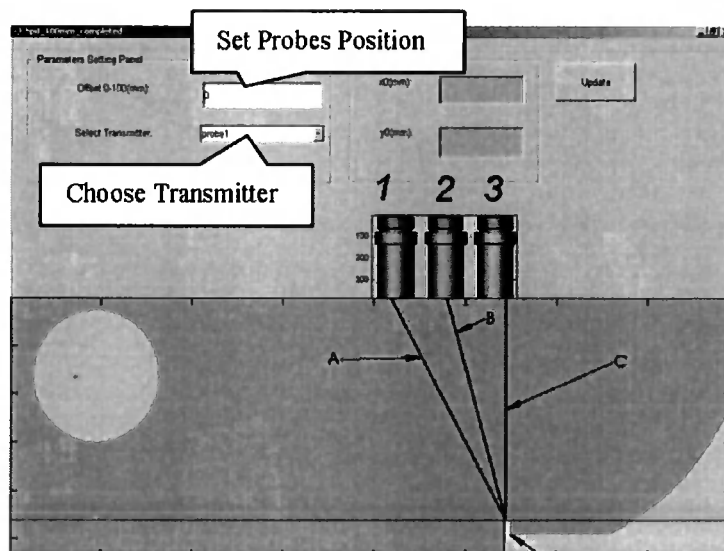


Figure3. 5 Matlab NPD GUI

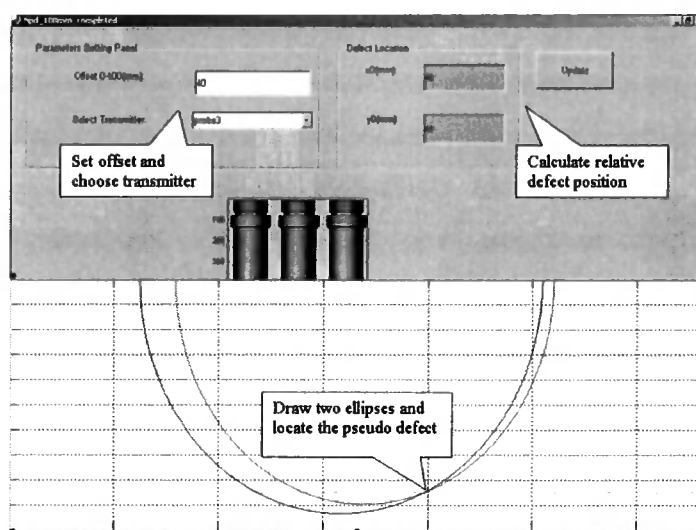


Figure3. 6 NPD GUI Example

3.4 Summary

In this chapter, the NPD algorithm was explained in detail. The mathematical models were designed and built using MATLAB tools to implement the NPD algorithm with two probes and three probes respectively. The algorithm was written into a Simulink block in order to be used for the automated code generation system. A Matlab GUI was also built to demonstrate the defect location procedure of the NPD algorithm. The results showed that the two and three probe geometries were suitable for detecting and locating the defect. However, in order to implement NPD in real-time, the three probe method is easier to implement due to timing considerations and analogue interfacing hardware.

CHAPTER 4

System Simulation Model

New and stronger demands on reliability of currently used NDT procedures and methods have stimulated the development of simulation tools of NDT. A realistic mathematical model of the ultrasonic inspection situation makes it possible to avoid, or at least reduce, time-consuming and costly experimental work. It can also be useful in the design of inspection routines as it can give an estimate of whether a postulated defect can be detected or not. This chapter describes such a mathematical model for NPD technique and its contribution to this endeavour.

Mathematical modelling of the ultrasonic NDT situation has become an emerging discipline with a broadening industrial interest in the recent decade. To qualify the procedures, extensive experimental work on test blocks is normally required. A thorough validated model has the ability to be an alternative and a complement to the experimental work in order to reduce the extensive cost that is associated with the previous procedure. The most significant advantage of a computational fast and against experiments validated and verified model is its capacity in parametric studies and in the development of new testing procedures.

In this chapter, separate model parts have been developed to cover the transmitting and receiving procedure, including the modelling of environment noise, the ultrasound attenuation and the processing and filtering of echoes from the defect. Simulink is a high level description language from the Mathworks which can provide a flexible simulation environment for hardware and software codesign DSP system. The use of Simulink intrinsically offers all potentialities and toolboxes of MATLAB. This is very useful to evaluate the simulation results and process the real measured results[19]. The rapid DSP prototype and its hardware and software are presented in next chapter.

4.1 Simulink Model

Simulink is a simulation tool for modeling, simulating, and analysing dynamic systems. It supports linear and nonlinear systems, modeled in continuous time, sampled time, or a hybrid of the two. Systems can also be multirate[20]. Because Simulink is integrated with Matlab, many functions from the Matlab analysis tools and application toolboxes, such as Signal Processing Toolbox and Filter Design Toolbox, can be accessed as Simulink blocks for building System Models and analysing simulation results.

Figure 4.1 illustrates a Simulink model built to simulate an NPD system. The main sections included are:

- Signal Generation: Generating various pulse signal
- Transmission: Simulating ultrasound transmitting in steel
- Filter: Cancelling environment noise using IIR and FIR filters
- Correlation: Locating received signal

Some system default parameters are set as follow:

- F_s (sampling frequency): 50MHz
- f (pulse frequency): 5MHz
- Gain (represent the analog amplifier): 200
- Pseudo Defect Depth (defect position, unit:mm): 85mm
- Ultrasonic Velocity: 5900m/s
- d (probe offset unit mm): to be set
- RTDX_ctrl (transmitter selector): to be set

The transmitted pulse is a specifically selected shape such as a sinewave in this model. The received signal consists of two parts: a shifted and attenuated version of transmitted pulse and random noise, resulting from interfering radio waves, thermal noise in the electronics, etc. Since the ultrasound travels at a known rate in steel, 5900 metres per second, the shift between the transmitted and received pulse is a direct measure of the transmission distance. Firstly, the IIR and FIR filters lowpass filter reduces the noise level and increase the signal-to-noise ratio, then the correlation determines where the given shape signal locates.

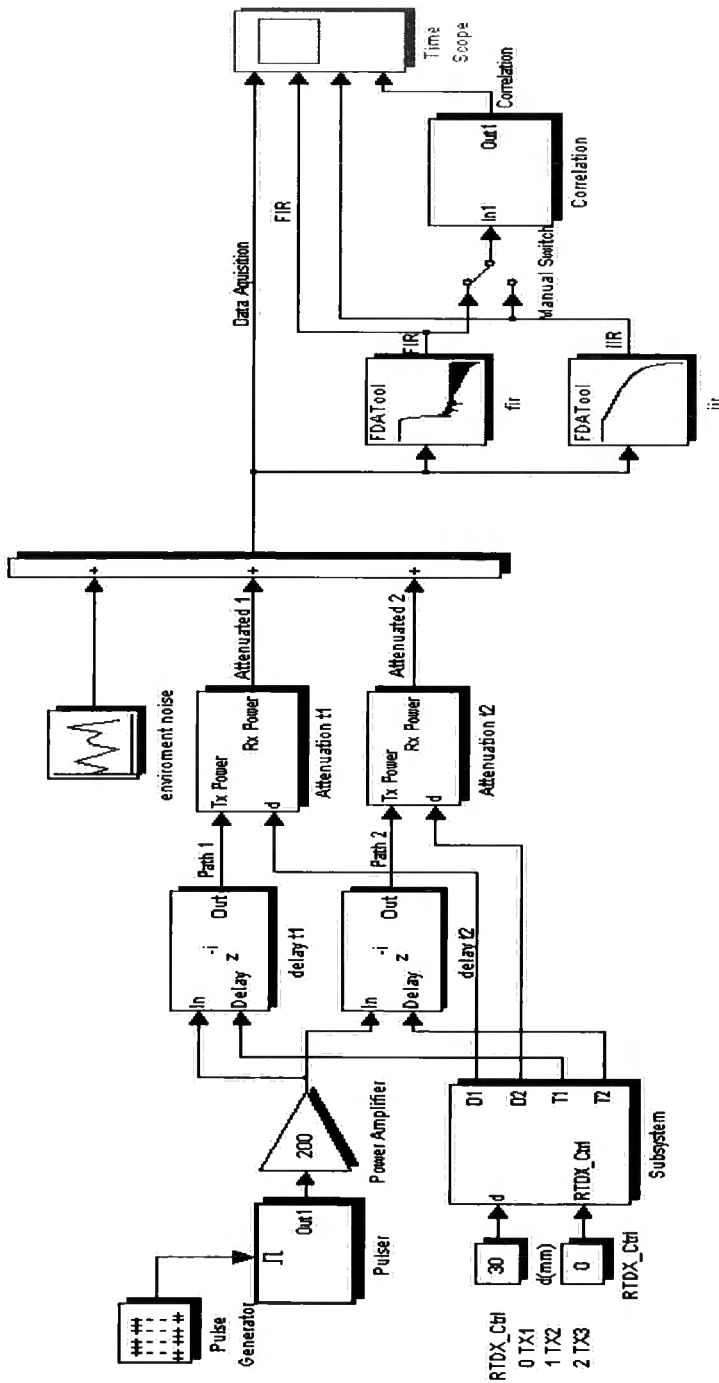


Figure 4. 1 Ultrasonic Detection System Simulink Model

4.2 Signal Generation

As shown in Figure 4.1, the pulser block generates a certain shape of waveform. It is triggered by a pulse generator block, the repetition period of which can be set according to the testing conditions. Different waveforms behave slightly different on various

material structures. The shape of the triggered signal at the transmitting end may affect the data acquired at the receiving end. There should be one certain waveform of ultrasound at a certain frequency which can gain the best testing result for a tested object under the same testing conditions. Experiments need to be carried out in practical testing to verify the effect of varying the waveform on the V1 steel calibration block. Sine wave, Square wave and Sawtooth are three fundamental signal shapes used in experiments and the Sine wave is the chosen in most engineering testing cases. In this project, three periods of a 5MHz sine wave is produced with a 50MHz sampling frequency (10 samples per period), to not only exceed the requirement of the Nyquist-Shannon sampling theorem and to effectively avoid aliasing, but to give an adequate representation of the signal shape.

The sampling theorem is one of the most significant theorems in the field of signal processing. It indicates that a continuous signal can be properly sampled, only if it does not contain frequency components above one-half of the sampling rate[21]. If B is the bandwidth and Fs is the sampling rate, then the theorem can be stated mathematically as follow

$$2 * B \leq Fs \dots\dots\dots (4.1)$$

4.3 Attenuation

In the field of NDT (Non-destructive Testing), attenuation is defined as the loss in acoustic energy that occurs between any two points of travel. This loss may be caused by absorption, scattering or other material characteristics. The sound attenuation is caused by the structure of the test object but is also strongly dependent on the frequency and the wave mode of the applied probe. Ultrasound attenuation relies on many factors such as absorption, scattering, transducer loading and diffraction patterns. Basically the sound attenuation increases with an increase in the frequency[1]. The general equation of ultrasound attenuation is:

$$\frac{p}{p_0} = e^{-\alpha d} \dots\dots\dots (4.2)$$

p_0 is ultrasound pressure at the start point and p is the ultrasound pressure at the end point of the travel path whose length is d . α (alpha) is the coefficient of attenuation for a given material. The attenuation coefficient is a factor which is determined by the degree of attenuation in sound wave energy per unit of distance the ultrasound travels. It is composed of two parts, (1) (absorption) proportional to frequency, (2) (scattering) dependent on the ratio of grain or particle size to wavelength. Normally the units of attenuation are in dB and the attenuation coefficient is in dB per unit length. Attenuation of metals is up to 10 dB/m depending on various structures. Since the attenuation is frequency dependent, a single attenuation coefficient only applies to a single frequency.

4.4 Time Delay and Environment Noise

Ultrasound transmission in a test object is simulated by calculating the time delay from the probe positions set by offset parameter and transmission mode controlled by the value of RTDX_Ctrl. In the subsystem shown in Figure 4.2, D1 and D2 are the distances of two transmission paths and major axes for two separate ellipses. These values are used for calculating ultrasound attenuation.

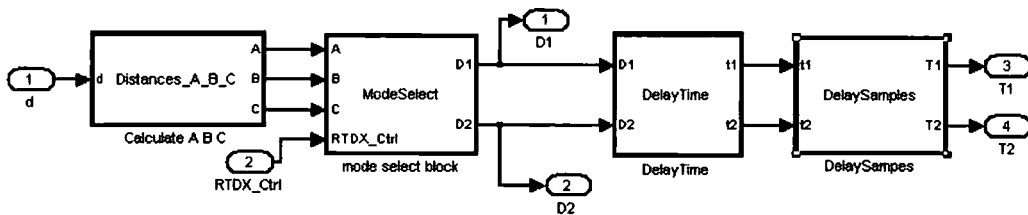


Figure 4. 2 Transmission Subsystem

In the root model, the Variable Integer Delay block delays the discrete-time input at the *In* port by the integer number of sample intervals specified by the input to the *Delay* port. The Random Source block generates a frame of M values drawn from a Gaussian pseudorandom distribution, where M is specified in the Samples per frame parameter whose value is set to 1 for this model. Here the mean of the noise is zero while the variance is one to simply simulate the environment noise.

4.5 Digital Filters

Digital filters are used for the purposes of reducing environment noise and increasing Signal-to-noise ratio. Digital filters can achieve far superior results for these tasks than their counterpart analogue filters. The most popular digital filters are designed using the Matlab Filter Design Toolbox and the simulation results are analysed and compared using the Signal Processing Toolbox.

Three kinds DSP methods – lowpass Infinite Impulse Response (IIR) filter, lowpass Finite Impulse Response (FIR) filter, Correlation were employed on dissimilar pulse signal adding random noise to verify the improvement of SNR.

4.5.1 IIR Filter

Infinite Impulse Response (IIR) Filter defines a class of digital filters that may have both zeros and poles on the z-plane. As such, IIR filters are not guaranteed to be stable and almost always have nonlinear phase responses. For a given filter order (number of IIR feedback taps), IIR filters have a much steeper transition region roll-off than FIR filters. Example IIR filters include the Chebyshev filter, Butterworth filter and Bessel Filter. In practice electrical engineers find IIR filters to be fast and cheap, but with poorer bandpass filtering and stability characteristics than FIR filters. In this model, Butterworth is chosen as an example IIR filter. The other filter type is also available in simulation modelling.

The Butterworth function is a mathematical function used to produce maximally flat filter magnitude responses with no consideration of phase linearity or group delay variations. Filter designs based on a Butterworth function have no amplitude ripple in either the passband or the stopband. However, for a given filter order, Butterworth designs have the widest transition region of the most popular filter design functions.

Figure 4.3 depicts the magnitude and phase response and the IIR filter parameters are listed below.

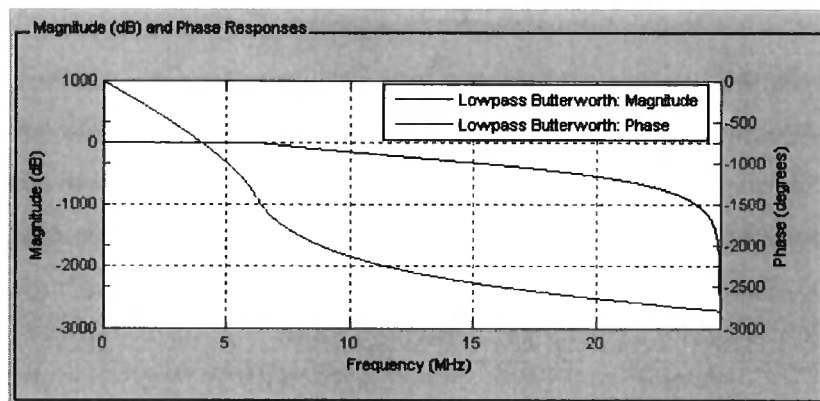


Figure 4. 3 IIR Butterworth Lowpass Filter

- Response Type: Lowpass
- Filter Type: Butterworth
- F_s (sampling frequency): 50MHz
- F_{pass} (passband frequency): 6MHz
- F_{stop} (stopband frequency): 8MHz
- A_{pass} (passband attenuation): 1dB
- A_{stop} (stopband attenuation): 80dB
- Order: 31

4.5.2 FIR Filter

Finite Impulse Response (FIR) Filter defines a class of digital filters that has only zeros on the z-plane. The key implications of this are that FIR filters are always stable, and have linear phase responses (as long as the filter's coefficients are symmetrical). For a given filter order, FIR filters have a much more gradual transition region roll-off than digital IIR filters. Figure 4.4 depicts the magnitude and phase response and the FIR filter parameters are listed below.

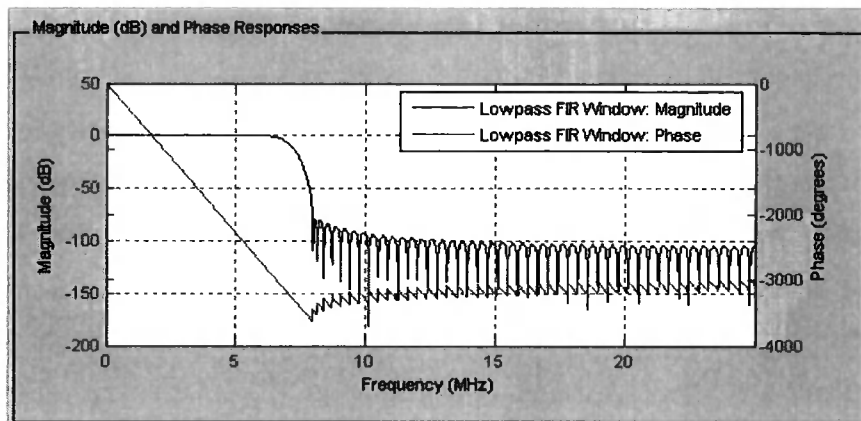


Figure 4. 4 FIR Kaiser Lowpass Filter

- Response Type: Lowpass
- Window Type: Kaiser
- Fs: 50MHz
- Fpass: 6MHz
- Fstop: 8MHz
- Apass: 1dB
- Astop: 80dB
- Order: 126

Comparing these two filters, the FIR filter has a linear phase response for the passband where IIR filter has a non-linear one. In applications such as ultrasonic detection where timing is critical, a linear filter is required to gain a constant group delay. For the magnitude response, the FIR filter has a sharper roll-off transition region and lower stopband attenuation than its counterpart. When all the parameters of the IIR and FIR filters are set to be the same, the order of FIR filter is 126, which is much higher than its counterpart IIR filter whose order is only 61. As a higher filter order means a more critical requirement for system performance, it will affect the speed of real-time signal processing. Hence, the filter parameters need to be adjusted to meet the requirement of the real-time system in practical applications. The effects of these two filters are compared and analysed in the simulation result section.

4.5.3 Correlation

Correlation is a mathematical operation that is very similar to convolution. It uses two signals to produce a third signal which is called the cross-correlation of the two input signals. If a signal is correlated with itself, the resulting signal is instead called the autocorrelation. Correlation is the optimal technique for detecting a known waveform in random noise. That is, the peak is higher above the noise using correlation than can be produced by any other linear system [21].

Figure 4.5 shows the correlation subsystem. The XCORR block in the correlation subsystem computes cross-correlation of two inputs – the received signal and the original generated three-period sinusoid.

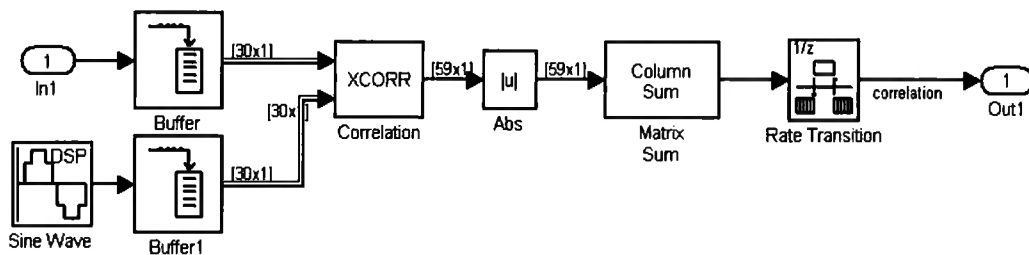


Figure 4. 5 Correlation Subsystem

4.6 Simulation Result

The result of the simulation is shown in Figure 4.6. The first diagram shows the original received signal buried in environmental noise and hard to be recognised. In the following three diagrams, IIR, FIR and correlation are implemented on the original received signal to improve the probability of detection. It is shown that both the FIR filter and correlation have made the required data easier to be picked out as anticipated, while the result of the IIR filter does not meet the expectation. Because the FIR filter has a linear phase response in its passband and thus a constant group delay as shown in Figure 15, the waveform of the filtered signal does not change as much as that filtered by the IIR filter, which has a non-linear phase response in its passband as shown in Figure 14. The signal-to-noise ratio is used to analyse the affects of IIR filter, FIR filter and correlation.

Signal-to-noise ratio (SNR) is an engineering term for the power ratio between a signal (meaningful information) and the background noise. Because many signals have a very

wide dynamic range, SNR is often expressed in terms of the logarithmic decibel scale. In decibels, the SNR is 20 times the base-10 logarithm of the Amplitude (A) ratio, or 10 times the logarithm of the Power (P) ratio as shown in equation 4.3.

$$\text{SNR (dB)} = 10 \log_{10} \left(\frac{P_{\text{signal}}}{P_{\text{noise}}} \right) = 20 \log_{10} \left(\frac{A_{\text{signal}}}{A_{\text{noise}}} \right) \dots\dots\dots (4.3)$$

SNR for four simulation signals are calculated and compared in Table 2. It disposes the same information as shown in Figure 4.3. The purpose of this simulation is to compare the effects of different filters with the parameters and to analyse the efficiency. All these signal processing methods increase the SNR as anticipated. Among them, the FIR filter's performance is the best.

Table 4. 1 Signal-to-noise Ratio Comparison

Signal	SNR(dB)			
	Test 1	Test 2	Test 3	Test 4
Original Received	14.08	13.51	14.40	16.09
IIR Filtered Signal	16.53	14.28	14.67	16.1
FIR Filtered Signal	18.58	17.92	18.90	20.08
Correlation Signal	17.74	18.02	17.15	18.67

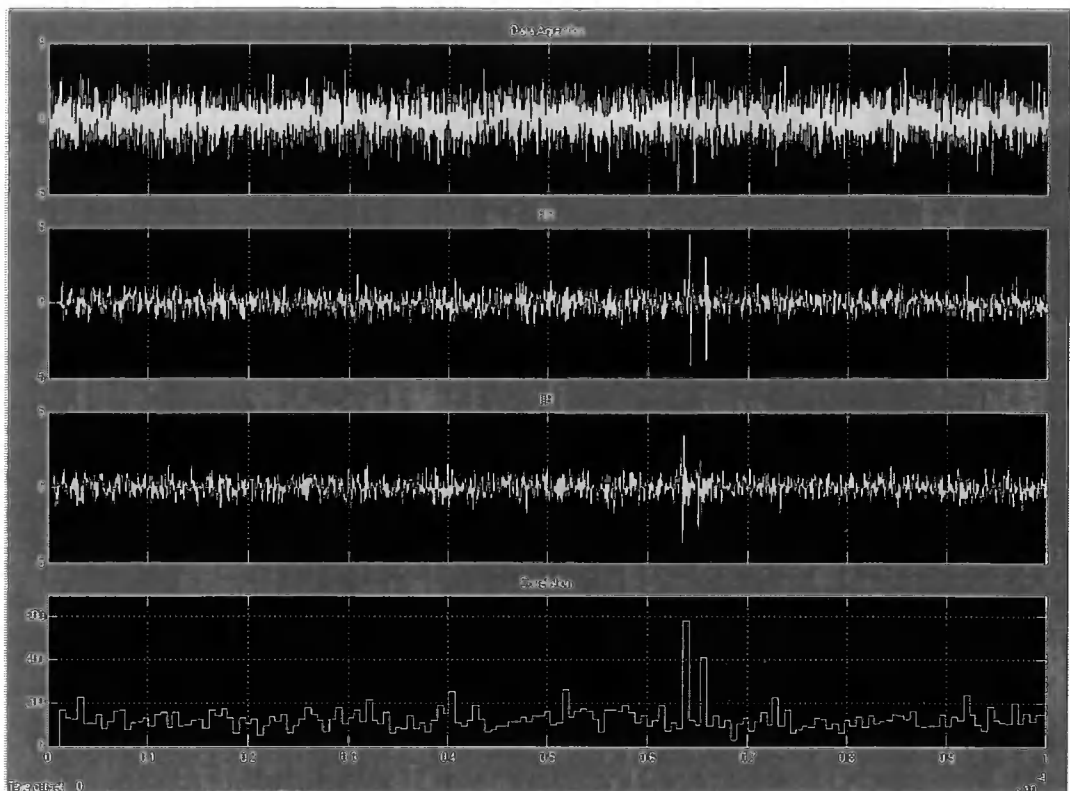


Figure 4. 6 Simulation Result

4.7 Summary

This chapter describes how Simulink is incorporated into a model of the complete ultrasonic test system, using simulated input data. Separate parts covering the transmitting and receiving procedures have been considered, including the signal generation, the environment noise and the ultrasound attenuation. The model is then used to investigate and design different filtering techniques to improve the signal to noise ratio such that the probability of detection can be increased. It was found that the 126 tap FIR filter provided the best improvement.

CHAPTER 5

DSP System Architecture

This chapter describes the hardware and software used to implement the NPD algorithm simulated in Chapter 4. Firstly an overview of the TI TMS320C6713 DSK (DSP Starter Kit) board and the Signalware AED_330 FPGA-based analog expansion daughter card is given, including the on-board components and their functionalities. Secondly the accompanying code development tools for developing diverse applications with the hardware are introduced. Finally a rapid real-time DSP prototype is introduced to integrate the hardware and software.

The hardware components on both the DSK and the daughter card have been indicated to present the integrated DSP system, with the emphases on their performances in this project. The daughter card offers new possibilities to the DSK by adding the high performance FPGA and high speed signal converters. The software solutions for the DSK board support the rapid development of real-time DSP prototypes but cannot be employed on the daughter card as well due to the current constraints of the Matlab Simulink Tools. Therefore, an audio processing example was implemented without the daughter card to demonstrate the low frequency real-time system, and the daughter card was programmed with Code Composer Studio to obtain a high frequency performance.

5.1 System Hardware

- TMS320C6713 DSK
- AED_330 Analog Expansion Daughter card

5.1.1 Texas Instruments TMS320C6713 DSK

The TMS320C6713 DSK is a cost-effective Development Board designed to develop applications for TI TMS320C6713 floating-point DSPs (Digital Signal Processor). Here DSPs is used to distinguish the DSP (Digital Signal Processing) Technique. The C67x

DSPs are a part of the High-performance TMS320C6000 generation of TI DSP platforms. These dynamic DSPs can be used for a wide variety of high performance applications like medical imaging and instrumentation. The DSK board and its block diagram are shown in Figure 5.1 and Figure 5.2 respectively[22]. In this project the C6713 DSK is used for real-time implementation of the NPD algorithm.

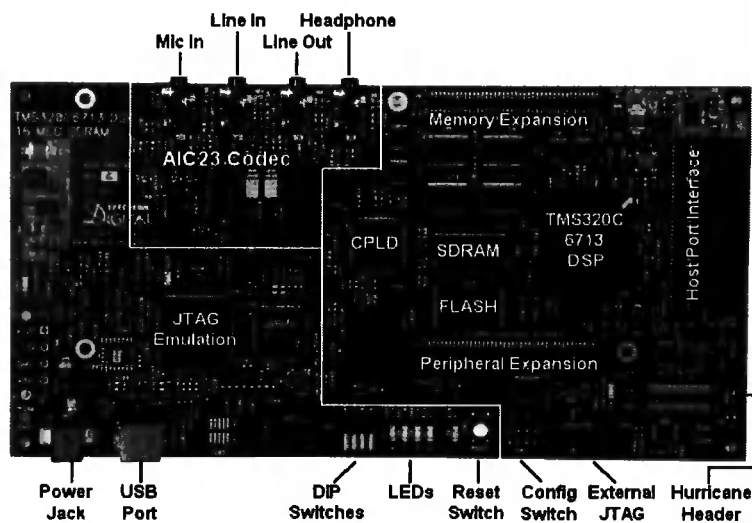


Figure 5. 1 Taxes Instrument TMS320C6713 DSK

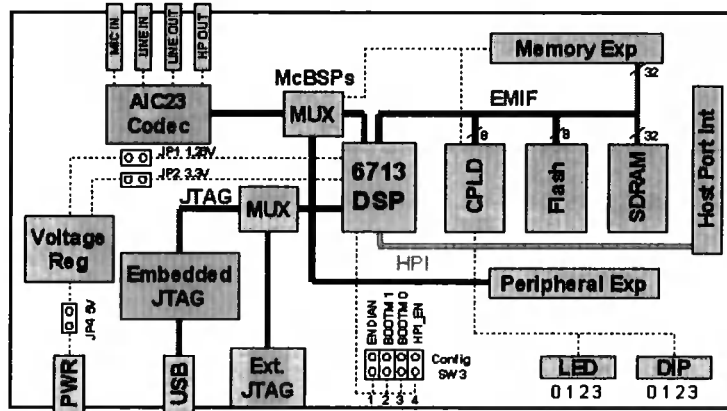


Figure 5. 2 TMS320C6713 DSK Block Diagram

The main features of the 6713 DSK board are listed in Table 5.1. The DSP chip interfaces to on-board peripherals through a 32-bit wide EMIF. The SDRAM, Flash, CPLD and third party add-in daughter card are all connected to the EMIF bus. The EMIF clock is derived from the PLL settings and configured in software at 90MHz. This number is based on an internal PLL clock of 450MHz required to achieve 225 MHz operation with a divisor of 2 and a 90MHz EMIF clock with a divisor of 5.

Table 5. 1 TMS320C6713 DSK Features

Feature	Details
TMS320C6713 DSP	225 MHz, floating point, 256 Kb internal RAM/Cache
CPLD	Programmable "glue" logic
External SDRAM	16 Mbytes, 32-bit interface
External Flash	512Kbytes, 8-bit interface (256Kb usable)
AIC23 Codec Stereo	8KHz –96KHz sample rate, 16 to 32 bit samples, mic, line-in, line-out and speaker jacks
4 User LEDs	Writable through CPLD
4 User DIP Switches	Readable through CPLD
3 Configuration Switches	Selects power-on configuration and boot modes
Daughter card Expansion Interface	Allows user to enhance functionality with add-on daughter cards
HPI Expansion Interface	Allows high speed communication with another DSP
Embedded JTAG Emulator	Provides high speed JTAG debug through widely accepted USB host interface

Figure 5.3 shows a memory map with the address space of a generic C6713 DSP on the left and specific details of how each region is used on the right. The internal memory locates at the beginning of the address space by default. The EMIF has 4 equally sized regions called chip enable spaces (CE0 ~ CE3) with their own dedicated chip enable signal and configuration registers. On the 6713 DSK, the on-board SDRAM is connected to CE0 of the EMIF while the Flash memory and programmable CPLD registers share CE1. The SDRAM uses the EMIF's internal synchronous DRAM controller while the Flash and CPLD use simple asynchronous memory signals. CE2 and CE3 are used to access devices on any add-on daughter cards.

Address	C67x Family Memory Type	6713 DSK
0x00000000	Internal Memory	Internal Memory
0x00030000	Reserved Space or Peripheral Regs	Reserved or Peripheral
0x80000000	EMIF CE0	SDRAM
0x90000000	EMIF CE1	Flash CPLD
0xA0000000	EMIF CE2	Daughter Card
0xB0000000	EMIF CE3	

0x90080000

Figure 5. 3 DSK Memory Map

5.1.1.1 C6713 DSP Core

The TI C6713 DSK was equipped with a 225 MHz TMS320C6713 Floating Point DSP and has 265Kbytes internal memory. It is capable of delivering up to 1800 million instructions per second (MIPS) and 1350 million floating-point operations per second (MFLOPS). The C67x DSPs use the Very Long Instruction Word (VLIW) architecture, which uses multiple functional units to execute multiple instructions in parallel. The internal memory of C6713 DSP has a two-level (L1 and L2) hierarchy to makes best use of the small amount of on-chip memory. The L1 memory is split into Program and Data Caches whereas L2 consists of unified Cache/ Mapped RAM. There are lot of peripherals on the C6713 DSP besides the VLIW core and the Two-level Memory that are useful for data movement, interfacing with other DSPs, adding a daughter card etc. The EDMA controller that usually controls the data transfer between the DSP and the external peripherals can only interact with L2. The CPU mostly interacts with the L1 memory level but also can access the L2 memory through L1. Using this two-level memory architecture, the CPU can save its precious time from data transfer for processing.

5.1.1.2 EDMA (Enhanced Direct Memory Access)

The EDMA controller included on the C6713 DSPs is a highly efficient data transfer engine which serves the purpose of releasing the DSPs from data transfer between the

DSPs and the peripherals outside the DSPs, between the on-chip peripherals or between the on-chip peripherals and the memory.

The EDMA controller has several enhancements to the DMA peripheral typically found on all processors for managing the data movement between the memory and the outside peripherals. Particularly, the EDMA controller does not use the same bus for accessing the memory as the CPU uses for accessing the operands. Combining with the two-level memory architecture of the DSPs, this access method reduces the interference between the data transfer and CPU processing and increases the DSPs' performance.

5.1.1.3 Timer

The C6713 DSP has two 32-bit Timers that can serve a variety of purposes. The Real-Time Operating System (RTOS) kernel - DSP/BIOS normally uses one of the available on-chip timers as a source for its system clock. The timers can also be used for timing events, counting events, generating pulses, interrupting the CPU and sending synchronization events to the EDMA controller. C6713 DSPs uses CPU/4 clock as the internal clock source to the timer.

For the C6713 DSPs, the default input clock frequency for the timers is the CPU clock rate divided by four. Each of the on-chip Timers has a period count register (PRD), timer count register (CNT), and a timer control register (CTL) for configuring its operation. The timer period value is set to the value in the PRD register. When the timer starts from reset, the value in CNT register is incremented for every tick of the input clock source. This value is incremented until it reaches the value in the PRD register, upon which a timer interrupt occurs and the timer is reset. With the control bits in the control register, the input source can be set to either internal or external clock, and the output mode can be set to timer output or general purpose output. [23][24].

5.1.1.4 EMIF (External Memory Interface)

EMIF is a 32-bit bus on which external memories and other devices can be connected.

All external memory accesses of the C6713 DSK are done through the EMIF. The EMIF generates external bus signals using a programmable controller to provide glueless interfaces to synchronous and asynchronous memories. The EMIF clock rate is determined by the PLL configuration. The EMIF has an independent divisor which can

be any integral number. For normal DSK operation, the EMIF divisor should be 5 for a bus speed of 90MHz (450MHz / 5). The EMIF must be set up before code is loaded into an external memory space[22].

5.1.1.5 CPLD (Complex Programmable Logic Device)

The CPLD is used to implement glue logic that ties the board components together. The CPLD has a register based user interface that allows the user to configure the board by reading and writing to its 4 memory-mapped registers in software. The registers are mapped into EMIF CE1 data space at address 0x90080000. The 6713 DSK includes 4 LEDs and a 4 DIP switches as a simple way to provide the user with interactive feedback. All can be accessed by reading and writing using the CPLD registers. The CPLD also provides the control of the daughter card interface and signal. Table 5.2 shows the definitions of these 4 registers.

Table 5. 2 CPLD Registers

Register	Definition
USER_REG	To read the state of the 4 DIP switches and turn the 4 LEDs on or off
DC_REG	To monitor and control the daughter card interface
VERSION	To indicate the board and CPLD versions
MISC	To set the McBSP for on-board codec or off-board daughter card

5.1.1.6 SDRAM (Synchronous Dynamic Radom Access Memory)

Asynchronous and Synchronous DRAM

Asynchronous DRAM refers to the fact that the memory is not synchronized to the system clock. The memory value appears on the bus a certain period of time later after a memory access begins. In this way, the signals are not coordinated with the system clock. Asynchronous memory works fine in lower-speed memory bus systems but is not suitable for high-speed access required by real-time processing.

On the contrary, synchronous DRAM or SDRAM is synchronized to the system clock; all signals are tied to the clock so timing is much tighter and better controlled. This type of memory is much faster than asynchronous DRAM and can be used to improve system performance. It is more suitable for higher-speed memory access of real-time systems.

The 16 Megabytes on board SDRAM is mapped at CE0 (address 0x80000000) on the 32-bit EMIF and must be configured in software for proper operation. One of the key SDRAM parameters is the refresh period. SDRAM must be continuously refreshed or they will become unstable and lose their contents. The SDRAM used on the C6713 DSK must refresh one row every 15.6 microseconds to maintain data integrity. This configuration uses a value of 1400 (0x578 in hex notation) to specify a refresh period of 1400 bus cycles with a 90MHz EMIF clock period (11.11 nanoseconds)[25].

5.1.1.7 Daughter Card Interfaces

The DSK provides three expansion connectors that can be used to accept plug-in daughter cards. The daughter card allows users to extend their DSK platform's capabilities and provide customer and application specific I/O. The expansion connectors are for memory, peripherals, and the Host Port Interface (HPI). The three expansion connectors are all 80-pin 0.050 x 0.050 inches low-profile connectors designed for high-speed interconnections. Each connector includes multiple ground, +5V, and +3.3V power signals so that the daughter card can obtain power directly from the DSK. The peripheral expansion connector additionally provides both +12V and -12V to the daughter card.

Only Memory and Peripheral Interfaces are used by the AED_330 daughter card in this project. The memory connector provides access to the DSPs' asynchronous EMIF signals to interface with memories and memory mapped devices. It supports byte addressing on 32-bit boundaries. The peripheral connector brings out the DSPs' peripheral signals like McBSPs, timers, and clocks. Both connectors provide power and ground to the daughter card.

Most daughter card signals are not modified on the board except a few daughter card control signals like DC_RESET and DC_DET, which are accessible through the CPLD DC_REG register. The DSK also multiplexes the McBSP0 and McBSP1 for on-board or external use. This function is controlled through the CPLD MISC register.

5.1.1.8 McBSP (Multi-channel Buffered Serial Ports)

On board peripherals include two McBSPs which are important for building real-time data transmission of audio systems. The McBSP consists of a data path and a control

path, both of which are connected to external devices. McBSP0 is used as the unidirectional control channel and it should be programmed to send a 16-bit control word to either the on-board codec or the mounted daughter card. The control channel is only used when configuring the codec; it is generally idle during data transmission. McBSP1 is used as the bi-directional data channel. Many data formats are supported based on three variables - sample width, clock source and serial data format.

5.1.1.9 AIC23 Codec

The DSK board is equipped with an on-board AIC23 Codec and four 3.5 mm audio jacks (microphone input, line input, line output, and headphone output) for signal transmission and audio processing. Codec stands for coder/decoder. The job of the AIC23 is to code analog input samples into a digital format for the DSPs to process, and then decode data coming out of the DSP to generate the processed analogue output. Digital data is sent to and from the codec on McBSP1. The signal can be sampled as 16-bit elements at a highest rate of 96 kHz by the on-board codec. The codec can select the microphone or the line input as the active input. The analogue output is driven to both the line out (fixed gain) and headphone (adjustable gain) connectors

5.1.1.10 JTAG (Joint Test Action Group)

JTAG refers to a set of design rules introduced by TI for testing, programming and debugging chips. JTAG interface allows greater visibility into the internal state of a chip using only five extra pins. The code development tools on the host PC use the JTAG interface to debug programs non-intrusively through JTAG emulator hardware. The JTAG emulator provides a target-host communication mechanism that is fast, flexible and does not need any hardware running on the target.

The 6713 DSK board includes a JTAG emulator that can directly access the register and memory state of the C6713 DSP chip through a standardised JTAG interface port. When a user wants to monitor the progress of his program, Code Composer (the development environment) sends commands to the emulator through its USB host interface to check on any data the user is interested in. MATLAB GUI can be used together with this interface to download the file from the host computer to the DSK board for transmission.

5.1.2 Analogue Daughter card

The Block Diagram of the AED_330 analog daughter card is shown in Figure 5.4. This card is mounted on the DSK via memory and peripheral expansion interfaces which allow the daughter card full access to all of the DSPs' resources. Two 12-bit ADCs and two DACs are mounted in the mixed signal area. Analogue connectors include four SMB coax connectors and a 20 pin 25 mm ribbon cable connector which are adjacent to the breadboard for connecting analog signals. The inputs to the ADCs and the outputs of the DACs lead directly to the breadboard area on which conditioning circuits can be constructed. The ADC and DAC have their digital interfaces connected directly to a FPGA which provides a flexible digital interface to the DSPs[26]. Additional analogue components can be mounted on the card by using different areas provided. Two dual amplifiers can be mounted to provide a variety of circuits to convert single-ended inputs to differential, filter input signal or buffer two separate signals. Two single amplifiers can be mounted for filtering and buffering output signals. Surface-mount(SOIC) and DIP analog components can be mounted on the bread board area.

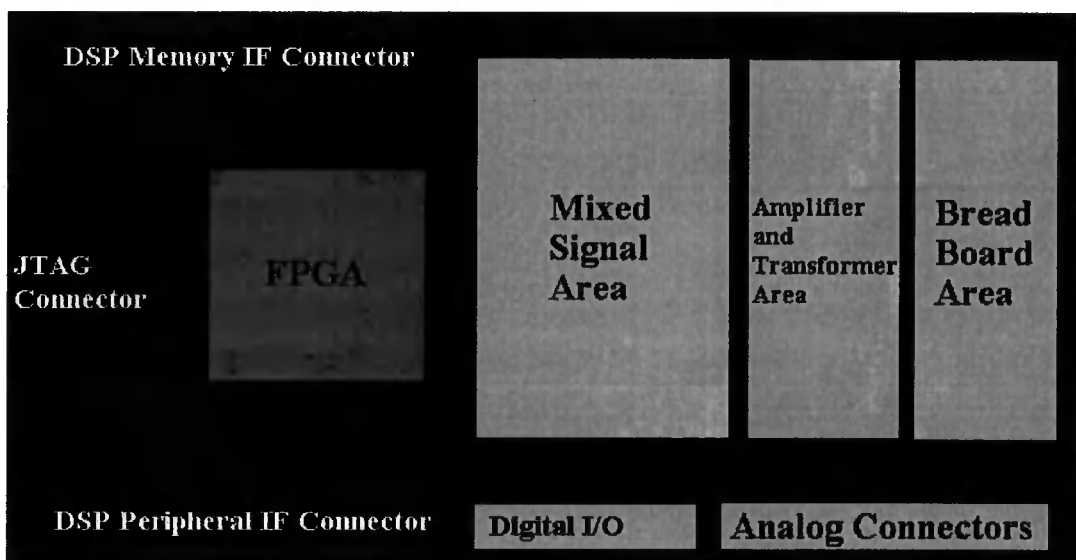


Figure 5. 4 AED_330 Daughter Card Block Diagram

5.1.2.1 FPGA

The AED_330 daughter card uses a Xilinx Vertex-E FPGA. Field-programmable gate arrays (FPGA) are used to synthesize the hardware and provide a fast and cost-effective way of prototyping hardware systems in a laboratory environment. The FPGA between

the DSPs and the converters allows blocking and FIFO buffering of signals before they are placed in the DSPs' memory. This optimises the use of DSPs' memory and memory bus bandwidth which is often a limiting factor in DSP applications. The FPGA provides an input decimation filter which limits the bandwidth with sharp digital filter edges. It also allows the application to work with higher initial sample rates than the DSPs can handle; constructs high speed output samples for the DACs and input samples from ADCs; and connects to the external digital I/O connector to the clock/control lines of the converters, allowing synchronization of the converters with both external signals and DSP signals[26].

FPGA configurations are used to configure the digital logic in the FPGA to interface between the devices mounted in the mixed signal area and the DSPs' parallel EMIF bus or the serial McBSP ports. The AED_330 is initially configured and delivered with a test configuration that tests the interface between the FPGA and the DSP. The Xilinx ISE Series PC based development tools can be used to configure the FPGA.

The signal from the FPGA to the mixed signal area can control ADCs and DACs. The converter clocks can be derived from any of the clocks the DSK supplies to the daughter card, or via a digital I/O pin: an oscillator mounted in the breadboard area of the daughter card. Digital I/O number 1 (D_CNTL1, J15 pin 39) is specifically designed for this.

5.1.2.2 THS5661 DAC

The daughter card has two THS5661 DACs, which are 12-bit resolution and support update rates up to 100 MHz. According to the on board configuration, the full scale output voltage $V_{OUT_{FS}}$ is 1V and the V_{OUT1} pin is connected to ground. Therefore the differential output voltage $V_{OUT_{DIFF}}$ can be expressed as[27][28]:

$$V_{OUT_{DIFF}} = V_{OUT1} - V_{OUT2} = \frac{(4095 - 2CODE)}{4096} \times V_{OUT_{FS}} \dots\dots\dots (5.1)$$

5.1.2.3 THS1230 ADC

The daughter card also has two 12-bit THS1230 ADCs with a sampling rate range between 5 MHz and 30 MHz. There are three working modes. The on board ADCs

work in Mode 1 and thus have the differential analogue input gain of 1.0. Tests shows that the analogue input range for the ADCs is 0.6V~2.7V with a full scale input voltage of about 2V, represented by 4096 digital levels.

5.1.2.4 Digital I/O Connector

The FPGA connects the 24 digital I/O connect to the 74LVTH245 transceivers and then to a 40-pin double-row connector designated J15 on the daughter card. It has 24 digital I/Os, 6 grounds and 10 pins that are connected to pads adjacent to the breadboard area.

The digital transceiver, U19 and U20 on the daughter card, are 74LVTH245 and 74LVTH244 respectively. They buffer the digital signal between the FPGA and the connector J15. U19 buffers I/O number 9-16; U20 buffers I/O numbers 1-8 (odd numbers are input, even are output). They can support digital I/O up to 100 MHz. The buffer can be enabled or disabled all together, and the directions can be set by the FPGA 9-16 group of eight.

5.2 Development Tools

The C6713 DSK is accompanied by a set of code development tools, including a highly optimising C/C++ Compiler, Code Composer Studio Integrated Development Environment (IDE) and the DSP/BIOS kernel. Some of the information in TI Technical documents related to this project is included in this section to implement the system and an attempt has been made to include some additional description of interfacing the daughter card so as to appreciate the architecture in further detail.

- Code Composer Studio
- DSP/BIOS
- Software Libraries
- Matlab Tools

5.2.1 Code Composer Studio

Code Composer Studio (CCS) is an IDE package for the host PC, provided by TI to develop applications for its DSPs such as TMS320C6000 series. This package includes

tools for code generation, such as a C compiler, an assembler and a linker. It has graphical capabilities and supports real-time debugging. It provides an easy-to-use software tool to build and debug programs. Therefore, it simplifies building of sophisticated real-time applications and cuts down the development time[29]. The main features of CCS are listed below:

- Highly optimising C/C++ Compiler
- Assembly Code generation tools
- Support for DSP/BIOS
- Advanced Emulation Drivers
- Real-time Analysis with RTDX
- Highly-effective Debugger
- Project Manager
- Code Editor

5.2.2 DSP/BIOS

DSP BIOS is a scalable real-time operation kernel which includes many benefits such as pre-emptive multi-threading in the form of hardware interrupt (HWI) or software interrupts (SWI), periodic tasks and idle functions, as well as a configuration tool used to configure peripheral devices. It also can be used to define many data scheduling and data synchronisation structures[30]. The three main components in DSP/BIOS are listed as follow:

- DSP/BIOS Configuration tool
- DSP/BIOS Real-time Analysis Tools
- DSP/BIOS API

The DSP/BIOS configuration tool is useful for creating and configuring DSP/BIOS objects like HWI, message logs (LOGs) etc. This tool can also be used for configuring memory, thread priorities and interrupt handlers. The DSP/BIOS Real-time Analysis tools are useful for viewing program activity, gathering statistics about threads and data logging. DSP/BIOS also provides implicit instrumentation in programs that utilise its multi-threading capabilities. DSP/BIOS Application Programming Interface (API) is a

collection of over 150 functions that are callable from C/C++ or assembly [31]. Application programs make use of DSP/BIOS by making calls to its API.

Real-time analysis can be performed using real-time data exchange (RTDX). RTDX allows for data exchange between the host PC and the target DSK, as well as analysis in real time without stopping the target. Communication with on-chip emulation support occurs to control and monitor program execution through the JTAG.

The real time analysis tool has many features to assist in the debugging process. These include message logs, variable watch windows, graphs, and real time operation analysis and program flow diagrams.

It was found that a substantial amount of design time had to be invested in understanding all these features. Running simple programs proved challenging until the basic operation of the system was fully understood. The investment time had to be warranted for the features required in the remaining steps of the system design.

5.2.3 Software Libraries

TI provides several optimized software libraries to develop application and implement algorithm on the C6713 DSPs. Three libraries were included in this project. They are TMS320C6000 Chip Support Library (CSL), TMS320C67x Fast RTS Library and TMS320C6713 DSK Board Support Library (BSL).

The chip support library (CSL) provides a C-language interface for configuring and controlling C6713 DSPs' on-chip peripherals like Timers, EDMA, McBSP, GPIO etc. [32]. Each of the on-chip peripherals is covered by a single API module of the CSL. The CSL assists the DSP/BIOS in configuring and accessing the DSPs' peripherals. The benefits of using CSL are listed as follows:

- Standard Protocol-to-Program Peripherals
- Automated pre-initialization via the CSL GUI
- Basic Resource Management
- Symbolic Peripheral Descriptions

Similarly, the BSL provides a C-language interface to configure and control the devices present on the C6713DSK[33].

The TMS320C67x Fast RTS Library is a set of assembly optimised floating-point math functions like sine, cosine, log etc that can be called by C[34]. These set of functions are hand-optimised for the C67x architecture and thereby result in the considerable saving of execution time.

5.2.4 Support for Daughterboard Interfaces

The DSP/BIOS and Chip Support Library provide the software interface to the EMIF, McBSPs, the EDMA and the daughterboard. The various mixed signal devices (ADC and DAC) are supported on either the EMIF memory bus or one of the serial ports depending on the daughterboard FPGA configuration.

DSP BIOS can be used to setup and configure the DSPs' peripherals that are used with the daughter card. The timing requirements imposed by the FPGA configuration must be entered to setup the EMIF bus. Data addresses and blocking requirements of the mixed signal devices must be entered to setup the EDMA peripherals. The result of the DSP BIOS setup is that the data appears in the DSP memory in the formats established by the mixed signal devices and the FPGA configuration[26].

5.2.5 Matlab Tools

The MATLAB Embedded Target for TI C6000 DSP and Real-Time Workshop can create executable code for the C6713 DSK. Additionally, one of the Real-Time Workshop build options builds a Code Composer Studio project from the C code generated by Real-Time Workshop.

All the features provided by Code Composer Studio (CCS), such as tools for editing, building, debugging, code profiling, and project management can work with MATLAB, Simulink, Real-Time Workshop, and the supported hardware to develop applications. Besides, Matlab also provides an interface between the PC host and the DSK target. The required Matlab tools are listed below:

- Simulink Signal Processing Blockset

- Real-Time Workshop
- Real-Time Workshop Embedded Coder
- The Embedded Target for TI C6000 DSP
- Matlab Link for CCS

5.2.6 FPGA Configuration

A test FPGA configuration provided with the daughter card by Signalware defines a hardware interface between the DSP and the daughter card. It can be used for simple buffering and control of the mixed signal devices. This test configuration was designed to test the major features of the daughter card, including the ADCs, DACs, and the 16 digital I/O lines.

Several memory-mapped 16-bit wide control registers are set in the FPGA to provide flexibility for programming. To work with the 32-bit C6713 DSPs which is byte addressing, these control registers are addressed as if they were 32-bit (4 bytes) wide with zero for bits 0 and 1. The registers and their address are shown in Table 5.3. Although the high order bits are shown as zero, they have to be set to some value to address the daughter card that depends on the DSP target board. For C6713 DSK, the daughter card is addressed at EMIF CE2 (0xA0000000~0xFFFFFFFF). The address bits that are not connected to the FPGA (bits 13 to 6 of byte address) are also shown as zero, but they are “don’t care”. The table also gives the test values which are the values when the example DSP program loads into the registers for 100MHz daughter card clock with 256 samples per frame. The test values give maximum performance that the DSK board provides. By default, the daughterboard clock equals the CLKOUT2 clock on the DSK board (225Mhz/2).

The test data word sent from the FPGA to the DSP is composed of two 16 bit fields. The first field (bit 0 ~ 15) is the interrupt clock counter incrementing at the CLKOUT2 rate. The second field (bit 16 ~ 31) is a counter value that increments each time the DSP reads a data word. Interrupt Start and Interrupt Period registers are 16 bit counts of board clock from start up to first interrupt and from one interrupt to the next. The interrupt counting is visible in the Interrupt Down Counter register.

Table 5.3 FPGA Control Registers

Register Name	Byte Addressing	Readable/Writable	Test Value
Digital I/O	0x00100000	R/W	0x0001
Digital I/O Control	0x00100004	R/W	0x3000
Interrupt Start	0x00120004	R/W	0x0100
Interrupt Period	0x00120008	R/W	0x0100
Interrupt Down counter	0x0012000C	Read only	N/A

5.2.6.1 Digital I/O Register

Each bit of the Digital I/O register corresponds to the value of one digital I/O pin. Bit 0 refers to digital I/O 1; bit 1 refers to digital I/O 2, and so forth. For groups of 8 bidirectional I/O, 74LVTH245 transceivers (U19 and U20) are used. The Digital I/O register is either an R/W register when the transceivers are set to output or read only when the transceivers are set to input.

5.2.6.2 Digital I/O Control Register

The Digital I/O Control register is used to enable and control the buffers and transceivers.

5.2.6.3 Status register

The Status register can be read to reveal FIFO error conditions. All bits will normally be zero. A value of one indicates an error. Bits 0 ~ 7 of the register indicate A/D error including the A/D FIFO overflow or underflow and any A/D device error. Bits 8 ~ 16 indicate the similar D/A errors. When an error occurs, it is latched in into the Status register. When the DSP reads from the A/D Data address, one word is read from the A/D FIFO. If a read is performed when the FIFO is empty, an A/D FIFO underflow will occur. When the DSP writes to the D/A data address, one word is written into the D/A FIFO. If a write is performed when the FIFO is full, a D/A FIFO overflow will occur. When the XCNTL0 (J10 Pin64) is set to high, both the ADCs and DACs start to transfer data. Some D/A data should be written to the D/A FIFO before the system starts to avoid the D/A FIFO immediately underflow.

5.2.6.4 Start register and Period register

The start register and Period register are used to control the interrupt line (J10 Pin53). The DSP should initiate an EDMA read from the A/D FIFO when it sees a rising edge on the interrupt line. Before the system starts, the value from the start register is loaded into a counter. Once the system starts, the counter counts down once every time a word is written into the A/D FIFO. When the counter reaches zero, another rising edge occurs on the interrupt line and the counter is reloaded with the value from the period register. This procedure continues till the system stops. The value of the down counter can be read any time by reading the Interrupt down counter register.

5.2.6.5 A/D Clock Rate Register

The A/D clock rate register controls the sampling rate of the ADC. The A/D clock rate equals the daughter card clock rate divided by the A/D clock rate register plus one as shown in the equation:

$$\text{ADC_CLK Rate} = \text{CONV_CLK Rate} / (\text{ADC_CLK_LOAD} + 1) \dots \dots \dots (5.2)$$

The DSK clock is not necessarily the same as the CPU clock or the daughter card clock. The value chosen for the rate must result in a clock rate that meets ADC specified clock frequencies. The clock that is sent to the converter is actually a pulse that has the width of one daughter card clock cycle. The pulse is generated when a down counter counts down the value of the A/D clock down counter register. The value of the down counter can be read at any time by reading the A/D clock down counter register.

5.2.6.6 D/A Clock Rate Register

The D/A clock rate register control the D/A sample rate in the same way as the A/D clock rate register. The A/D and D/A sample rates can be set to different values.

$$\text{DAC_CLK Rate} = \text{CONV_CLK Rate} / (\text{DAC_CLK_LOAD} + 1) \dots \dots \dots (5.3)$$

5.3 Real-Time DSP Prototype

Before attempting to implement the NPD algorithm on the DSK board, a prototype was developed for the PC using the MATLAB environment.

The basic system consists of one DAC that outputs the generated pulse signal for detection; two ADCs capture signals which are then processed by the C6713 DSPs. DSPs are concerned primarily with real-time signal processing. Real-time processing requires the processing to keep pace with some external event, whereas non-real-time processing has no such timing constraint. The external events to keep pace with in this project are the A/D conversion, D/A conversion and data transfer.

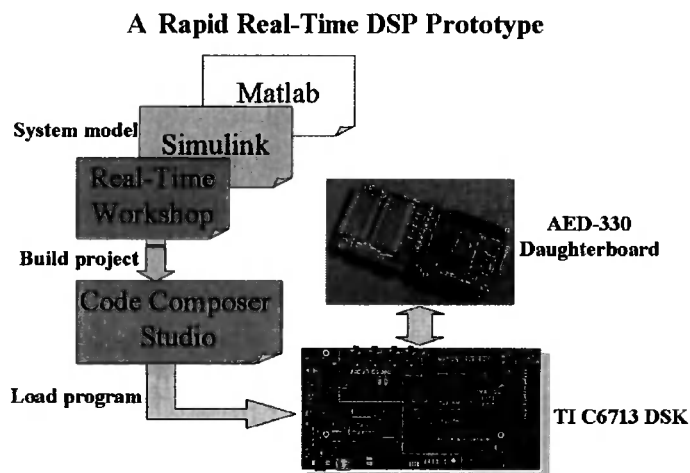


Figure 5. 5 A Rapid Real-Time DSP Prototype

Figure 5.5 depicts the architecture of a rapid DSP prototype for the real-time testing system. Firstly, a Simulink model is built using the Matlab Embedded Target for DSP and DSP blockset which enable the rapid prototyping of real-time software for the TMS320C6713 floating-point DSPs and generates efficient code for the processor directly from the Simulink model. The generated code is readable and editable for manual optimization. The Embedded Target automates the creation of a link to the IDE, which provides board support software for the DSK board. It then invokes the compiler and linker to create a DSPs executable file and finally downloads the executable to the DSK board and sets it running for real-time algorithm evaluation. The AED-330 analogue expansion daughter card is mounted on the DSK to gain high sample rate for A/D and D/A conversion. Variable frequency and wave shape pulse signals was used in order to gain the optimum testing conditions. To remove the randomly distributed background noise that disturbs the recognition of the defect echoes and increase the behaviour of the system, several DSP algorithms such as correlation are applied and different filters including FIR filter and IIR filter can be chosen for real-time analysis as discussed in chapter 4.

A low frequency pulser and receiver are implemented using the on-board codec of the DSK. An 18 kHz sine signal, sampled by the maximum 96 kHz sampling frequency of the codec, is generated with a lookup table created by Matlab and sent out. The on-board DIP switch is programmed to control the generation. The received signal was logged and stored in the 16 Megabytes SDRAM of the DSK, to be analysed and processed off-line. Because the sampling frequency of the codec limits the signal frequency that can be generated, the analogue daughter card was added to solve this problem. However, the third party daughter card does not support the rapid prototype method illustrated above as it can not be represented as a block in Simulink model. Therefore, all programs related to the daughter card need to be built and debugged with CCS using C.

The daughter card has one test programme without using the software support tools such as DSP/BIOS and chip support library provided by Texas Instruments. This test programme is self-running and cannot be relied on for complicated application requiring interruption and real-time control. The daughter card requires a general hardware driver to be built in order to interface with the DSK using CCS with the support of DSP/BIOS and CSL. The DSP/BIOS kernel contains functions for capturing information about the running program without halting execution. Captured information can be uploaded in real-time to the host using the RTDX protocol with the physical JTAG link. CCS contains visual tools for displaying program information. These tools can be thought of as a software logic analyser. This unique feature of CCS facilitated by the real-time capability of DSP/BIOS is to be used to build the new daughter card driver to substitute the self-running test programme. Peripherals such as MCBSP, EMIF and EDMA can be initialised, configured and programmed graphically using DSP/BIOS, so there is no need to memorise register bit-fields for peripheral options. And this is the first task in any further development as it is the critical point of the hardware system for real-time testing.

5.4 DSK Application Example

This section describes an application which receives and processes an audio signal and then outputs it to a set of headphones. This was implemented in the CCS IDE using the Chip Support Library with the DSP/BIOS. This development environment gives the

designer great programming flexibility, but requires a significant amount of time and effort to fully realise a system and hence benefit from the CCS tools. It enables full access to the functionality of third party daughter cards such as the AED330 used in this project. This includes controlling the ping pong buffer, EDMA transfer and DSP/BIOS real-time analysis and scheduling.

This example was studied and included because it gives a clear explanation of the data transfer methods which are very useful for understanding the software structure of the daughter card test programme, thus, providing a sound basis for a pulser/receiver application programme.

5.4.1 Description

The dsk_app example digitally processes audio data from the line input on the AIC23 codec and plays the result on the headphone and line output. It uses the McBSP and EDMA to efficiently handle the data transfer without intervention from the DSP. Digital audio data is received from the codec on McBSP1. The audio data is a series of 16-bit signed integers representing the amplitude of the input waveform at a particular point in time. Since the AIC23 is a stereo codec, the audio input consists of both left and right audio channels. Data is received in a frame consisting of two elements, one 16-bit sample from the left channel followed by one 16-bit sample from the right channel. Frames are received at the DSK's default sample rate, 48 kHz.

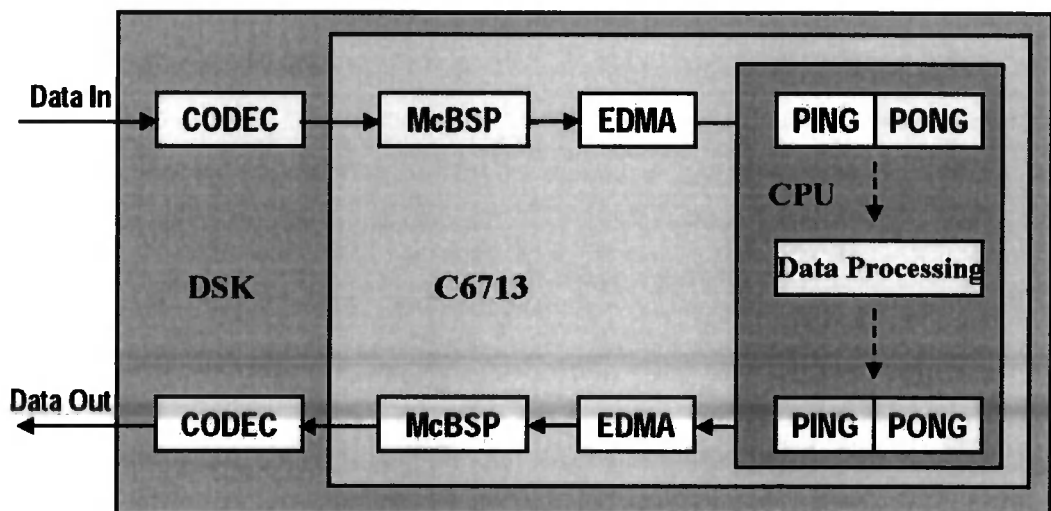


Figure 5. 6 DSK Application Example Hardware Diagram

The EDMA is configured to take every 16-bit signed audio sample arriving on McBSP1 and store it in a buffer in memory until it can be processed. Once it has been processed, it is sent back out through McBSP1 to the codec for output. One EDMA channel is used to transmit data to the codec while another is used to receive data from the codec. The example uses EDMA to relieve the DSP from the duty of data transfer. The EDMA controller takes incoming audio data directly from McBSP1 and places it in a memory buffer. It also takes data from a memory buffer and sends it to McBSP0 to generate the audio output. Separate EDMA channels are used to transmit and receive audio data. When running the program, if no DIP switches are pressed, the example simply passes the audio from the line-in to the audio outputs. LED2 and LED3 toggle as the data is being transferred. If the DIP0 is depressed, LED0 blinks once per second. If DIP1 is pressed, a dummy load that takes 20-25% of the processor time is added.

Two special features, Ping-pong buffering and EDMA linked transfer implement an especially robust and efficient data transfer infrastructure. Both features are illustrated in the hardware diagram of this example shown in Figure 5.6.

5.4.2 Ping-Pong Buffering

At the highest level, the EDMA controller reads audio data from the McBSP and places it in a buffer in memory. On the data receive side there are two logical buffers, receive PING and receive PONG. When the first data comes in it is placed in the PING buffer. When it is full, new data is redirected to the PONG buffer and the DSP is free to process the PING data without fear of it being overwritten. When the PONG buffer fills up, the configuration is reversed. The ping-pong data transfer continues indefinitely with one buffer always hosting the active transfer and one remaining stable for the DSP to operate on. If only one buffer is used, the DSP must process all of the data between the instant the buffer fills up and the next audio sample arrives. When ping-pong buffers are used, the DSP can take as long as the time it takes to fill an entire buffer to process the data, making it much easier to meet a real-time schedule.

Separate input and output buffers are used to decouple the receive side from the transmit side while data is being processed. The output buffers are also of the ping-pong variety so there are a total of four logical buffers, receive PING, receive PONG, transmit PING and transmit PONG.

5.4.3 EDMA Linked Transfers

The other data transfer feature is called linked transfers. When the EDMA finishes with the PING side and needs to switch to the PONG side, the source and destination pointers need to be changed to point at the new buffer. When linked transfers are used, the new address can be stored in a link configuration structure and automatically loaded by the EDMA controller when the current transfer is complete. The reconfiguration can also be handled by the DSP in a software interrupt service routine but using linked transfers removes the scheduling requirement that the software finish before the next sample is received to get uninterrupted audio. A detailed explanation of the EDMA controller and the linked transfer is given in reference[35].

5.4.4 DSP/BIOS Real-time Analysis and Schedule

A real-time system is a system that must satisfy the explicit response-time constraints or risk severe consequences. It consists of a controlling system and a controlled system. The DSP/BIOS GUI Configuration Tool, as a part of the Code Composer Studio, is the operating system in this project. It controls the real-time performance by configuring the Hardware Interrupt (HWI), Software Interrupt (SWI), Task (TSK) and background threads (IDL). Figure 5.7 shows the priority of these four thread types and the thread pre-emption.

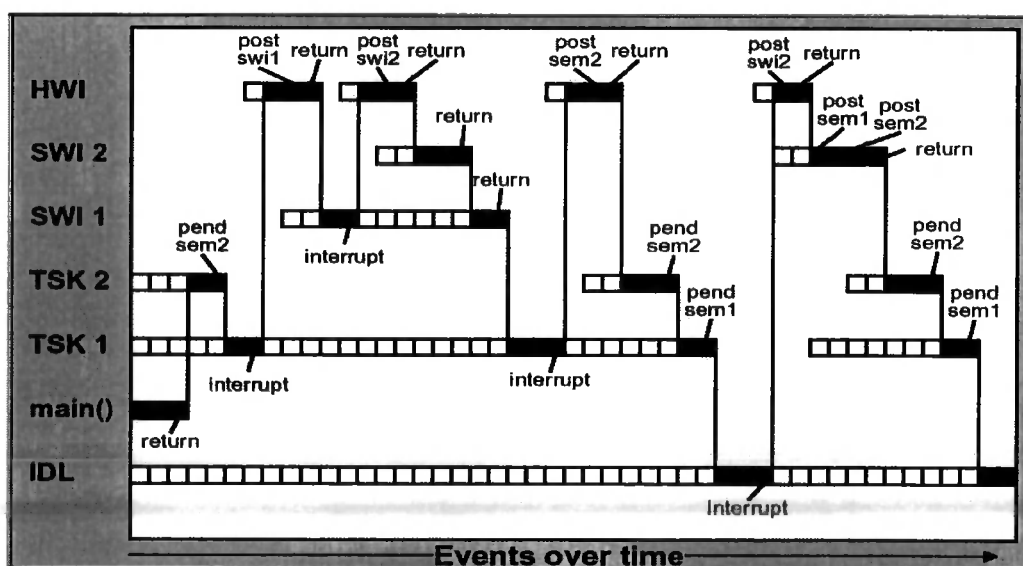


Figure 5. 7 Real-time analysis using DSP/BIOS

When the program starts running, the individual DSP/BIOS modules are initialized as configured in `dsk_app.cdb` with the DSP/BIOS configuration tool. The `main()` function is then called as the main user thread. In this example `main()` performs application initialisation and starts the EDMA data transfers. When `main` exits, control passes back entirely to DSP/BIOS which services any interrupts or threads on an as-needed basis. When there is no work to be done an idle thread is run. EDMA interrupts will pre-empt the idle thread.

The `edmaHwi()` interrupt service routine is called when a buffer has been filled. It contains a state variable named `pingOrPong` that indicates whether the buffer is a PING or PONG buffer. The `edmaHwi()` switches the buffer state to the opposite buffer and calls the SWI thread `processBuffer()` to process the audio data. The `processBuffer()` is responsible for manually transferring receive data to the transmit buffers. It can be replaced with code that processes the data rather than copying it. Two periodic threads, `blinkLED()` and `load()` run asynchronously with the audio processing as a demonstration of DSP/BIOS multitasking.

The DSP/BIOS provides Real-time scheduling, Real-time analysis (RTA) and Real-time data exchange (RTDX). Real-time analysis is performed using RTDX. It allows for data exchange between the host PC and the target DSK, as well as in real time without stopping the target. Key statistics and performance can be monitored in real time. Through the JTAG, communication with on-chip emulation support occurs to control and monitor program execution.

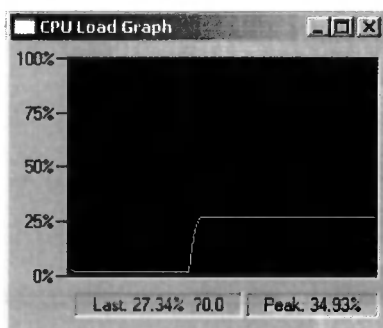


Figure 5. 8 CPU Load Graph

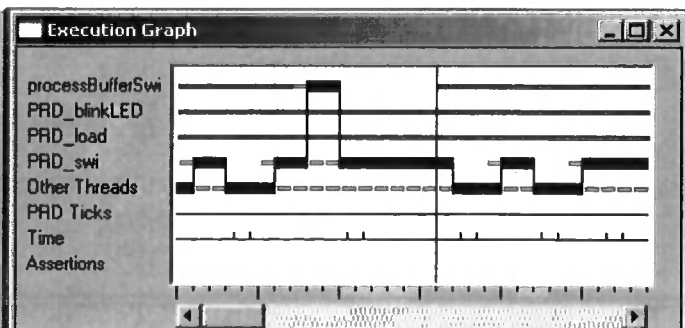


Figure 5. 9 Execution Graph

In this example, RTDX is enabled and set for non-continuous mode with a buffer size of 1024. RTDX allows data transfer between a host and target devices without interfering

with the target application. The data can be analyzed and visualized on the host using any host client. The CPU load graph is enabled to display what percentage of the total cycles is spent doing real work as shown in Figure 5.8. Figure 5.9 shows the DSP/BIOS execution graph, in which the processBufferSwi is at the highest priority and can interrupt the PRD_BlinkLED and the PRD_load threads in order to guarantee real-time processing.

5.5 Real-time Rapid Prototype Example

The application described in this section is an acoustic noise cancellation system employed using the Matlab-Simulink rapid real-time prototyping system discussed in section 5.3. This includes an Embedded Target for the TI TMS320C6000 DSPs Platform which integrates Simulink and MATLAB with TI eXpressDSP tools and deploys embedded code onto TI C6000 DSPs. It is basically a software assistant to develop and validate DSP designs from concept through to code and automates rapid prototyping on TI DSK. The process consists of creating a Simulink model which include blocks, specific to the target processor. The build then used to carry out a sequence of procedures. Firstly, C code is generated by Real-Time Workshop and is used to create a Code Composer Studio project. It then automatically compiles and links files to create an executable file which is finally downloaded to the target processor and run. All the features provided by CCS, such as tools for editing, building, debugging, code profiling, and project management, can be accessed using MATLAB, Simulink, Real-Time Workshop. [36].

5.5.1 Simulink Model and RTDX Result

The acoustic noise canceller application for a TI C6713 floating-point DSP was created using the C6713 Board Support and RTDX blocks(see section 6.2.3). The Simulink model for the noise canceller system is shown in Figure 5.10. The waterfall plot in Figure 5.11 generated using MATLAB and the Link for Code Composer Studio, shows the filter taps adjusting adaptively to cancel the noise.

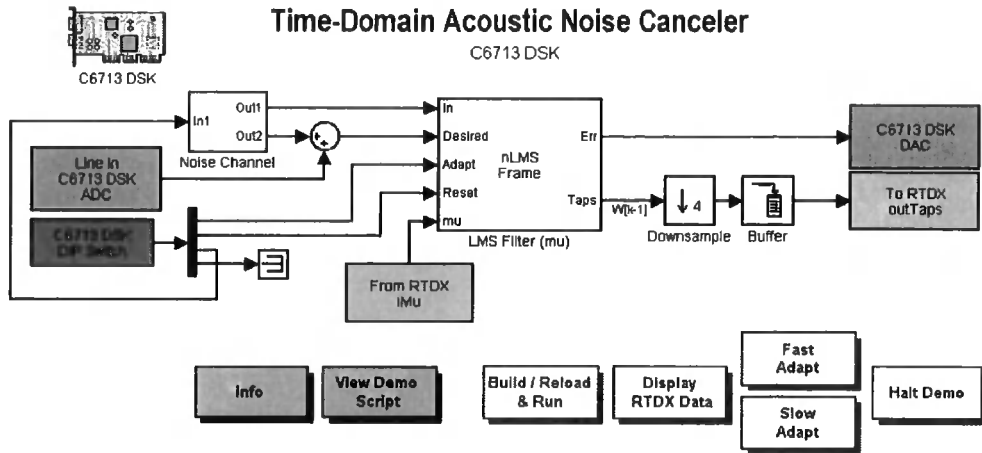


Figure 5. 10 Simulink Real-time Model: Time-Domain Acoustic Noise Canceller

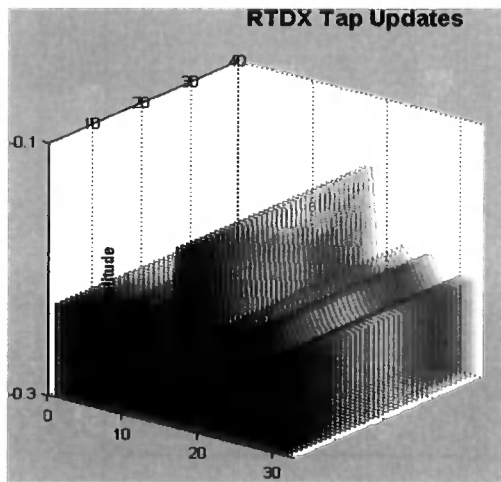


Figure 5. 11 Waterfall Plot of Filter Parameters

5.5.2 Board Support Blocks

The C6713 DSK board support blocks provide access to I/O, peripherals, and other utilities on each of the supported boards. These blocks (ADC, DAC, LED, Switch, and Reset) are parameterised with Simulink dialog boxes[36]. Prototype code can be automatically generated for a supported DSK board, combining these blocks with standard blocks from Simulink, the Signal Processing Blockset, and other blocksets. The Embedded Target for TI C6000 DSP, together with Real-Time Workshop, the Link for Code Composer Studio, and TI development tools, automates the process of code generation, compiling, linking, downloading, and executing embedded signal processing applications on the DSK board.

5.5.3 From/To RTDX Block

From/To RTDX block are used in this model to implement the real-time data exchange. From RTDX adds an input channel to send control signal from the PC to the DSK. Similarly, To RTDX adds an output channel to the Simulink model. In this model, the To RTDX block creates a channel to send the adapt filter parameters from the DSK back to the PC. These parameters are sent back to the PC and display in a waterfall plot which updates in real-time.

5.6 Summary

The hardware and the associated development tools were described in this chapter, together with some application examples for illustration. A TMS320C6713 DSK and a high-speed analogue daughter card were chosen as the base hardware platform. The hardware components on both the DSK and the daughter card have been integrated to produce the complete DSP system. The daughter card offers new possibilities to the DSK by adding the high performance FPGA and high speed signal converters. The Matlab Simulink real-time rapid prototyping method is described, but was not used in this project since it could not easily support the third party daughter card. An audio processing example was implemented without the daughter card to demonstrate the low frequency real-time system, and the daughter card was programmed with Code Composer Studio to obtain a high frequency performance.

CHAPTER 6

AED330 Daughter Card Experiments

This chapter describes a daughter card test program for testing the features of onboard components and the data transition between the DSP core on the DSK and signal converters on the daughter card based on the default FPGA configuration. The program was revised to generate an output 40 kHz signal with various waveforms. A custom circuit was then built to amplify and bias the output signal such that it could be received within the range (0.6 V to 2.7 V) of one of the ADCs.

The test program is written in ANSI C and is intended to provide an initial test for the board to show that the mixed signal part and the FPGA are working. This program is primarily for hardware operation and it does not use either DSP/BIOS or CSL. It is suggested by Signalware, the producer of the expansion daughter card that these support tools should be used in developing custom applications[26].

6.1 Test Program Description

In the test program, interfaces are mapped into the daughter card memory space using the EMIF. The definition of the interface consists of addresses and data transferred over the EMIF. These addresses are relative locations within the daughter card memory space. The location of the daughter card memory space is EMIF CE2 defined by the memory map of the C6713 DSK starting at 0xA0000000. These addresses can be read and written directly from the DSPs. In this project EDMA is required to access high speed mixed signal devices at these addresses.

The test program provides a framework to develop DSP code for the daughter card. This program controls the hardware directly to attain a very high speed. It uses EMIF to transfer data from the ADC to the DSP and uses EDMA channel to transfer the data without interrupting the CPU. The CPU only processes when a block of data is ready.

The test program can use either the EMIF bus or the McBSP (for lower speed devices on the selected daughter card) to transfer data to D/A devices.

The test program is a data acquisition and signal generation program. Because the EMIF data bus has a limited bandwidth, the program runs the ADCs and DACs separately to attain higher sampling rate rather than running all converters simultaneously. There are three steps for this program.

1. The test program first reads data from the ADCs, stores some samples and sums a large number of samples to get information on the operation of the ADCs. It sets up the EDMA registers, starts the EDMA, starts the FPGA and waits for interrupts indicating a frame of data is ready. It writes a 0x0100 to the Start and Period Registers, so that every time it sees a rising edge on the interrupt line, it reads 256 words from the A/D FIFO. If the A/D clock rate is set too fast, the DMA will not be able to keep up with reading the samples and the A/D FIFO will overflow. The A/D FIFO overflow can be indicated either by the status register or the XSTAT0 line (J10 Pin66). The fastest A/D sample rate for the AED_330 on the 6713 DSK in this project is set to be 10 MHz per channel. This is done by set the ADC clock rate register of the FPGA to 8 in equation 6.1.

$$\text{ADC or ADC clock rate} = \text{Conversion CLOCK} / (\text{ADC_CLK_REG} + 1) \dots (6.1)$$

According the daughter card manual, the conversion clock should equal to the onboard EMIF clock which is 90 MHz. However, the test program provided showed ambiguous information which conflicted with the user manual. Tests were made to find out the clock frequency the daughter card used and the result is discussed later.

2. After taking in several frames of data from the A/D FIFO, the DSP sets the XCNTL0 (J10 Pin64) line low to stop the ADC and print the data acquired. Then it operates the digital I/O in a pattern that allows each bit to be activated individually for output for about 0.5 second.

3. Finally, the program generates a waveform with the DACs which can be observed with an oscilloscope. The DSP writes the words to fill the D/A FIFO. Then the XCNTL0 line is set to high again to start the DACs. The previous written data is transferred from the D/A FIFO to the DACs. A pulse is sent to the DSP on the TINP1

line (J10 Pin50) when the DACs receive a new value. The pulse is used by the DSP to drive a counter. When the counter reaches half the FIFO size, another group of words are written to the D/A FIFO, so that the D/A FIFO will neither overflow nor underflow.

If the DAC sample rate is too fast, the DSP will not be able to write to the FIFO fast enough and a D/A FIFO underflow will occur. The slowest DAC sample rate is the daughter card clock divided by 0xFFFF. The D/A FIFO overflow can be indicated either by the status register or the XSTAT1 line (J10 Pin65). The fastest DAC sample rate for the AED_330 on the 6713 DSK in this project is set to be 9 MHz per channel. This is done by setting the DAC clock rate register of the FPGA to 9 in equation 6.1.

6.2 Test Program Source Files

Four source files are included in the test program project in CCS. They are AED_Main.c, AED_DMS_EDMA.c, AED_330.c and 6x1x_BRD.c.

6.2.1 AED_Main

This is a general purpose main program used to transfer data from the daughter card to the DSK. This file is very application independent and can be used for a number of applications without modification. It was kept unchanged in this project.

6.2.2 AED_DMS_EDMA

This source file contains functions for the configuration and control of DMA and EDMA, including register setup, transfer start and transfer type. It can sufficiently control EDMA for simple applications such as data collection and it remained the same in this project.

6.2.3 AED_330

This source file is the only one that was modified in this project. The application dependent functions included define the data processing of the daughter card. It is suggested that this file needs to be replaced to create a program for an application of the daughter card. Because it was expected to build an application which is also a combination of signal generation and data acquisition, the desired application should be similar to the test program. This file was included but reprogrammed to generate a 40

kHz sinusoid pulse for the transmitter. The real-time processing is defined in AED_330.c by five functions which are listed in Table 6.1.

Table 6.1 Daughter Board Test Program Functions

Function	Description
appl_parm()	Allows the application to define the size of the buffers, size of the transfer words and number of buffers used by the EDMA for transfer of data form the daughter card. (Printing is possible in this code)
appl_init()	Allows the application to initialize any internal data and buffers before the data transfer begins. (Printing is possible in this code)
appl_process()	Allows the application to process a frame of data which is passed to the function from the main program. This function can terminate the application with a non-zero return code. (No printing is possible in this code)
appl_idle()	Allows the application to do any background processing it wants to do between processing frames of data. This function can terminate the application with a non-zero return code. (No printing is possible in this code)
appl_end()	Allows the application to do any final processing before termination. Signal generation code is included. (Printing is possible in this code)

6.2.4 6x1x_BRD

This source file is another main program for all AED applications employing expansion memory interface for access to the daughter board. It includes daughter card dependant functions such as FPGA_enable/disable and FPGA start/stop. These functions support the other three source files and generally are not supposed to be modified for any application.

6.3 Daughter Card Clock Frequency Test

The signal generated by function appl_end() is shown in Figure 6.1. The function creates a 512 elements lookup table called DAC_table which is located in the DSPs internal memory. The digital output range is between 0x0000 and 0x0FFF. The output signal was also measured by an oscilloscope with a voltage from 0V to 1V and a frequency of 33.33 kHz. The program only reads 240 samples from the lookup table in order to avoid underflow as explained in section 5.2.6.3. Sincethe DAC sample rate is 9 MHz, then the output frequency is DAC sample rate divided by sample number per period,37.34 kHz. This conffliction was verified by changing the DSK main clock and EMIF clock frequency using PLL (Phase Locked Logic). It was found that the

frequency of the DAC output signal changes when the main DSK clock changes, but remains the same when only the frequency of EMIF changes. The daughter card uses the CLKOUT2/EMIF clock (J10 Pin78) as the conversion CLOCK which was mentioned to be CPU Clock/2 by the daughter card manual. Thus, the software code suggests the output frequency should be 112.5MHz which does not agree with either the measured 33.33kHz or calculated 37.34kHz.

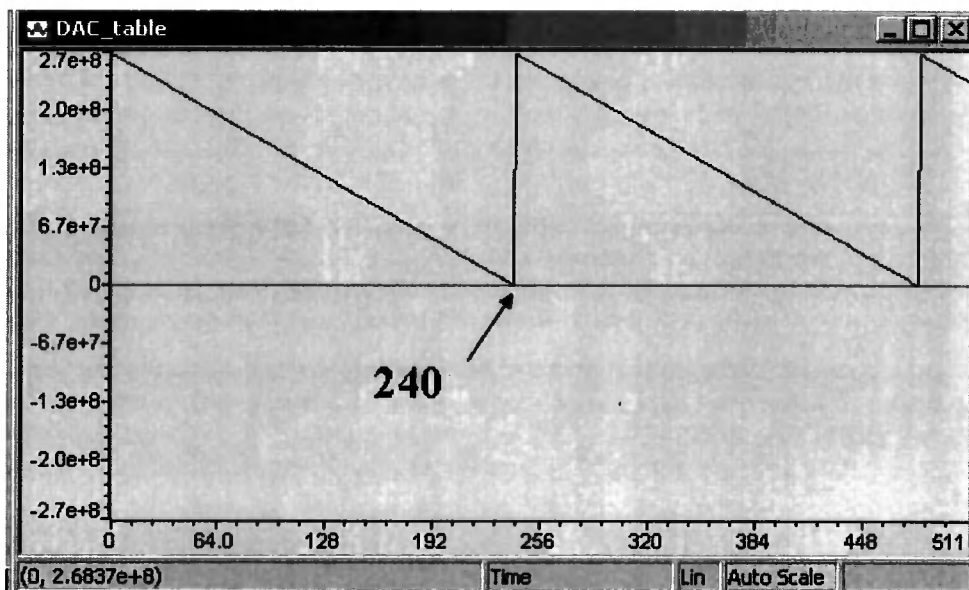


Figure 6. 1 Test Program DAC_table

The C6713 DSP is designed to operate at 225MHz with a 50MHz external oscillator. For normal operation on the 6713 DSK, the internal phased lock loop (PLL) is configured with a multiplier of 9 and a divisor of 2 to obtain the 225MHz clock from the 50MHz reference. When the DSP comes out of reset, the PLL is inactive and the 6713 runs at 50MHz. The PLL can be configured by user applications. The 6713 DSK Board Support Library initializes the PLL with the call `DSK6713_init()`. The EMIF clock rate is also determined by the PLL configuration. The EMIF has an independent divisor which can be any integral number. This can be done by programming DSK gel file. For normal DSK operation, the EMIF divisor should be 5 for a bus speed of 90MHz ($450\text{MHz} / 5$).

By calculating from the frequency of DAC output signal, with 240 samples per period and the value of DAC clock register set to be 8. An expected sample rate for the daughter card should be 80MHz. Experiments have been carried out to find out where

this sample rate derived from. EMIF frequency was tested from J10 P78 on the daughter card. It was noticed that the pin number marked on the daughter card J10 connector is wrong. The even and odd columns should be exchanged. Table 6.2 shows the frequency of the DAC output signal controlled by the PLL multiplier. Table 6.3 shows the DAC sampling frequency does not changed according to the EMIF frequency, what conflicted with the information given by the daughter card manual. The real DAC sampling frequency on the daughter card is calculated from the tested DAC frequency.

Table 6. 2 PLL Multiplier Control Daughter Card Sampling Frequency

PLL Multiplier	CPU Frequency	EMIF Frequency	DAC Frequency	Real Sampling Frequency
9 (default)	225MHz	90 MHz	33.33 kHz	8 MHz
10	250 MHz	100 MHz	36.9 kHz	8.9 MHz
11	275 MHz	110 MHz	40.59 kHz	9.7 MHz
12	300 MHz	120 MHz	44.44 kHz	10.7 MHz
13	325 MHz	130 MHz	50.10 kHz	12 MHz
14	350 MHz	140 MHz	FPGA FIFO Overflow	
15	375 MHz	150 MHz	Cannot run test program	

Table 6. 3 PLL Divider Control EMIF Frequency

PLL Divider(div3)	EMIF Frequency	DAC Frequency	Real Sampling Frequency
5	90 MHz	33.33 kHz	8 MHz
4	112.5 MHz	33.33 kHz	8 MHz
3	150 MHz	Cannot run test program	

In order to find where the daughter card DAC sampling frequency derives from, further study of the FPGA configuration is required. With the default FPGA configuration, the 40 kHz output signal can be obtained by either setting the PLL or changing the number of samples per period.

6.4 40 kHz Ultrasonic Transceiver Circuit

A 40 kHz transmitter-receiver ultrasonic system was designed and built with the DSK and the daughter card to either transmit a designed wave shape pulse signal or receive and log a signal generated by an external source. The current circuit which simply implements a transceiver system may be incomplete at the present stage and need to be improved. The 40 kHz pulser was triggered every 5 ms, giving a PRF (Pulse Repetition Frequency) of 200Hz. The receive circuit biases the received signal to 1.65V to place AC signal received in the middle of ADC input range which is from 0.6V to 2.7V. The

bias and amplify circuit is shown in Figure 6.2. This bias receiver circuit can be used for all data acquisition applications for the daughter card. Components used are listed as follow:

- SCS401T/R Ultrasonic Sensors (40 kHz)
- OPA627 op-amp $\pm 18\text{V}$ bandwidth 16MHz
- LM79-05(-5V) typical application: fixed output regulator
- Buffer op-amp OPA277
- Differential op-amp OPA105/INA105

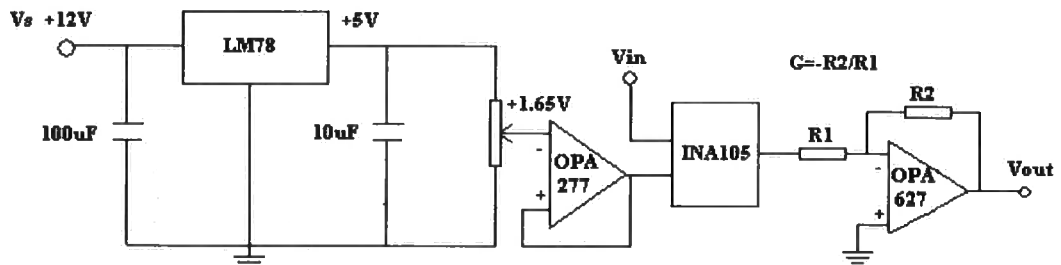


Figure 6. 2 Receive Circuit

Figure 6.3 and Figure 6.4 shows the transmitted(yellow) and received(green) signals using three periods of square wave and a half wave sine wave separately. The 40 kHz ultrasonic signals generated by the DSK were sent out from the SMB analogue port on the daughter card and reflected back from a 30 mm wall. Critical timing control based on interrupt programming was investigated and tried but a synchronously transceiver system was not successfully achieved. More software programming work is required in this part to build a complete ultrasonic detection system to implement the NPD algorithm.

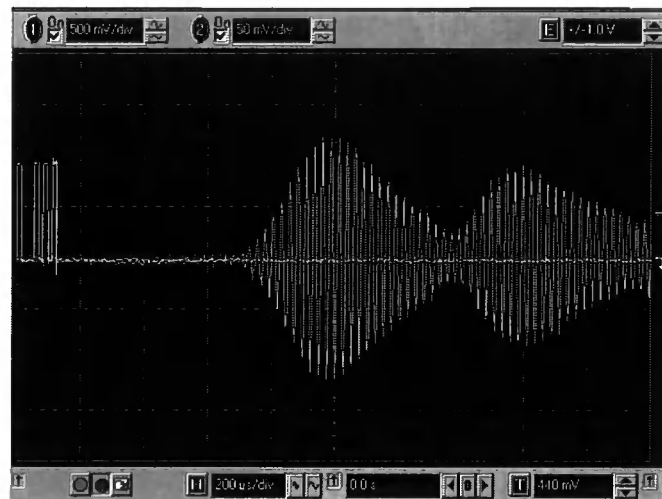


Figure 6. 3 Tx-Rx using 3 Periods Square Wave

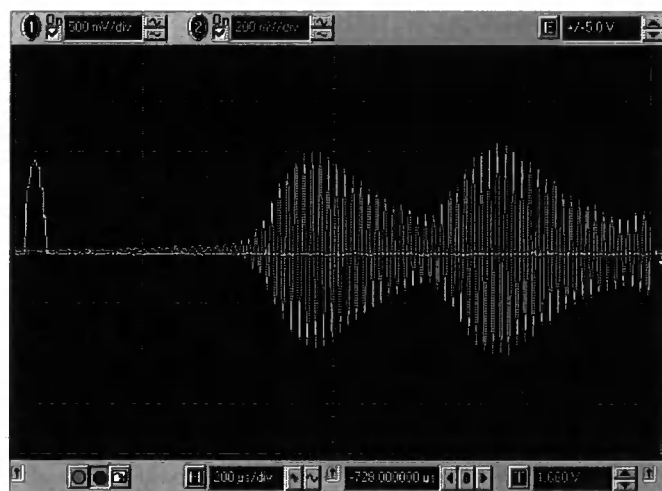


Figure 6. 4 Tx-Rx using Half Period Sine Wave

6.5 High Voltage High Frequency (HVHF) Amplifier

A high-voltage driver is needed to drive the very low impedance transducer described in chapter 2. The challenge is to boost the output of a conventional amplifier to high voltages. Effort has been made to find a commercial instrument or op amp to meet the high voltage high frequency requirement. However, available AC high-voltage amplifier modules are limited to low frequency ranges. Hence, a custom amplifier is designed, the design idea of which presents a simplified AC high-voltage amplifier that uses an n-channel MOSFET.

A basic single stage class A amplifier was designed. Class A amplifiers amplify over the whole of the input cycle. They are the usual means of implementing small-signal amplifiers. They are not very efficient—a theoretical maximum of 50% is obtainable, but for small signals, this waste of power is still extremely small, and can easily be tolerated. It is only when we need to create output powers with appreciable levels of voltage and current does Class A become problematic. In a Class A circuit, the amplifying element is biased such that the device is always conducting to some extent, and is operated over the most linear portion of its characteristic curve – transfer function. Because the device is always conducting, even if there is no input at all, power is wasted. This is the reason for its inefficiency[37].

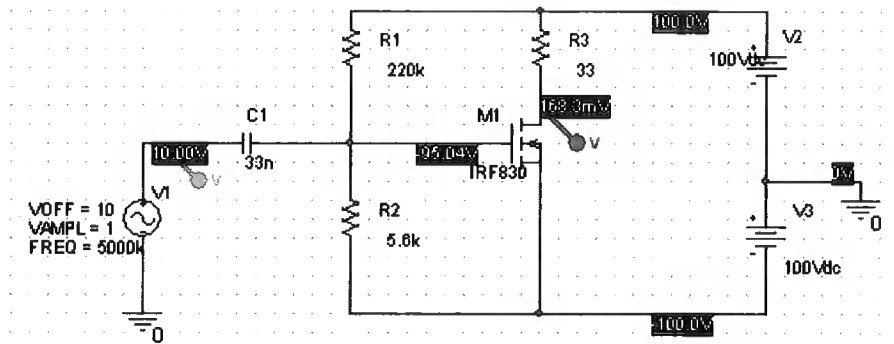


Figure 6. 5 Custom Amplifier Circuit

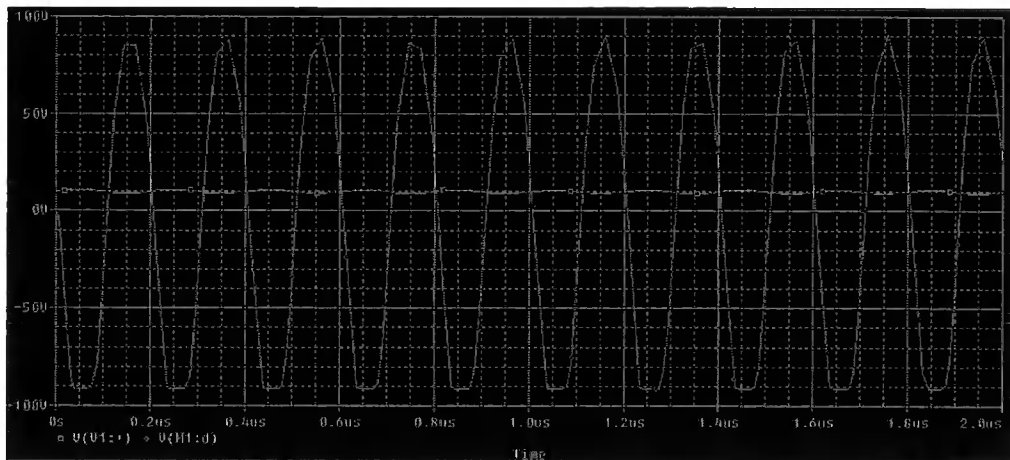


Figure 6. 6 PSPICE Simulation Result

ORCAD and PSPICE design and simulation packages were used to reduce the amount of testing required after construction and allow component values to be selected and tested much quicker and more safely than on a PCB. The bias-voltage circuit shown in

Figure 6.5 comprises a biasing-resistor pair R1 and R2; the result is a symmetrical output with zero central voltage. Figure 6.6 shows a sinusoidal input of 1V p-p at 5000 kHz (5MHz) and an output of 180V p-p. The AC gain of the signal stage amplifier is approximately 200.

The PCB has not been built because of the high power dissipation of the circuit which requires improvement. The resistor R3 and the transistor would get very hot with over 300 W dissipated in each. Heat generation can impair circuit operation. Circuits operate slower at high temperatures, and have a reduced reliability. Hence, a heat sink is essential for the IRF830 circuit. The unsatisfactory aspects of the amplifier design require were considered and a push-pull amplifier can be a solution to this problem. On the other hand, an instrument amplifier could be another efficient solution as op-amps provide more flexibility and better performance for amplification circuit.

6.6 Summary

This chapter includes work carried out in applying the DSK and daughter card to transmit and receive signals from ultrasonic transducers with the ultimate aim of applying NPD in real-time. The test program of the daughter card was discussed in detail based on the default FPGA configuration. This FPGA configuration was to be revised in further research to gain a higher sampling frequency per channel for both ADCs and DACs on the daughter card. A voltage bias and amplification circuit was built for the daughter card ADCs to receive signals within the range between 0.6V and 2.7V. To test the basic principles, a 40 kHz system was investigated in which analogue interfacing hardware was designed and implemented. A high speed (MHz) high voltage amplifier was designed but not implemented during this project.

CHAPTER 6

AED330 Daughter Card Experiments

This chapter describes a daughter card test program for testing the features of onboard components and the data transition between the DSP core on the DSK and signal converters on the daughter card based on the default FPGA configuration. The program was revised to generate an output 40 kHz signal with various waveforms. A custom circuit was then built to amplify and bias the output signal such that it could be received within the range (0.6 V to 2.7 V) of one of the ADCs.

The test program is written in ANSI C and is intended to provide an initial test for the board to show that the mixed signal part and the FPGA are working. This program is primarily for hardware operation and it does not use either DSP/BIOS or CSL. It is suggested by Signalware, the producer of the expansion daughter card that these support tools should be used in developing custom applications[26].

6.1 Test Program Description

In the test program, interfaces are mapped into the daughter card memory space using the EMIF. The definition of the interface consists of addresses and data transferred over the EMIF. These addresses are relative locations within the daughter card memory space. The location of the daughter card memory space is EMIF CE2 defined by the memory map of the C6713 DSK starting at 0xA0000000. These addresses can be read and written directly from the DSPs. In this project EDMA is required to access high speed mixed signal devices at these addresses.

The test program provides a framework to develop DSP code for the daughter card. This program controls the hardware directly to attain a very high speed. It uses EMIF to transfer data from the ADC to the DSP and uses EDMA channel to transfer the data without interrupting the CPU. The CPU only processes when a block of data is ready.

The test program can use either the EMIF bus or the McBSP (for lower speed devices on the selected daughter card) to transfer data to D/A devices.

The test program is a data acquisition and signal generation program. Because the EMIF data bus has a limited bandwidth, the program runs the ADCs and DACs separately to attain higher sampling rate rather than running all converters simultaneously. There are three steps for this program.

1. The test program first reads data from the ADCs, stores some samples and sums a large number of samples to get information on the operation of the ADCs. It sets up the EDMA registers, starts the EDMA, starts the FPGA and waits for interrupts indicating a frame of data is ready. It writes a 0x0100 to the Start and Period Registers, so that every time it sees a rising edge on the interrupt line, it reads 256 words from the A/D FIFO. If the A/D clock rate is set too fast, the DMA will not be able to keep up with reading the samples and the A/D FIFO will overflow. The A/D FIFO overflow can be indicated either by the status register or the XSTAT0 line (J10 Pin66). The fastest A/D sample rate for the AED_330 on the 6713 DSK in this project is set to be 10 MHz per channel. This is done by set the ADC clock rate register of the FPGA to 8 in equation 6.1.

$$\text{ADC or ADC clock rate} = \text{Conversion CLOCK} / (\text{ADC_CLK_REG} + 1) \dots (6.1)$$

According the daughter card manual, the conversion clock should equal to the onboard EMIF clock which is 90 MHz. However, the test program provided showed ambiguous information which conflicted with the user manual. Tests were made to find out the clock frequency the daughter card used and the result is discussed later.

2. After taking in several frames of data from the A/D FIFO, the DSP sets the XCNTL0 (J10 Pin64) line low to stop the ADC and print the data acquired. Then it operates the digital I/O in a pattern that allows each bit to be activated individually for output for about 0.5 second.

3. Finally, the program generates a waveform with the DACs which can be observed with an oscilloscope. The DSP writes the words to fill the D/A FIFO. Then the XCNTL0 line is set to high again to start the DACs. The previous written data is transferred from the D/A FIFO to the DACs. A pulse is sent to the DSP on the TINP1

line (J10 Pin50) when the DACs receive a new value. The pulse is used by the DSP to drive a counter. When the counter reaches half the FIFO size, another group of words are written to the D/A FIFO, so that the D/A FIFO will neither overflow nor underflow.

If the DAC sample rate is too fast, the DSP will not be able to write to the FIFO fast enough and a D/A FIFO underflow will occur. The slowest DAC sample rate is the daughter card clock divided by 0xFFFF. The D/A FIFO overflow can be indicated either by the status register or the XSTAT1 line (J10 Pin65). The fastest DAC sample rate for the AED_330 on the 6713 DSK in this project is set to be 9 MHz per channel. This is done by setting the DAC clock rate register of the FPGA to 9 in equation 6.1.

6.2 Test Program Source Files

Four source files are included in the test program project in CCS. They are AED_Main.c, AED_DMS_EDMA.c, AED_330.c and 6x1x_BRD.c.

6.2.1 AED_Main

This is a general purpose main program used to transfer data from the daughter card to the DSK. This file is very application independent and can be used for a number of applications without modification. It was kept unchanged in this project.

6.2.2 AED_DMS_EDMA

This source file contains functions for the configuration and control of DMA and EDMA, including register setup, transfer start and transfer type. It can sufficiently control EDMA for simple applications such as data collection and it remained the same in this project.

6.2.3 AED_330

This source file is the only one that was modified in this project. The application dependent functions included define the data processing of the daughter card. It is suggested that this file needs to be replaced to create a program for an application of the daughter card. Because it was expected to build an application which is also a combination of signal generation and data acquisition, the desired application should be similar to the test program. This file was included but reprogrammed to generate a 40

kHz sinusoid pulse for the transmitter. The real-time processing is defined in AED_330.c by five functions which are listed in Table 6.1.

Table 6.1 Daughter Board Test Program Functions

Function	Description
appl_parm()	Allows the application to define the size of the buffers, size of the transfer words and number of buffers used by the EDMA for transfer of data form the daughter card. (Printing is possible in this code)
appl_init()	Allows the application to initialize any internal data and buffers before the data transfer begins. (Printing is possible in this code)
appl_process()	Allows the application to process a frame of data which is passed to the function from the main program. This function can terminate the application with a non-zero return code. (No printing is possible in this code)
appl_idle()	Allows the application to do any background processing it wants to do between processing frames of data. This function can terminate the application with a non-zero return code. (No printing is possible in this code)
appl_end()	Allows the application to do any final processing before termination. Signal generation code is included. (Printing is possible in this code)

6.2.4 6x1x_BRD

This source file is another main program for all AED applications employing expansion memory interface for access to the daughter board. It includes daughter card dependant functions such as FPGA_enable/disable and FPGA start/stop. These functions support the other three source files and generally are not supposed to be modified for any application.

6.3 Daughter Card Clock Frequency Test

The signal generated by function appl_end() is shown in Figure 6.1. The function creates a 512 elements lookup table called DAC_table which is located in the DSPs internal memory. The digital output range is between 0x0000 and 0x0FFF. The output signal was also measured by an oscilloscope with a voltage from 0V to 1V and a frequency of 33.33 kHz. The program only reads 240 samples from the lookup table in order to avoid underflow as explained in section 5.2.6.3. Sincethe DAC sample rate is 9 MHz, then the output frequency is DAC sample rate divided by sample number per period,37.34 kHz. This conffliction was verified by changing the DSK main clock and EMIF clock frequency using PLL (Phase Locked Logic). It was found that the

frequency of the DAC output signal changes when the main DSK clock changes, but remains the same when only the frequency of EMIF changes. The daughter card uses the CLKOUT2/EMIF clock (J10 Pin78) as the conversion CLOCK which was mentioned to be CPU Clock/2 by the daughter card manual. Thus, the software code suggests the output frequency should be 112.5MHz which does not agree with either the measured 33.33kHz or calculated 37.34kHz.

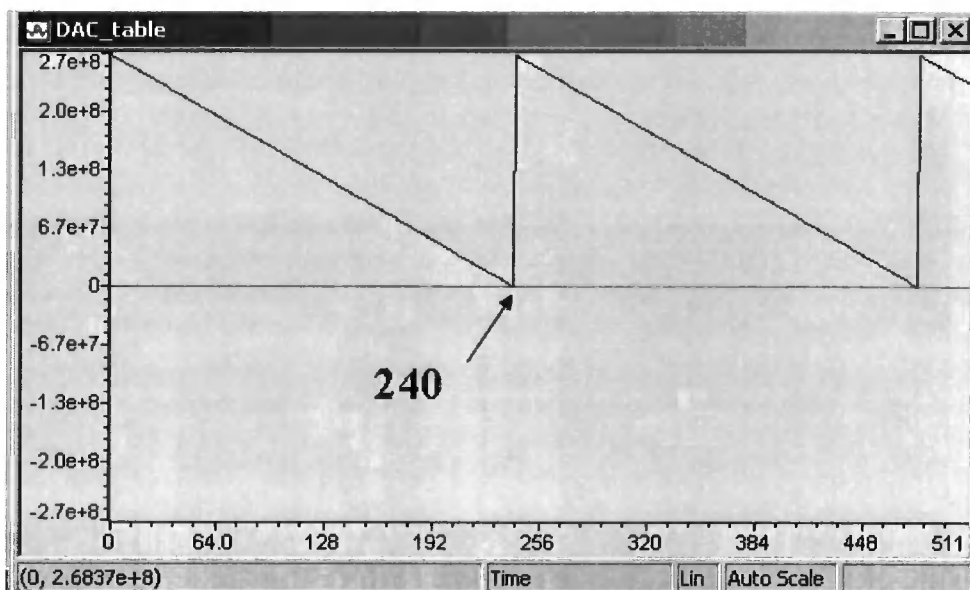


Figure 6. 1 Test Program DAC_table

The C6713 DSP is designed to operate at 225MHz with a 50MHz external oscillator. For normal operation on the 6713 DSK, the internal phased lock loop (PLL) is configured with a multiplier of 9 and a divisor of 2 to obtain the 225MHz clock from the 50MHz reference. When the DSP comes out of reset, the PLL is inactive and the 6713 runs at 50MHz. The PLL can be configured by user applications. The 6713 DSK Board Support Library initializes the PLL with the call `DSK6713_init()`. The EMIF clock rate is also determined by the PLL configuration. The EMIF has an independent divisor which can be any integral number. This can be done by programming DSK gel file. For normal DSK operation, the EMIF divisor should be 5 for a bus speed of 90MHz ($450\text{MHz} / 5$).

By calculating from the frequency of DAC output signal, with 240 samples per period and the value of DAC clock register set to be 8. An expected sample rate for the daughter card should be 80MHz. Experiments have been carried out to find out where

this sample rate derived from. EMIF frequency was tested from J10 P78 on the daughter card. It was noticed that the pin number marked on the daughter card J10 connector is wrong. The even and odd columns should be exchanged. Table 6.2 shows the frequency of the DAC output signal controlled by the PLL multiplier. Table 6.3 shows the DAC sampling frequency does not change according to the EMIF frequency, what conflicted with the information given by the daughter card manual. The real DAC sampling frequency on the daughter card is calculated from the tested DAC frequency.

Table 6. 2 PLL Multiplier Control Daughter Card Sampling Frequency

PLL Multiplier	CPU Frequency	EMIF Frequency	DAC Frequency	Real Sampling Frequency
9 (default)	225MHz	90 MHz	33.33 kHz	8 MHz
10	250 MHz	100 MHz	36.9 kHz	8.9 MHz
11	275 MHz	110 MHz	40.59 kHz	9.7 MHz
12	300 MHz	120 MHz	44.44 kHz	10.7 MHz
13	325 MHz	130 MHz	50.10 kHz	12 MHz
14	350 MHz	140 MHz	FPGA FIFO Overflow	
15	375 MHz	150 MHz	Cannot run test program	

Table 6. 3 PLL Divider Control EMIF Frequency

PLL Divider(div3)	EMIF Frequency	DAC Frequency	Real Sampling Frequency
5	90 MHz	33.33 kHz	8 MHz
4	112.5 MHz	33.33 kHz	8 MHz
3	150 MHz	Cannot run test program	

In order to find where the daughter card DAC sampling frequency derives from, further study of the FPGA configuration is required. With the default FPGA configuration, the 40 kHz output signal can be obtained by either setting the PLL or changing the number of samples per period.

6.4 40 kHz Ultrasonic Transceiver Circuit

A 40 kHz transmitter-receiver ultrasonic system was designed and built with the DSK and the daughter card to either transmit a designed wave shape pulse signal or receive and log a signal generated by an external source. The current circuit which simply implements a transceiver system may be incomplete at the present stage and need to be improved. The 40 kHz pulser was triggered every 5 ms, giving a PRF (Pulse Repetition Frequency) of 200Hz. The receive circuit biases the received signal to 1.65V to place AC signal received in the middle of ADC input range which is from 0.6V to 2.7V. The

bias and amplify circuit is shown in Figure 6.2. This bias receiver circuit can be used for all data acquisition applications for the daughter card. Components used are listed as follow:

- SCS401T/R Ultrasonic Sensors (40 kHz)
- OPA627 op-amp $\pm 18\text{V}$ bandwidth 16MHz
- LM79-05(-5V) typical application: fixed output regulator
- Buffer op-amp OPA277
- Differential op-amp OPA105/INA105

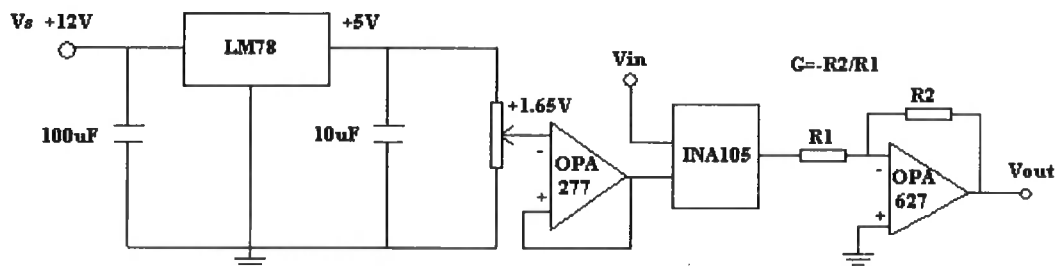


Figure 6. 2 Receive Circuit

Figure 6.3 and Figure 6.4 shows the transmitted(yellow) and received(green) signals using three periods of square wave and a half wave sine wave separately. The 40 kHz ultrasonic signals generated by the DSK were sent out from the SMB analogue port on the daughter card and reflected back from a 30 mm wall. Critical timing control based on interrupt programming was investigated and tried but a synchronously transceiver system was not successfully achieved. More software programming work is required in this part to build a complete ultrasonic detection system to implement the NPD algorithm.

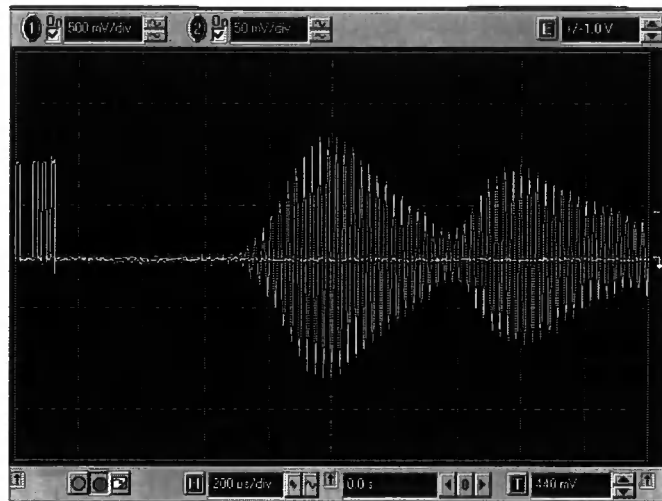


Figure 6. 3 Tx-Rx using 3 Periods Square Wave

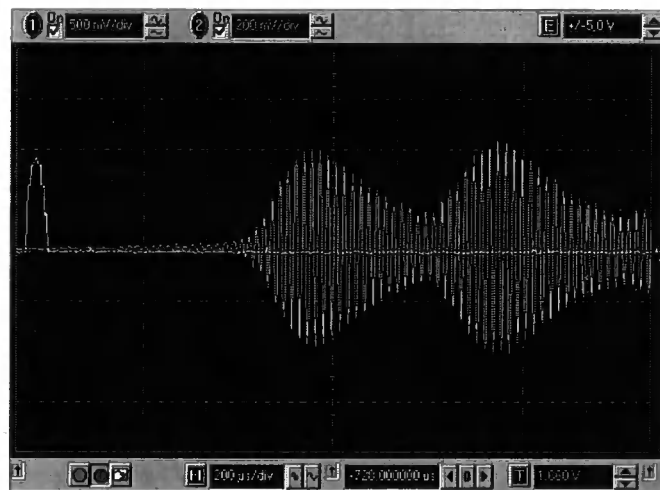


Figure 6. 4 Tx-Rx using Half Period Sine Wave

6.5 High Voltage High Frequency (HVHF) Amplifier

A high-voltage driver is needed to drive the very low impedance transducer described in chapter 2. The challenge is to boost the output of a conventional amplifier to high voltages. Effort has been made to find a commercial instrument or op amp to meet the high voltage high frequency requirement. However, available AC high-voltage amplifier modules are limited to low frequency ranges. Hence, a custom amplifier is designed, the design idea of which presents a simplified AC high-voltage amplifier that uses an n-channel MOSFET.

A basic single stage class A amplifier was designed. Class A amplifiers amplify over the whole of the input cycle. They are the usual means of implementing small-signal amplifiers. They are not very efficient—a theoretical maximum of 50% is obtainable, but for small signals, this waste of power is still extremely small, and can easily be tolerated. It is only when we need to create output powers with appreciable levels of voltage and current does Class A become problematic. In a Class A circuit, the amplifying element is biased such that the device is always conducting to some extent, and is operated over the most linear portion of its characteristic curve – transfer function. Because the device is always conducting, even if there is no input at all, power is wasted. This is the reason for its inefficiency[37].

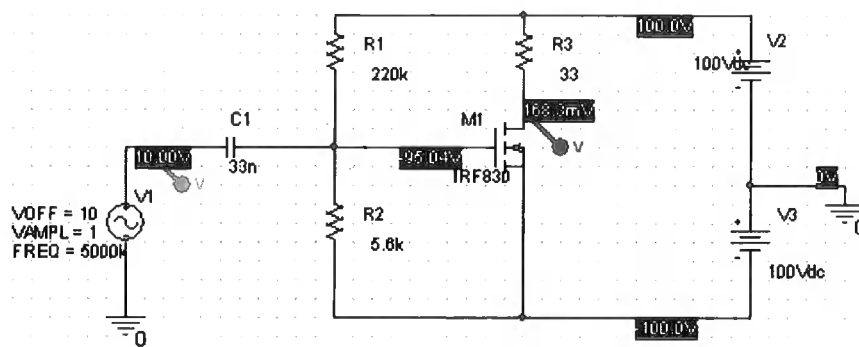


Figure 6. 5 Custom Amplifier Circuit

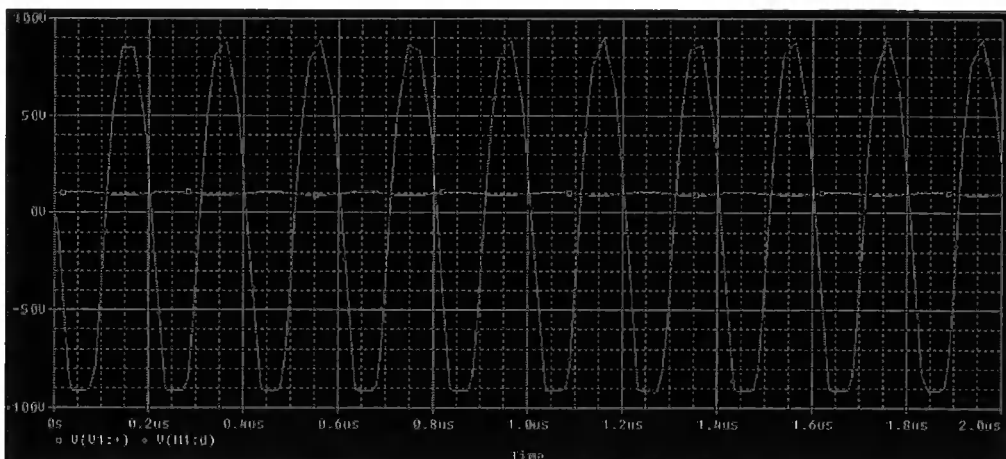


Figure 6. 6 PSPICE Simulation Result

ORCAD and PSPICE design and simulation packages were used to reduce the amount of testing required after construction and allow component values to be selected and tested much quicker and more safely than on a PCB. The bias-voltage circuit shown in

Figure 6.5 comprises a biasing-resistor pair R1 and R2; the result is a symmetrical output with zero central voltage. Figure 6.6 shows a sinusoidal input of 1V p-p at 5000 kHz (5MHz) and an output of 180V p-p. The AC gain of the signal stage amplifier is approximately 200.

The PCB has not been built because of the high power dissipation of the circuit which requires improvement. The resistor R3 and the transistor would get very hot with over 300 W dissipated in each. Heat generation can impair circuit operation. Circuits operate slower at high temperatures, and have a reduced reliability. Hence, a heat sink is essential for the IRF830 circuit. The unsatisfactory aspects of the amplifier design require were considered and a push-pull amplifier can be a solution to this problem. On the other hand, an instrument amplifier could be another efficient solution as op-amps provide more flexibility and better performance for amplification circuit.

6.6 Summary

This chapter includes work carried out in applying the DSK and daughter card to transmit and receive signals from ultrasonic transducers with the ultimate aim of applying NPD in real-time. The test program of the daughter card was discussed in detail based on the default FPGA configuration. This FPGA configuration was to be revised in further research to gain a higher sampling frequency per channel for both ADCs and DACs on the daughter card. A voltage bias and amplification circuit was built for the daughter card ADCs to receive signals within the range between 0.6V and 2.7V. To test the basic principles, a 40 kHz system was investigated in which analogue interfacing hardware was designed and implemented. A high speed (MHz) high voltage amplifier was designed but not implemented during this project.

CHAPTER 7

Conclusion and Further Research

7.1 Conclusion

In this thesis, research covered two main areas, ultrasonic testing and the development of a real-time DSP system. In the first area, the principle of ultrasonic testing and its utilities in the realm of industry was introduced; descriptions of typical ultrasonic transducers, current ultrasonic testing methods and the structure of a PC based ultrasonic testing system were also included in order to demonstrate a new ultrasonic testing technique, Normal Probe Diffraction (NPD), which was presented and compared with the conventional pulse-echo method and the state of the art Time of Flight Diffraction (TOFD) method.

The second part gave an overview of real-time DSP systems including hardware and software and a rapid prototype for the implementation of various DSP applications. The rapid prototype of a low frequency system was implemented on the TI TMS320C6713 DSK, which is a DSP development tool containing one of the latest floating point digital signal processors, TMS320C6713. The foundation of the DSK hardware was also examined. This prototype is especially suitable for audio processing as the on-board codec was configured to run at several typical frequencies for sampling audio signals. A high sample rate was gained by adding an analogue expansion daughter card which mainly contains two ADCs, two DACs and an FPGA. The rapid prototyping system using MATLAB Simulink model does not support the third part commercial daughter card and it had to be programmed using C language in the Code Composer Studio environment.

In conclusion, research of the NPD technique, DSPs architectures and programming methods has been done and a simulated system model has been built and analysed. The aim of this project was to implement the NPD algorithm in real time and the project was scheduled based on using the rapid prototype to automatically generate executive code

from Simulink Model without complex C programming. The author found that it was a very challenging task to compile the desired software code onto the expansion daughter card within a couple of months without sufficient and effective technical support from the daughter card producer. Abundant TI manuals are required for the fully understanding of the functionalities of DSK hardware components and software programming. The aim of the project was not fulfilled partly because the author lacked the ultrasonic testing knowledge and was unfamiliar with the CCS program. However, the author has learnt a lot ultrasonic testing knowledge, DSP system architecture and C programming from this project and it is believed that this project would be fully completed if an extension on the due date is applied.

7.2 Further Research

Further research leading from this project include,

- Daughter card driver design and Software Program
- FPGA Configuration
- Real-time NPD Implementation

Several problems were encountered during the hardware and software development and further research is required to solve these problems and complete the project. The further research includes the hardware driver design and software programme for the third party expansion daughter card; FPGA configuration and programming for various applications of the DSK – daughter card system; the implementation and the efficiency analysis of the NPD algorithm.

Daughter card driver design and Software Program

The daughter card was only supplied with a software program to test the hardware was functioning correctly. A generic device driver for the daughter card was not provided to use the card with the DSK board. The required driver therefore, needs to be written in conformance to the DSP/BIOS IOM device driver model and handles communication to and from the McBSP, and uses the EDMA to transfer the data[38]. Timer and Interrupt configurations are also needed for the software program. Further study in software programming and DSP/BIOS tools will be indispensable to complete this part.

FPGA Configuration

The method used to configure the Vertex E FPGA on the AED_330 daughter card is to use the Xilinx iMPACT tool in the boundary scan mode (JTAG). The reconfiguration of the FPGA was not tried but it could be another challenge to improve the flexibility of the real-time DSP system.

Real-time NPD Implementation

It was supposed that a real-time NPD system could be developed by designing a Simulink Model from which executive code could be generated directly and can be downloaded to the DSK board to implement the NPD algorithm in real-time using MATLAB Real-Time Workshop toolbox. The MATLAB Embedded target for TIC6713 DSP, the software bridge between MATLAB and the C6713 DSK should make it possible to smoothly and incrementally transition from Simulink model to full hardware implementation. However, this method was found to be unsuitable for this project since Real-time Workshop did not include blocks to communicate with third party daughter cards. Custom blocks could be written, but it is debateable whether this would be more efficient than using the CCS IDE directly to create the application. Thus, it is suggested that further development is carried out using CCS projects.

The real-time system will lead to a great improvement in verifying and realising NPD. The system will make the experiment data easy to be acquired, analysed and visualised.

References

- [1] Rose, J.L., *Ultrasonic Waves in Solid Media*. 1999, Cambridge: Cambridge University Press.
- [2] Halmshaw, R., *Mathematics and Formulae in NDT*. 2nd ed. 1993, Northampton: The British Institute of Non-Destructive Testing.
- [3] *Nondestructive Material Testing with Ultrasonics, The e-Journal of Nondestructive Testing & Ultrasonics-ISSN:1435-4934, Issue Vol. 5 No. 9 - September 2000*
- [4] Zhang, G. Hu, H. and Ta, D., *Ultrasonic Detection of the Metallurgical Defects in the Steel and its Evaluation by Neural Network Based on the Wavelet Transform Noise Suppression*, *Kdy Engineering Materials Vols. 270-273 (2004)* pp. 160-167
- [5] Wolfram, A. *Automated ultrasonic inspection. WCNDT conference. 2000. Rome, Italy*
- [6] Shin, B.-C. and J.-R.Kwon, *Ultrasonic transducers for continuous-cast billets. Sensors and Actuators A: Physical*, 1996. 51:p.173-177.
- [7] Kiessling, R., *Non-metallic inclusions in steel*. 1989, London: The Institute of Metals.
- [8] Dekkers, R., *Non-metallic inclusions in steel*. 2002, Katholieke Universiteit Leuven: Leuven. P. 7.
- [9] Singh, B. and S.K. Kaushik, *Influence of steel-making processes on the quality of reinforcement. The Indian Concrete Journal*, 2002(July): p. 407-412
- [10] P C Snowdon, S Johnstone, S Dewey, *A 2D static ultrasonic array of passive probes for improved Probability of Detection, Nondestructive Testing and Evaluation*, 19(3), pp. 111-120, 2003
- [11] R. Venteris, (2002) *Exploration of DSP architectures in ultrasonic measurement application, Ultragarsas Journal* 42(1)
- [12] M. Lach, M. Platte, A. Ries, *Piezoelectric materials for ultrasonic probes, NDTnet - September 1996, Vol.1 No.09*
- [13] *Nondestructive Material Testing with Ultrasonics, The e-Journal of Nondestructive Testing & Ultrasonics-ISSN:1435-4934, Issue Vol. 5 No. 9 - September 2000*
- [14] *The British TOFD standard BS 7706: Guide to Calibration and setting-up of the Ultrasonic Time of Flight diffraction (TOFD) technique for defect detection, location and sizing of defects.*
- [15] P C Snowdon, S Johnstone and S Dewey, "Improving the probability of detection for a 2D ultrasonic array using digital signal processing techniques" *Insight Vol 45 No 11 November 2003, P743-745*
- [16] Chen, C.-T., *Digital Signal Processing: Spectral Computation & Filter Design*. 2001, New York, U.S.A. , Oxford University Press.
- [17] Webb, P. and Wykes, C. (1995) "Suppression of second-time-around echoes in high firing rate ultrasonic transducers", *NDT & E International* 28(2), 89-93.
- [18] *Creating Graphical User Interfaces, The MathWorks, 2005*

- [19] L.M. Reyneri, A Simulink-based hybrid codesign tool for rapid prototyping of FPGA's in signal processing systems, *Microprocessors and Microsystems* 28(2004) 273-289
- [20] Using Simulink, The MathWorks, 2005.
- [21] Steven W. Smith, *Digital Signal Processing: A Practical Guide for Engineers and Scientists*, Newnes, 2003
- [22] Texas Instruments Inc., TMS320C6713 DSK Technical Reference, 2004.
- [23] Texas Instruments Inc., TMS320C6000 32Bit Timer Reference Guide, SPRU582A, Dallas, TX, Mar 2004.
- [24] Texas Instruments Inc., DSP/BIOS Timers and Benchmarking Tips, SPRA829, Dallas, TX, July 2002.
- [25] Micron Technology, Inc., 64Mb: x32 SDRAM Datasheet, 2000
- [26] Documentation Package for AED-330 Multi-Purpose Flex Analog Expansion Daughter card, Signalware Corporation, 2003.
- [27] Texas Instruments Inc., THS5661 12-BIT, 100 MSPS, DIGITAL-TO-ANALOG CONVERTER datasheet
- [28] Signalware Corporation, Document Package for AED Custom Modification
- [29] Texas Instruments Inc., Code Composer Studio Getting Started Guide, SPRU509C, 2001
- [30] Texas Instruments Inc., TMS320 DSP/BIOS User's Guide, SPRU423B, 2002
- [31] Texas Instruments Inc., TMS320C6000 DSP/BIOS API Reference Guide, SPRU403F, Dallas, TX, Apr 2003.
- [32] Texas Instruments Inc., TMS320C6000 Chip Support Library API Reference Guide, SPRU401I, Dallas, TX, May 2004.
- [33] Spectrum Digital Inc., TMS320C6713 DSK On-line Tutorial, Stafford, TX, May 2003.
- [34] Texas Instruments Inc., TMS320C67x Fast RTS Library Programmer's Reference, SPRU100A, Dallas, TX, Oct 2002.
- [35] Texas Instruments Inc., TMS3206000 Peripherals Reference Guide, SPRU190D, Dallas, TX, Feb 2001.
- [36] The MathWorks, Inc. Embedded Target for Texas Instruments C6000 DSPs User's Guide.
- [37] Adel S. Sedra, Kenneth C. Smith, *Microelectronics Circuits*, Fifth Edition, Oxford University Press, 2004
- [38] Texas Instruments Inc., A DSP/BIOS EDMA McBSP Device Driver for TMS320C6x1x DSPs, SPRA846, Dallas, TX, Dec 2002.

Normal Probe Diffraction – Improving the capability of industrial ultrasonic probe arrays

Lei Zhang, Sherri Johnstone, Paul Snowdon, School of Engineering, University of Durham, DH1 3LE
Steve Dewey, STC, Rotherham, Corus

Abstract

In bloom and billet mills, on-line defect detection systems exist, in which each probe is sequentially used to produce a radio frequency pulse, which is then reflected from the defect and detected by the same probe. The work carried out in this project shows that extra information can be obtained about the defect if the diffracted signal is also collected by neighbouring probes and digital signal processing algorithms are applied to improve the signal to noise ratio. This technique is similar to time-of-flight diffraction, but does not require angled probes, and is thus referred to as normal probe diffraction, NPD. The advantage of this method is that it is possible to apply it in real-time thus giving the possibility of improved on-line defect detection, sizing and orientation. This paper describes the physical principles of NPD together with the hardware and software development required to implement the system in real time. The results on a simulated defect show that it can be detected from a distance of 41mm using NPD as opposed to 15mm with the sequential single probe pulse-echo method.

Key words: Normal Probe Diffraction (NPD), Digital Signal Processing (DSP), real-time, ultrasonic detection, non-destructive testing (NDT)

1. Introduction

The defects of steel mainly include inclusions, bubbles and cracks, all of which can affect the quality of the steel to some degree, therefore their detection and recognition is becoming increasingly significant, due to the customer lead demand for higher quality products. In steelmaking, on-line defect position and real-time size detection are desired. Many methods have been tried and developed for achieving a reliable cost-effective solution. Ultrasonic detection is commonly used in this field of non-destructive testing (NDT) in the steel industry. Traditional ultrasonic defect detection systems use an array of probes in which each probe pulses and receives sequentially. One new ultrasonic detection technology-Normal Probe diffraction (NPD) has been proven to enhance the probability of detection for steel testing in the previous research[1]. In this work, the necessary real-time system is simulated with software and the corresponding hardware is to be realised and tested to demonstrate the result. In order to gain the best testing effect, an ultrasonic pulser is designed to generate a variable frequency and pulse shape which can be completely and flexibly controlled in real-time. A high voltage power amplifier is also designed to get a good response from the transducers. To remove the randomly distributed background noise that disturbs the recognition of the defect echoes and increase the behaviour of the system, several Digital Signal Processing (DSP) algorithms are applied and different filters can be chosen for real-time analysis

as well. The developed real-time system will help increase the probability of detection of defects in steel billets and produce low-cost system solution for ultrasonic billet inspection in steel industry.

2. Previous Research

The previous research has investigated the potential within a current multi-probe ultrasonic detection system installed at a steel mill. Extensive laboratory experiments were carried out using the transducer array geometry, to extract additional information from passive probes. The apparatus was set up as shown in Figure1 [2].

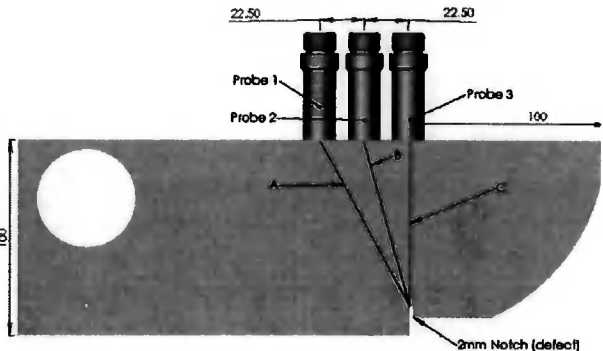


Figure 1 Probe Geometry

Figure 2 shows the increase of probability of detection using the standard single-probe-multi-receiver (SPMR) system over the conventional single-probe-single-receiver (SPSR) system. It shows that the NPD system starts detecting the defect at a lateral distance of 41mm from the defect

whereas the pulse-echo probe needs to be within a range of 15mm. The physical principle behind this system uses diffracted waves from the edge of the defects and thus it is particularly effective for the increased detection and sizing of centre-line defects. This technique is defined as Normal Probe

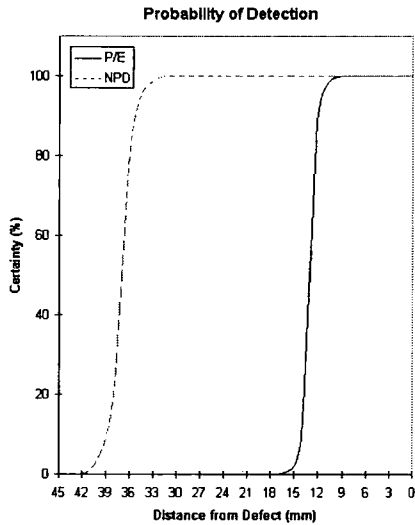


Figure 2 Comparison of Detection Range for NPD and Pulse-Echo techniques

Diffraction (NPD), which has been successfully applied offline on a V1 calibration block and a single billet, but has not yet been applied for real-time control.

Experiments show that the defect detection range can be increased by collecting the diffracted pulse on all the neighbouring probes. This is due to the defect being detected several times per pulse. The research project involves in developing a real-time laboratory based prototype which can detect defects using two methods: the standard single probe pulse echo technique and NPD, and testing the system on a V1 calibration block and a steel billet. In this project, the transmitting and receiving electronics are developed to enable the NPD technique to be applied in real-time.

3. Real Time Implementation

A good real-time implementation should be reliable, low power consuming, compact and always runs in real-time[3]. Sufficient amount of instructions per second and quick enough transport speed must be considered and calculated during the design procedure to meet the requirement of short delays between inputs and outputs in real-time implementation.

This system uses general purpose digital signal processing microprocessors for solving signal processing problems in real-time, particularly focus on using the Texas Instruments (TI) TMSC6713 DSK (Digital Signal Processing Starter Kit) with the C6713 kernel floating processor to implement programs written in assembly and C. The TI C6713 DSK is for general real-time signal processing applications. The main applications taking place in this project are digital filter design using different DSP algorithms. These filters are characterized and applied on the received data. TI Hardware/software development tools (Code Composer Studio and DSP/BIOS) provide I/O channels for data exchange with Matlab in real-time.

System testing applies MATLAB and Simulink including several toolboxes. The MATLAB Embedded Target for TI C6000 DSP enables the rapid prototyping of real-time software for C6713 floating-point processor and generates efficient code for the processor directly from a Simulink model using MATLAB Real-Time Workshop. The generated code is readable and editable, and the code profiler identifies regions of generated code that may benefit from manual optimization. The Embedded Target for TI C6000 DSP automates the creation of Link for Code Composer Studio project, provides board support for the C6713 DSK board, invokes Link for Code Composer Studio to create a DSP executable and downloads the executable to the DSK board for real-time algorithm evaluation. It also employs the link to enable interactive debugging and systematic testing of the DSP programs.

4. System Architecture

The system is available for testing single input and output channels with dual transducers (transmitter/receiver) and can be expanded for multi-channel testing as well. This system combines analogue and digital electronics technology together. The digital part consists of pulser generation and signal processing, while the analog part includes pulse amplification and A/D (Analog-to-Digital), D/A (Digital-to-Analog) conversion. A single channel system is illustrated in figure 3. The digital pulse signal generated by C6713DSK, with a variable pulse repetition frequency (PRF), is converted to analogue signal by AED330 analog daughtercard and amplified by a high voltage high frequency amplifier. The custom amplifier is designed and fabricated to give out a high voltage



Figure 3 Single Channel Test System Block Diagram

output above 200V. The echoed signal is received, digitised and buffered for the further use of data analysis by a program loaded on the DSK. The program implements the functions of frequency spectrum analysis, an IIR (Infinite Impulse Response) or FIR (Finite Impulse Response) filter and defect depth calculated from transceiver time delay.

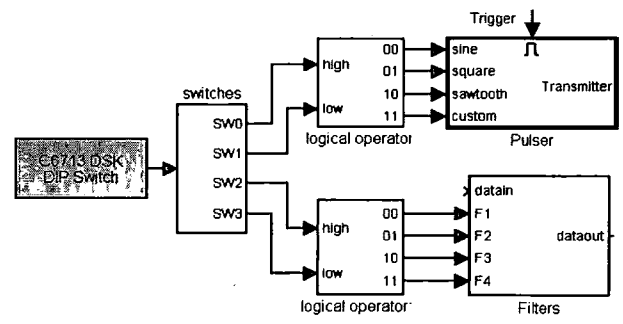


Figure 4 DIP Switches Controlling system

Table 1 DIP Switches

D0	D1	PULSE	D2	D3	FILTER
0	0	Sinewave	0	0	IIR Band pass
0	1	Square	0	1	IIR Low pass
1	0	Sawtooth	1	0	FIR Band pass
1	1	Custom	1	1	FIR Low pass

The 6713DSK includes four DIP switches as a simple way to provide the user with flexible interactive control. These four switches are divided into two groups. One is used to control the waveforms of the generator's outputs, the other offers four different choices for the filter applying upon the echoed signal. Figure 4 Shows the controlling system built with Simulink and Table 1 indicates the corresponding switch setting modes.

6. Conclusion

The real-time system leads to a great improvement in verifying and realising NPD. Much information discarded by conventional test methods of ultrasonic billet inspection can be used due to modern advances in DSP. Therefore, the system not only improves the test integrity and sensitivity, but also makes the experiment data easy to acquire, analyze and visualise. After the successful simulation of the

signal-channel system, a probe array based on the geometry in a typical ultrasonic defect detection system is to be built and driven by using sequential transmitter and parallel receiver processing units. The electronic hardware to achieve this goal is to be designed, constructed and tested in the following research.

7. Further Research

The single channel ultrasonic detection system discussed in this paper can be replicated to develop a multi-channel system by adding a software control structure for control and synchronization of single component[4]. FPGA architecture will give the multi-channel system the ability to perform in real-time. In NPD multi-channel system, each transducer is assigned to be the transmitter sequentially and the other transducers receive echoed signal. As multiple receivers can be set up to test in 3D, more diffracted signal are detected and more information is obtained. It is expected that the position and size of defect can be tested as well.

References

[1] PC Snowdon, S Johnstone, S Dewey, (2003), *A 2D static ultrasonic array of passive probes for improved Probability of Detection*, Nondestructive Testing and Evaluation, 19(3), pp. 111-120
 [2] PC Snowdon, S Johnstone, S Dewey, (2003), *Improving the probability of detection for a 2D ultrasonic array using digital signal processing techniques*, Insight 45(11)
 [3] R. Venteris, (2002) *Exploration of DSP architectures in ultrasonic measurement application*, Ultragarsas Journal 42(1)
 [4] R. L. Tutwiler, S Madhavan, K. V. Mahajan, (1999), *Design of a Test System to Characterize Very High-Frequency Ultrasound Transducer Arrays*, SPIE 3664(182)

Real-Time DSP System for Normal Probe Diffraction Technique

Lei Zhang, Sherri Johnstone

Affiliation

School of Engineering, University of Durham, County Durham DH1 3LE, UK

0191 3342542

Lei.zhang3@dur.ac.uk

Steve Dewey

Corus plc. Swinden Technology Centre, Rotherham, South Yorkshire S60 3AR, UK

Abstract

In steelmaking, on-line defect position and real-time size detection are desired. Many methods have been tried and developed for achieving a reliable cost-effective solution. Ultrasonic detection is commonly used in this field of non-destructive testing (NDT) in the steel industry. Traditional ultrasonic defect detection systems use an array of probes in which each probe pulses and receives sequentially. One new ultrasonic detection technology-Normal Probe diffraction (NPD) has been proven to enhance the probability of detection for steel testing in the previous research.

In this project, a rapid Digital Signal Processing (DSP) prototype for realising the real-time system is modelled and simulated to implement the NPD technique. A DSP integrated development board is used to implement the NPD algorithm and process the digital signal in real-time. An analog expansion daughterboard is also applied in order to gain a fast digital-to-analogue conversion speed for the desired high frequency pulse signal. Variable frequency and wave shape pulse signals can be used in order to gain the best testing effect. A custom high frequency high voltage power amplifier is also designed to get a good response from the transducers. To remove the randomly distributed background noise that disturbs the recognition of the defect echoes and increase the behaviour of the system, several DSP algorithms such as correlation are applied and different filters including FIR filter and IIR filter can be chosen for experiments as well.

The developed real-time system will help increase the probability of detection of defects in steel billets and produce low-cost system solution for ultrasonic billet inspection in steel industry.

1. Introduction

Various defects such as inclusions, bubbles and cracks can affect the quality of the steel and may cause tremendous waste in the steel industry; therefore the detection and recognition of these defects without destructing the tested object is becoming increasingly significant. In steelmaking, on-line defect position and real-time size detection are desired under the urgent requirement for higher quality products. Many methods have been tried and developed for achieving a reliable cost-effective solution. Ultrasonic detection is commonly used in this field of non-destructive testing (NDT) in

the steel industry. Traditional ultrasonic defect detection systems use an array of probes in which each probe pulses and receives sequentially. One new ultrasonic detection technology-Normal Probe diffraction (NPD) has been proven to enhance the probability of detection for steel testing in the previous research ⁽¹⁾. In this work, the necessary real-time system is simulated with software and the corresponding hardware is to be realised and tested to demonstrate the result. In order to gain the best testing effect, a high voltage amplifier is designed for the high frequency output ultrasonic to get a good response from the transducers and gain a better feedback from the tested object. A variable frequency and pulse shape can be completely and flexibly controlled in real-time. To remove the randomly distributed background noise that disturbs the recognition of the defect echoes and increase the behaviour of the system, several Digital Signal Processing (DSP) algorithms are applied and different filters can be chosen for real-time analysis as well.

2. Normal Probe Diffraction

2.1 Background Knowledge

The nature of the project dictates the specific areas of concentrated ultrasonic research, however all areas of wave propagation are to be briefly researched to ensure no potential avenue is overlooked.

The transducer forms the core of all non-destructive ultrasonic inspection procedures, and whether a work-piece can be inspected or not depends upon the acoustic properties they possess. The choice of the correct transducer is therefore indicative for the quality and the reliability of inspection results. Ultrasonic transducers work almost exclusively according to the piezoelectric effect, and there are four fundamental transducer types: Straight beam transducers, Angle beam transducers, Delay line transducers and Twin crystal transducers. In this project, the straight beam transducer is initially required and is dictated by the remit. This type of transducer has one main drawback, in that the poor recognition of near-to-surface discontinuities due to the width of the initial pulse, however in this project it is the core of the material that is of most interest.

Transducers also differ with respect to the size of the active piezoelectric elements, their frequency, bandwidth and the basic design. The selection of bandwidth is essential for achieving certain test results - narrow bandwidth for highly sensitive testing, or broad banded for high resolution testing. The sound field characteristics of a transducer, is generally derived from the diameter and the frequency of the piezoelectric element.

The Near Field is the region in an ultrasonic beam that is subject to variations of intensity due to diffraction effects. It extends from the source of radiation to a point just short of the far field. Diffraction is a particular example of wave interference and is common to all wave motion. Defect detection in the near zone should be avoided unless the characteristics of the probe used are accurately known. Figure1 shows the near field N , the angle of divergence of γ and the far field for a typical circular probe.

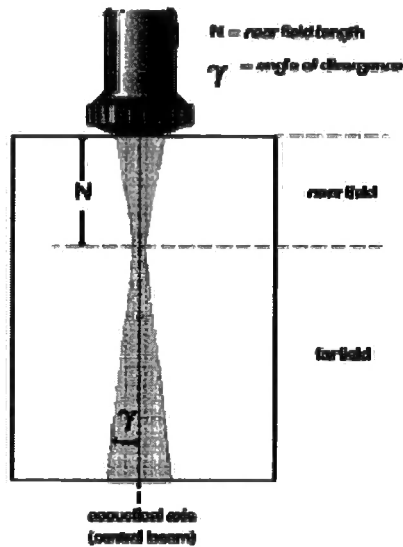


Figure 1 Near Field

The near field equation:

$$N = \frac{D^2 - \lambda^2}{4\lambda}$$

Where

- | | | |
|-----------|---|---|
| D | = | the diameter of a flat circular oscillator (probe/transducer) |
| λ | = | wavelength of the ultrasound |
| N | = | length of near zone |

Wavelength equation:

$$\lambda = \frac{c}{f}$$

Where

- | | | |
|-----------|---|-------------------|
| f | = | frequency |
| c | = | acoustic velocity |
| λ | = | wavelength |

Acoustic velocity is dependant on the material of propagation, and in general, is constant for any frequency and wavelength. The mode of the wave however does affect the velocity, in that longitudinal waves have greater velocity than transverse waves. In steel, longitudinal waves have an acoustic velocity of 5.9 km/s compared to transverse waves with an acoustic velocity of 3.2 km/s.

2.2 Ultrasonic Detection Methods

Ultrasonic detection techniques have developed at a tremendous rate to fulfil the requirement for high quality defect free material in many industrial and research applications. The basic method is Conventional Pulse-Echo Method. As dictated by its name, conventional Pulse-Echo method use an array of probes in which each probe

pulses and receives sequentially. This method was replaced gradually by some new techniques such as Time-of-Flight Diffraction (TOFD) and NPD, because these new methods collect extra information from diffracted signal which was previously discarded by the pulse-echo detection. The TOFD technique uses angled beam probes to pick up the diffracted signal, while NPD can get the same result with normal probes by using multi-receivers.

Both the TOFD and NPD ultrasonic technique relies on the diffraction of ultrasonic energies from 'corners' and 'ends' of internal structures in a component under test. This is in contrast to conventional pulse echo method which relies on directly reflected signals from internal structures and only can test the depth of the defect, while the latter two methods can detect the flaw in 2D and could be improved to 3D detection by using an array of probes.

2.3 Previous Research

The previous research has investigated the potential within a current multi-probe ultrasonic detection system installed at a steel mill. Extensive laboratory experiments were carried out using the transducer array geometry, to extract additional information from passive probes. The apparatus was set up as shown in Figure2.

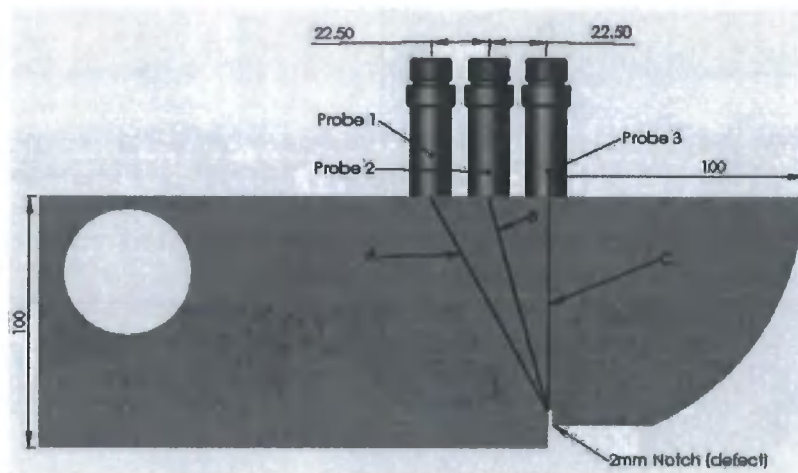


Figure 2 Normal Probe Diffraction

Figure 3 shows the increase of detection ability using the standard single-probe-multi-receiver (SPMR) system over the conventional single-probe-single-receiver (SPSR) system. It shows that the NPD system starts detecting the defect at a lateral distance of 41mm from the defect whereas the pulse-echo probe needs to be within a range of 15mm. The physical principle behind this system uses diffracted waves from the edge of the defects and thus it is particularly effective for the increased detection and sizing of centre-line defects. This technique is defined as Normal Probe Diffraction (NPD), which has been successfully applied offline on a V1 calibration block and a single billet, but has not yet been applied for real-time control.

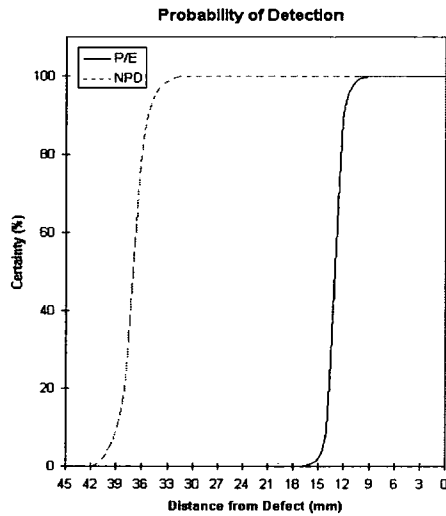


Figure 3 Comparison of Probability of Detection for NPD and Pulse-Echo

Experiments show that the defect detection range can be increased by collecting the diffracted pulse on all the neighbouring probes. This is due to the defect being detected several times per pulse. The research project involves in developing a real-time laboratory based prototype which can detect defects using two methods: the standard single probe pulse echo technique and NPD, and testing the system on a V1 calibration block and a steel billet. In this project, the transmitting and receiving electronics are developed to enable the NPD technique to be applied in real-time.

2.4 NPD Algorithm

The NPD algorithm uses three probes – one transmitter and two receivers. Each transmitter receiver pair are considered to be the foci of two ellipses, each of which pass through the defect. By solving these two ellipse equations, both the vertical offset/defect depth (y0) and the horizontal offset (x0) can be calculated to locate the defect. An ellipse and the coefficients are shown in Figure 4. The relative equations are also listed as follow.

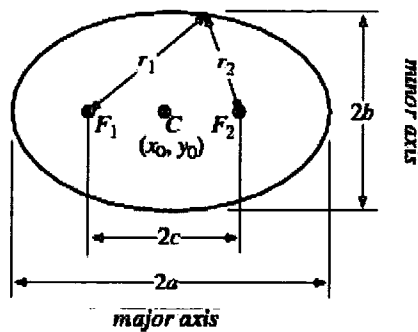


Figure 4 Ellipse

The ellipse equations:

$$\left(\frac{x}{a}\right)^2 + \left(\frac{y}{b}\right)^2 = 1$$

$$a^2 = b^2 + c^2$$

$$r_1 + r_2 = 2 * a$$

Table 1. Transmit Distance and Time

Path	Distance (mm)	Time (us)
A	96.18	16.3
B	87.93	14.9
C	85	14.4
Backwall	100	16.95

Note: $d = v * t$; $v = 5900 \text{ m/s}$

Table 1 gives out the tested distances of path A, B and C in millimetre, with the theoretical time in microsecond calculated from the distances with the velocity of 5900m/s. The experiment setups and ellipse graphs for double probes and triple probes are shown separately in Figure 5 and Figure 6. The distance between each two probes is set to 22.5mm and the depth of the defect (notch) is 85mm (2).

For double probe NPD, probe 1 transmits signal and then receives the diffracted signal, so the first path is 2 x B and forms a circle whose radius (R) is B. The second path is formed by transmitter probe 1 and receiver probe 2, making an ellipse whose major axis equals to B plus C.

Similarly, for triple probes NPD, probe 1 only transmits signal and forms two ellipses with receiver probe 2 and receiver probe 3. The major axes for each are A plus B and A plus C separately.

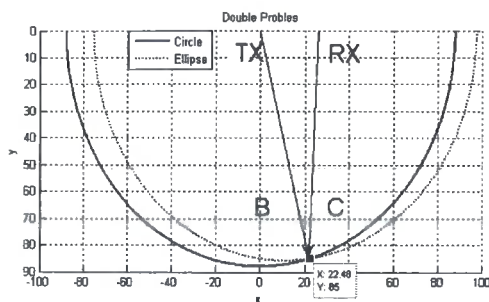
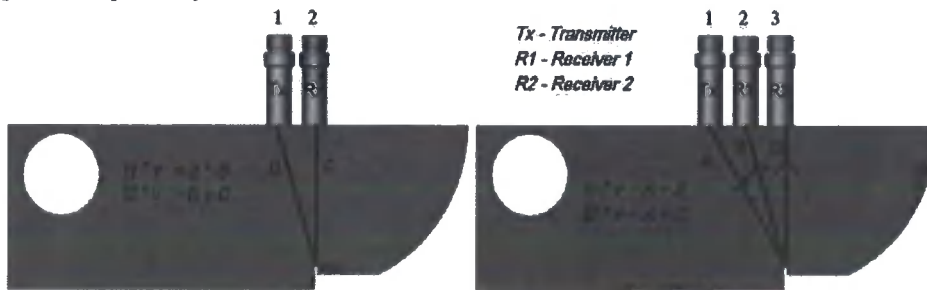


Figure 5 Double Probes Scheme

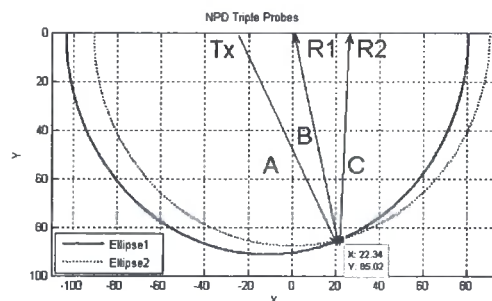


Figure 6 Triple Probes Scheme

2.5 NPD Simulation Model

Simulink Models have been built to simulate the Pulse-echo, Double Probes NPD and Triple Probes NPD algorithms. Figure 7 shows that by calculating the time delay of two transmit paths – t_1 and t_2 , the algorithm can locate the pseudo defect in 2 dimensions. These blocks can be called as individual functions during the idle time in real-time data acquisition.

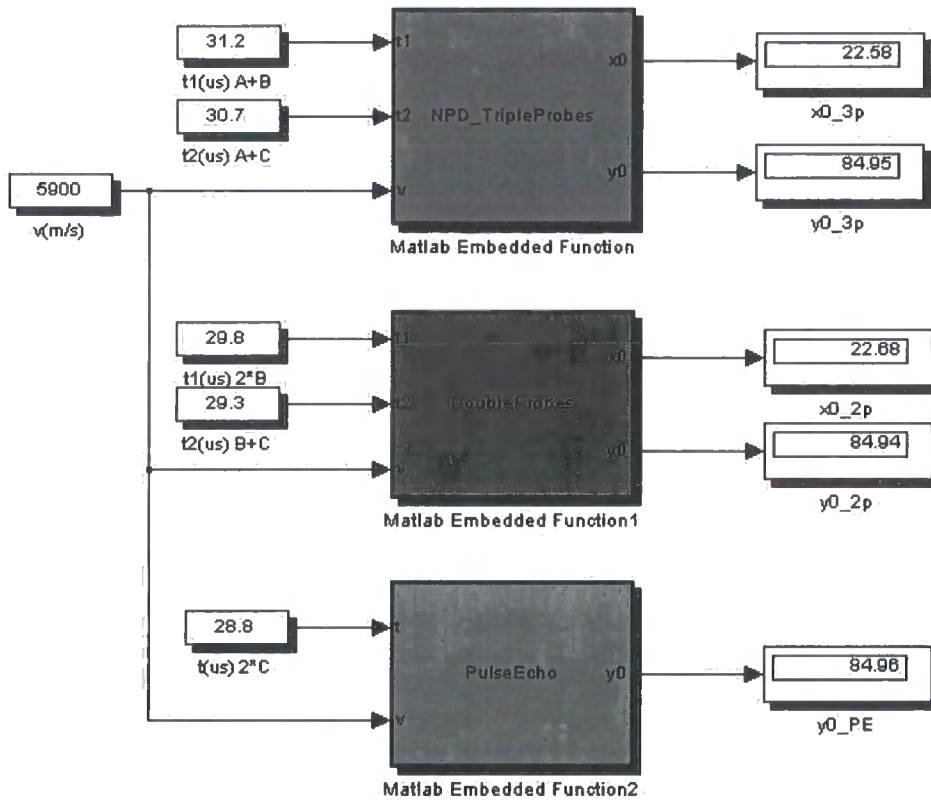


Figure 7 NPD Algorithm Simulation Model

3. DSP System

3.1 Hardware

- TMS320C6713 DSK
- AED_330 Analog Expansion Daughterboard
- High Voltage High Frequency Amplifier

3.2 Software

- Matlab and Simulink
- Code Composer Studio

3.3 System Architecture

Figure 8 depicts the architecture of a rapid Digital Signal Processing (DSP) prototype for the real-time testing system. Firstly a Simulink model is built using the MATLAB

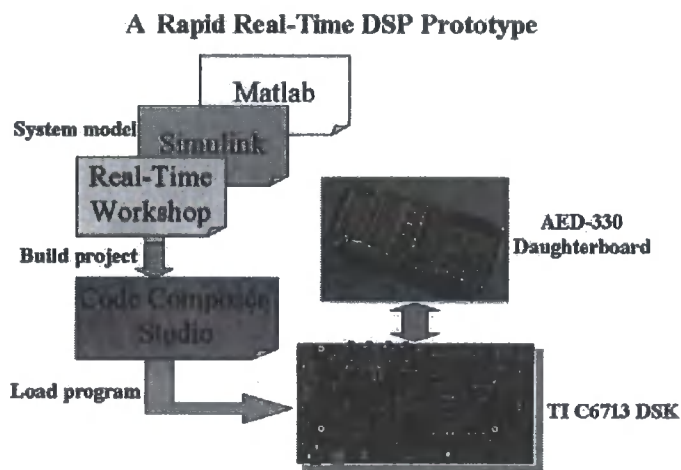


Figure 8 A Rapid Real-Time DSP Prototype

Embedded Target for DSP and DSP blockset which enable the rapid prototyping of real-time software for the TMS320C6713 floating-point processor and generates efficient code for the processor directly from the Simulink model. The generated code is readable and editable for manual optimization. The Embedded Target automates the creation of a link to the Integrated Development Environment, IDE, which provides board support software for the DSK board. It then invokes the compiler and linker to create a DSP executable file and finally downloads the executable to the DSK board and sets it running for real-time algorithm evaluation. An AED-330 analogue expansion daughterboard is mounted on the DSK to gain high speed digital to analogue and analogue to digital conversion for the desired high frequency pulse signal. Variable frequency and wave shape pulse signals can be used in order to gain the optimum testing conditions. A high voltage power amplifier is also designed to get a good response from the transducers(3). To remove the randomly distributed background noise that disturbs the recognition of the defect echoes and increase the behaviour of the system, several DSP algorithms such as correlation are applied and different filters including FIR filter and IIR filter can be chosen for real-time analysis as well .

3.4 System Model

3.4.1 Simulink Model

Figure 9 illustrates SIMULINK model built to simulate the real time system. Main subsystems included are:

- Pulser: Generating various pulse signal
- Delay: Calculating delay time according to distance
- Attenuation: Ultrasound power attenuation in solid material (steel)

- Filter: Cancelling environment noise using IIR and FIR filters
- Correlation: Locating received signal

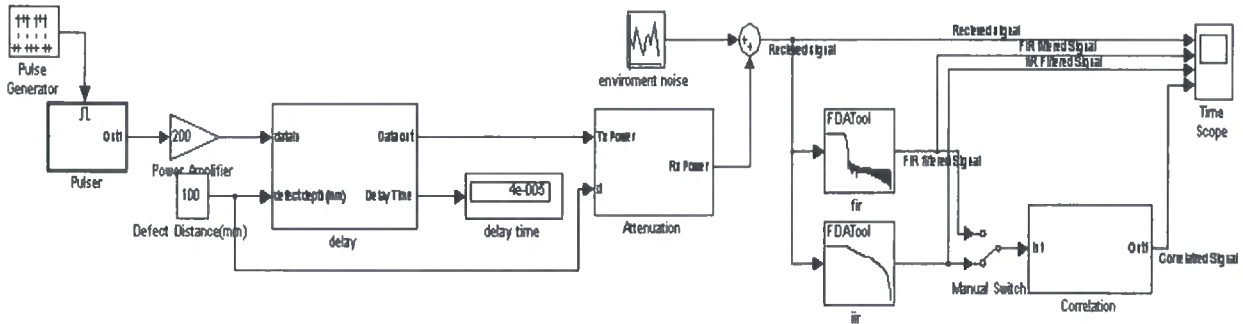
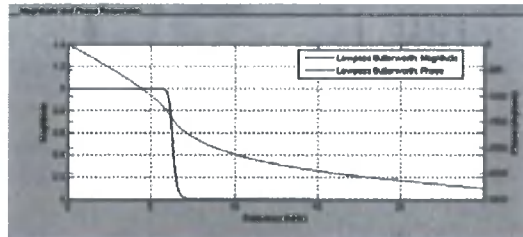


Figure 9 Ultrasonic Detection System SIMULINK Model

Some block and subsystem's parameters are set as follow:

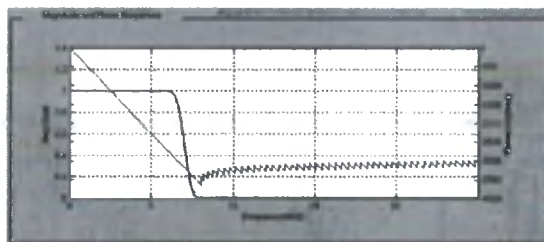
- F_s (sampling frequency): 50MHz
- f (sine pulse frequency): 5MHz
- Gain (represent the analogy amplifier): 200
- Defect Distance (defect position, unit:mm): 100mm

3.4.2 IIR Filter



- Response Type: Lowpass
- Filter Type: Butterworth
- F_s (sampling frequency): 50MHz
- F_{pass} (passband frequency): 6MHz
- F_{stop} (stopband frequency): 8MHz
- A_{pass} (passband attenuation): 1dB
- A_{stop} (stopband attenuation): 80dB
- Order: 31

3.4.3 FIR Filter



- Response Type: Lowpass
- Window Type: Kaiser
- Fs: 50MHz
- Fpass: 6MHz
- Fstop: 8MHz
- Apass: 1dB
- Astop: 80dB
- Order: 126

3.4.4 Simulation Result

The result of the simulation is shown by Figure 12, which indicates that after filtering and correlation, the amplitude of the interesting signal which is buried in environment noise has been increased and easy to be recognized. The signal-to-noise ratio can be used efficiently to analyse the simulation results.

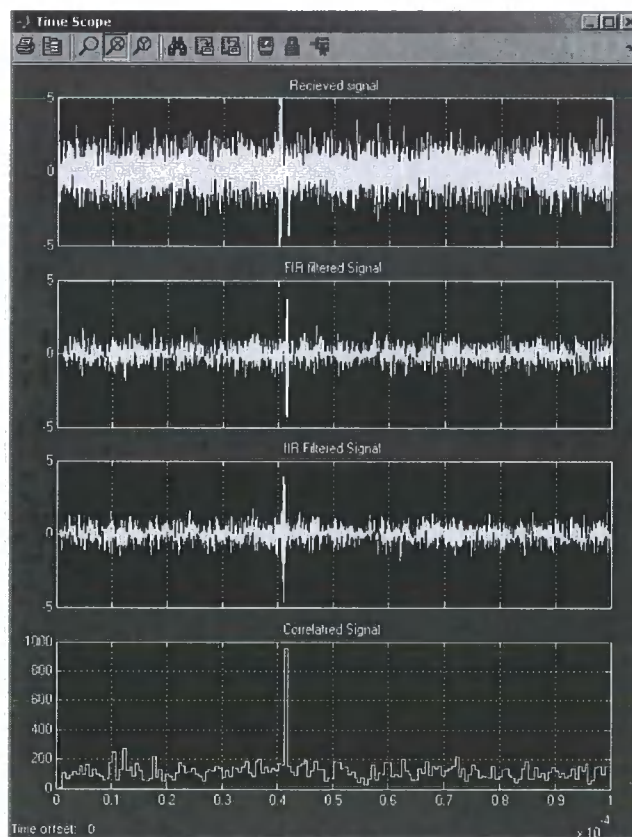


Figure12 Pulse-Echo Simulation result

4. Conclusion

The real-time system leads to a great improvement in verifying and realising NPD. Much information discarded by conventional test methods of ultrasonic billet inspection can be used due to modern advances in DSP. Therefore, the system not only improves the test integrity and sensitivity, but also makes the experiment data easy to acquire,

analyze and visualise. After the successful simulation of the signal-channel system, a probe array based on the geometry in a typical ultrasonic defect detection system is being built and driven using sequential transmitter and parallel receiver processing units. The electronic hardware to achieve this goal has been designed and constructed.

References

1. P C Snowdon, S Johnstone, S Dewey, (2003), A 2D static ultrasonic array of passive probes for improved Probability of Detection, *Nondestructive Testing and Evaluation*, 19(3), pp. 111-120
2. PC Snowdon, S Johnstone, S Dewey, (2003), Improving the probability of detection for a 2D ultrasonic array using digital signal processing techniques, *Insight* 45(11)
3. R. L. Tutwiler, S Madhavan, K. V. Mahajan, (1999), Design of a Test System to Characterize Very High-Frequency Ultrasound Transducer Arrays, *SPIE* 3664(182)
4. R. Venteris, (2002) Exploration of DSP architectures in ultrasonic measurement application, *Ultrasonics Journal* 42(1)

